Innovative Modelling Approaches for the Design, Operation and Control of Complex Energy Systems with Application to Underground Infrastructures

Doctoral Dissertation
Doctoral Program in Energy Engineering (29th Cycle)

Innovative Modelling Approaches *for the* Design, Operation *and* Control *of* Complex Energy Systems *with* Application *to* Underground Infrastructures

By

Sara Cosentino

******

Supervisor(s):
Prof. Romano Borchiellini, Co-Supervisor
Prof. Adriano Sciacovelli, Co-Supervisor
Prof. Vittorio Verda, Supervisor

Politecnico di Torino
2017

Declaration

I hereby declare that, the contents and organization of this dissertation constitute my own original work and does not compromise in any way the rights of third parties, including those relating to the security of personal data.

SARA COSENTINO

2017

A Giuseppe
per l'immensa pazienza e l'incommensurabile amore

Abstract

The ventilations systems play a key role in underground infrastructures for health and safety of occupants during normal operation as well as during accidents. Their performances are affected by selection of the optimal design, operation and control that is investigated by predicting air flow.

The calculation of ventilation flows and their interaction with fires can be done with different modelling approaches that differ in the accuracy and in the required resources.

The 3D computational fluid dynamics (CFD) tools approximate the flow behaviour with a great accuracy but they require high computational resources. The one dimensional (1D) models allow a compact description of the system with a low computational time but they are unsuitable to simulate thermal fluid-dynamic scenarios characterized by turbulence and gradients.

Innovative tools are necessary in order to make the analysis and optimization of these systems possible and accurate in a reasonable time. This can be achieved both with appropriate numerical approaches to the full domain as the model order reduction techniques and with the domain decompositions methods as the multiscale physical decomposition technique. The reduced order mode techniques as the proper orthogonal decomposition (POD) is based on the snapshots method provides an optimal linear basis for the reconstruction of multidimensional data. This technique has been applied to non-dimensional equations in order to produce a reduced model not depending on the geometry, source terms, boundary conditions and initial conditions. This type of modelling is adapted to the optimization strategies of the design and operation allowing to explore several configuration in reduced times, and for the real time simulation in the control algorithms.

The physical decomposition achieved through multiscale approaches uses the accuracy of the CFD code in the *near field* e.g. the region close to the fire source, and takes advantage of the low computational cost of the 1-D model in the region where gradients in the transversal direction are negligible. In last years, the multiscale approach has been proposed for the analysis of tunnel ventilation. Among the several CFD codes used in this field, the Fire Dynamic Simulator (FDS) is suitable for the multiscale modelling. This is an open source CFD package developed by NIST and VTT and presents the HVAC routine in which the conservation equations of mass, energy and momentum are implemented. Currently, the HVAC module does not allow one to consider heat and mass transfer, which significanltly limits the applications. For these reasons a multiscale simulator has been created through the fully integration of a 1D continuity, momentum, energy and mass transport equation in FDS modifying its source codes. The multiscale simulator thus obtained, is based on a direct coupling by means of a Dirichlet-Neumann strategy. At each 1-D-CFD interface, the exchange flow information occurs prescribing thermo-fluid dynamic boundary conditions. The 1-D mass transport equation computes the diffusion of the exhaust gas from the CFD domain and the relative concentration that is particularly interesting in the case of back layering of smoke. The global convergence of the boundary conditions at each 1-D-CFD interface has been analyzed by monitoring the evolution of thermo-fluid dynamic variables (temperature, velocity, pressure and concentration. The multiscale simulator is suitable for parametric and sensitivity studies of the design and the operation ventilation and fire safety systems. This new tool will be available for all the scientific community.

In this thesis, Chapter 1 provides a general introduction to the role of the system ventilation in underground infrastructures and to the innovative modelling strategies proposed for these systems. Chapter 2 offers a description of the 1D network modelling, its fluid-dynamic application to the Frejus tunnel and its

thermal application to ground heat exchangers. In Chapter 3, the proper orthogonal decomposition method is presented and its application to the optimal control of the sanitary ventilation for the Padornelo Tunnel is discussed. To demonstrate the applicability of POD method in other fields, boreholes thermal energy storage systems have been considered in same chapter. In particular, a multi-objective optimization strategy is applied to investigate the optimal design of these system and an optimization algorithm for the operation is proposed. Chapter 4 describes the multiscale approach and the relative simulator. The new open tool is used for modeling the ventilation system of the Monte Cuneo road tunnel in case of fire. Results show that in the case of the current configuration of the ventilation system, depending on the atmospheric conditions at portals, smoke might not be fully confined. Significant improvements in terms of safety conditions can be achieved through increase of in smoke extraction, which requires the installation of large dumpers and of deflectors on the jet fans. The developed tool shows to be particularly effective in such analysis, also concerning the evaluation of local conditions for people evacuation and fire-brigades operation.

Innovative Modelling Approaches For *the* **Design, Operation** *and* **Control** *of* **Complex Energy Systems** *with* **Application** *to* **Underground Infrastructures**

Content

List of Figures

List of Tables

Nomenclature

a,b,c	*Fan characteristic curve coefficients*
$\boldsymbol{A}$	*Incidence matrix*
$\overline{\boldsymbol{A}}$	*Amplitude matrix*
A	*Area [m^2]*
$\boldsymbol{C}$	*Covariance matrix*
C	*Concentration [ppm]*
c	*Gas specific heat [kJ/kg K]*
$\boldsymbol{D}$	*Diffusor tensor[m^2/s]*
Dh	*Hydraulic diameter [m]*

$\boldsymbol{F}$	*Momentum source term [Pa]*
f	*Major losses coefficient*
G	*Mass flow rate [kg/s]*
G_{ext}	*Mass flow rate exchanged with the external environment in a node [kg/s]*
g	*Gravity acceleration [m/s^2]*
h	*Specific enthalpy [kJ/kg]*
K	*Friction continuous loss*
L	*Branch length [m]*
$\dot{m}$	*Mass flow rate [kg/s]*
p	*Pressure [Pa]*
Pe	*Peclet number*
r	*Radial coordinates [m]*
r_{ex}	*External U-tube radius [m]*
r_g	*Borehole radius [m]*
r_i	*Inner U-tube radius [m]*
r_s	*Ground radius [m]*
S_p	*Source of contaminant [ppm/s]*
T	*Temperature [K]*
T_s	*Ground temperature [K]*
t	*Time [s]*
u	*Normal velocity [m]*
U	*Overall heat transfer coefficient [W/m^2 K]*
$\boldsymbol{U_{MxN}}$	*Snapshots matrix*
$\boldsymbol{v}$	*Velocity vector [m/s]*
x	*Longitudinal coordinate [m]*
β	*Minor losses coefficient*
ε_{II}	*Second law efficiency*

λ_j	*Eigenvalue*
ρ	*Air density [kg/m3]*
$\boldsymbol{\tau}$	*Stress tensor [Pa]*
ΔP_{fan}	*Pressure gain due to fan [Pa]*
ΔP_{fric}	*Pressure gain due to friction [Pa]*
ΔP_{pist}	*Pressure gain due to piston effect [Pa]*
Δt	*Time step [s]*
Δz	*Height variation [m]*
Φ_v	*Heat release rate [kW]*
Φ_v	*Heat losses [kW]*
Ω	*Perimeter [m]*

Chapter 1

Introduction

1.1 The role of the ventilation systems in underground infrastructures

Underground infrastructures are complex systems largely diffused in the transport hydroelectric plants (road tunnels and sub-way stations), in the mining sector and in energy sector (geothermal fields, gas pipelines, district heating). Regardless of the sector application, the presence of people focus the attention on the human health and safety in these facilities. Possible hazards are the contaminants due to vehicular traffic, to the working machines, to drilling and explosions stages, fires, smoke propagation etc.

In underground infrastructures subjected to vehicular traffic, among the potential toxic gases are usually considered (PIARC: Technical Committee C4 Road Tunnels Operation, 2012):

- carbon monoxide CO that is the reference emission for the assessment of the toxicity of exhaust gases;

- nitrogen oxide NO and nitrogen dioxide NO_2 that is the reference for the air quality;
- particulate matter PM responsible in the reduction of visibility.

These are constantly monitored by sensors located in the infrastructures. Their effects on human health depend on the exposure time. Regulations prescribe the threshold values considering the pollution dosage depending on the travel or stop time in the infrastructures (PIARC: Technical Committee C4 Road Tunnels Operation, 2012).

In facilities as mines in addition to the products of combustion or fumes from vehicle exhaust emissions, other potential toxic and hazard gases deriving from activities such as blasting are hydrogen sulphide H_2S, hydrogen H_2 and methane CH_4 (Mine safety operation divisions, 2008).

In these confined areas, the environmental comfort also depends on the air temperature and humidity. The increasing in the average temperature value is linked with low levels of thermal exchange between indoor and outdoor environments and with high internal heat gains and as the metabolic processes of the people inside facilities, train and vehicles operation, electrical equipment and heat re-radiated from the ground (Raines, 2009). The temperature of the soil increases with the depth due to the geothermal gradient and in deep facilities as mines, it can reach 40-45 °C with high internal heat gains (Bozhiiov, et al., 1997).

The continuous air circulation is required within the stations, tunnels and mines so as to dilute and remove hazardous substances, to control the thermal environment, to provide oxygen for humans and to ensure an appropriate level of visibility. In normal operating condition, all these requirements are obtained through the sanitary ventilation systems that supply fresh air.

In emergency conditions i.e. in presence of fire, the ventilation systems play a key role for safety and evacuation of the passengers and of the workers. The most immediate threat to life is not the direct exposure to fire, but smoke inhalation. A suitable visibility must be guaranteed during the rescue operations and evacuation. These conditions can obtained by a correct control of fire and of smoke propagation with an appropriate ventilation system. In the underground infrastructures, the smoke propagation is affected by several parameters as the facility geometry, the pressure difference, the inclination, the vehicular traffic and the ventilation system capacity (Gehandler, 2015).

All of these aspects must be included during the design, operation and control of the ventilation systems, resulting so complex from a thermal fluid-dynamic point of view. To study the whole behaviour, designers and engineers use predictive models. They are usually the mathematical formulation of the physical phenomenon of interest in the form of Partial Differential Equations (PDEs) (Beltrami, 1997; Gershenfeld, 1999; Bender, 2000). The spatial and the temporal discretization through numerical methods, converts the original set of PDEs in system of ordinary differential equations (ODEs) in one or more spatial coordinates.

1.1.1 Network modelling for the underground ventilation systems

The overall behaviour of the ventilation system can be approximated using 1D fluid-dynamics models under the assumptions that all the fluid-dynamic quantities are uniform in each tunnel cross section and gradients are only present in the longitudinal direction (Colella, et al., 2012). Several 1D models have been developed by national Institutions MFIRE (U.S., Bureau of Mines, 1995), ROADTUN (Dai & Vardy, 6-8 July,1994; West, et al., 28-30 Nov 1994), RABIT and SPRINT (Riess, et al., November 2000), Express'AIR and SES (NTIS, 1990).

The majority of the 1D models available in literature, considers the topological representation of the network of the underground facilities (Grant & Jagger, 2012). They are usually based on a generalized Bernoulli formulation including the buoyancy effects, the transient fluid-dynamic and the thermal phenomena, the piston effect and the transport of pollutant species (Colella, 2010).

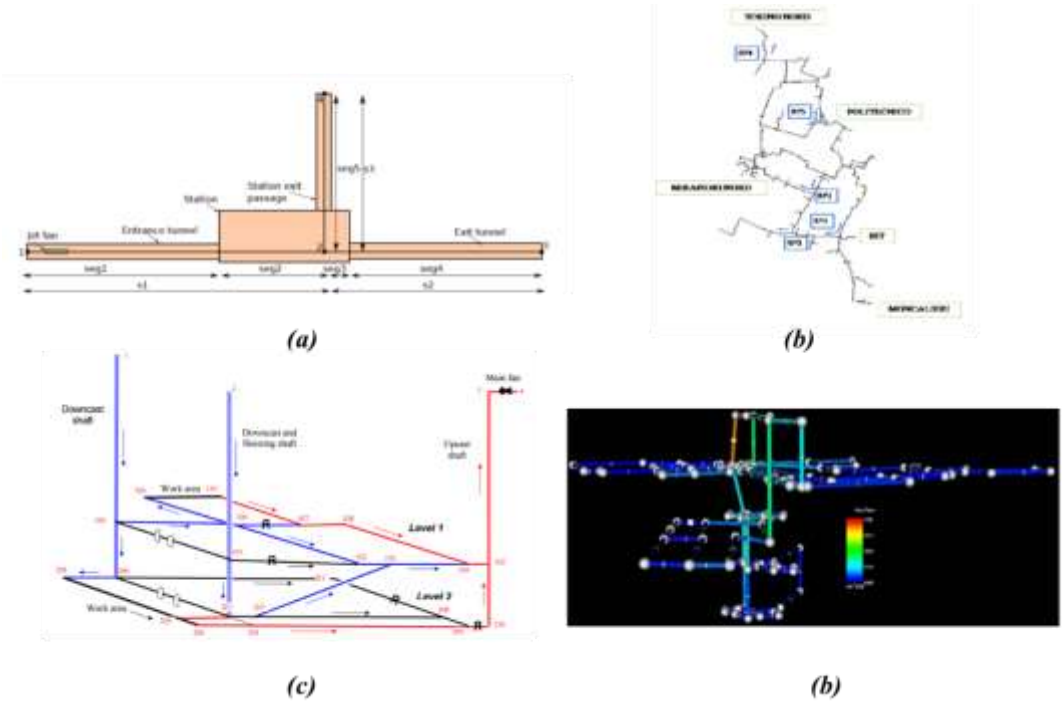

Figure 1.1*: Examples of network modelling applications: (a) subway station* **(Price, 2015)**, *(b) district heating network* **(Guelpa, 2016)**, *(c) mine ventilation systems* **(McPherson, 1993)** *and tunnel ventilation systems* **(Bracke, et al., 2006)**.

The network modelling covers several application fields as shown in *Figure 1.1*. This type of modelling ensures the compact description of the system of interest and the reduced computational costs. Chapter 2 offers a detail description of the 1D network model that includes the continuity, the momentum, the energy and mass transport equations.

The selection of the optimal design, operation and control of the ventilation during normal operation as well as during incidents has become an important issue. As previously said, the ventilation systems are affected by several design variables, complex topology and time-dependent operating conditions etc. The set of ODEs that describes these systems presents many degrees of freedom and the large amount of computations for finding the solution.

Nowadays, the modelling tools are required to analyse and to optimize such complex systems with accuracy and with a reasonable computational time. These last two characteristics are sometimes competitive, forcing the designer to choose either one. In the modelling field, innovative solutions must be investigated to preserve the computational resources and the reliability of the results. This can achieved through compact models based on the model order reduction techniques and the multiscale approach.

1.1.2 Model order reduction techniques: compact models for sanitary ventilation in underground infrastructures

Compact models are appropriate to perform the analysis and optimization of complex systems possible and accurate in an acceptable time. As defined by Schilders (Schilders, 2008), a compact model simplifies the full initial model selected for simulations with reduced CPU time and reliable results. A compact model can be achieved by using model order reduction (MOR) that consists in the selection of certain level of detail sufficient for the analysis of a system. In fact, these techniques try to capture the essential features of a system i.e. the most basic properties of the original model. These are preserved in the reduced model ensuring a certain accuracy. The global effect is a reduction of the computational complexity of the mathematical model in numerical simulations.

Originally developed in the area of systems and control theory (Schilders, 2008), MORs cover several field of research as the fluid dynamics (Lassila, et al., 2014), the structural dynamics (Besselink, et al., 2013), and the circuit design (Steinbrecher & Stykel, 2013).

Basically the methods of MOR can be classified in three categories:

- the methods based on Krylon subspaces;
- the methods based on the Singular Value Decomposition (SVD);
- the methods based on the combination of the previous procedures.

The SVD methods are largely applied in the case of non -linear problems as in computational fluid-dynamic field (Schilders, 2008)

Proper Orthogonal Decomposition (POD) belongs to this category and it is *a posteriori* reduction methods. It extract the essential information from a pre-existing full model of the interested problem and reduce it to a compact model.

The POD method proposed in this thesis starts from the non-dimensional form of the equations that describe the phenomena of interest adding the flexibility to its already known features, i.e. the accuracy and the reduced CPU time.

An accurate description of the POD technique developed in this work, is provided in Chapter 3.

Considering the advantages of this methodology, the application fields involve from the optimization strategies based on heurist algorithms for the design, the operation and control of energy systems to real time simulations (*Figure 1.2*). The design and operation of sanitary ventilation can require an optimization strategy to minimize the electricity consumption of the fans ensuring at the same time the environment comforts (temperature, pollutants, humidity etc.). Given the variability of the operating conditions and the too many variables, a POD model reduces the computational resources achieving the optimal solution in short time.

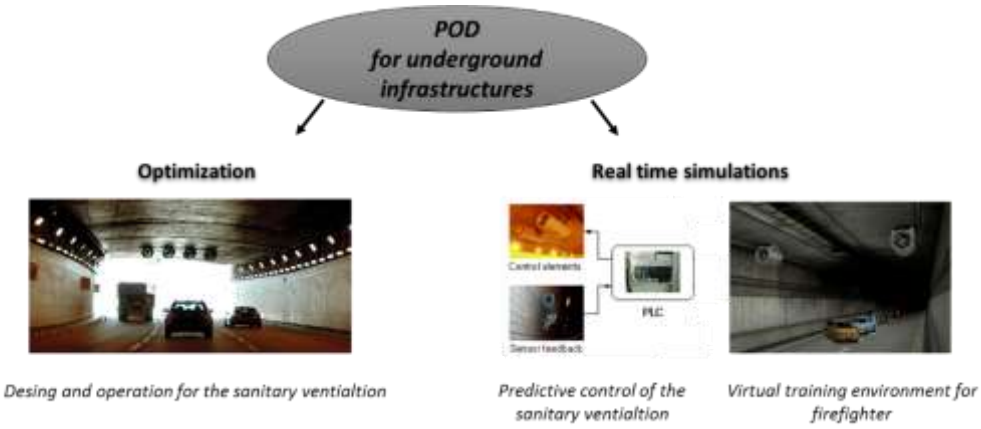

Figure 1.2: *Applications of POD technique for underground infrastructures.*

In the field of fluid networks, the POD strategy has been proposed for the optimization of the operating conditions of a district heating network aimed to the reduction of the pumping costs and the primary energy consumptions thanks a prediction of the evolution of heat power required during the daily transient (Guelpa, 2016).

The real time simulations are another interesting application of the reduced modelling. The latter can be implemented in the control algorithms of the ventilation system as the *predictive controller* determining the required air flow on the basis of the traffic type, the traffic intensity and the weather conditions. The use of the predictive control in the ventilation systems has been tested for the Ucka tunnel, Croatia in (Bogdan, et al., 2008) shown the benefit on the energy consumption. Authors have used empirical equations to predict the required air flow that do not consider the transient dynamic of the whole tunnel. This can take jet-fans to switch on and of with a needless energy consumption.

The use of a POD model to the prediction of air flow within a traditional logic control (i.e. Fuzzy Logic Control), allows an optimal regulation of the jet fans with a significant reduction of the electricity consumption.

In the field of fire safety, the virtual reality simulators are important tool because they allow to train fire fighters in the efficient mitigation of fires in a tunnel, using a computer generated virtual environment. This is a cheap and environmentally friendly alternative to real firefighting exercises that are currently carried out and that involve burning fuel in a disused tunnel (Beer, et al., 2002). In (Beer, et al., 2004) the virtual simulator accesses a database containing the results of CFD simulations for particular tunnel geometries with associated safety installations, particular fire hazard scenarios, etc. The very CPU demanding of the CFD calculations does not allow a real time simulation. The POD models could be implemented in a virtual reality simulator for tunnel fires, reproducing different situations and changing parameters of the simulation in real-time.

In this thesis the POD technique is separately applied on a fluid-dynamic problem and on thermal problem in mono-dimensional geometries.

1.1.3 Multiscale model for the ventilation systems of the underground infrastructures

Nevertheless, 1D models and the reduced models obtained by them result unsuitable to simulate the fluid behaviour in regions at high temperature gradients or in region at velocity gradients due to the assumption of a homogenous behaviour of the fluid flow in each cross section. Proper corrections and empirical correlations must be introduced to account the tri-dimensional behaviour of flow in such

regions. The results of 1D models for fire scenario can be affected by large uncertainties especially for smoke propagation and temperature profiles.

Commercial CFD codes as FLUENT (Inc., ANSYS, 2013), Flow3D and STAR-CD or open source codes as Fire Dynamic Simulator (FDS) (McGrattan, et al., 2013), OpenFoam (Greenshields, 2016) and SMARTFIRE (Taylor, et al., 1997) are usually adopted in fire safety engineering for the prediction of air flow and fire. The accuracy of CFD in the prediction of local flow field data i.e. velocity and temperature fields, is affected by the mesh size used for the domain discretization with consequent unsuitable computational costs for vast domain as in network infrastructures several kilometre long. For this reason, in most of the applications, the computational domain is limited to a small region i.e. close to the fire and the velocity and temperature profile in the rest of the domain are assumed known.

A possible solution for the modelling of network systems is represented by the multiscale approach. It is based on the physical decomposition of the domain and it divides the full domain in sub-regions assigning a model of different complexity as well as a different level of detail e.g. 1D and 3D. Unlike the previous strategy (POD technique), the multiscale approach does not approximate the initial set of ODEs through linear combination, but reduces a multi-dimension problem in only one dimension in the selected sub-domains.

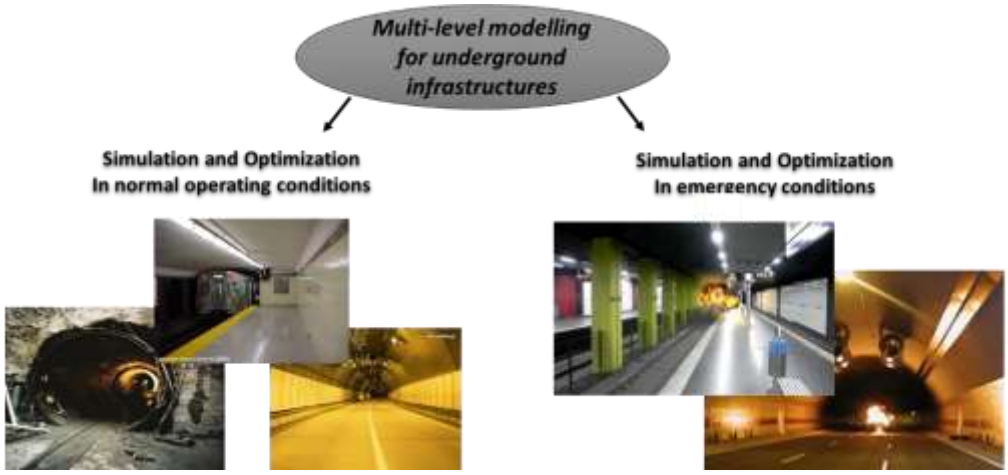

Figure 1.3: *Applications of the multiscale modelling for underground infrastructures.*

The multiscale modelling has been proposed for various fluid flow applications, e.g. to study the brain blood flow (Perdikaris, et al., 2016; Formaggia, et al., 2001). In the last decade, its application has been investigated for the ventilation and fire scenario in tunnels (Colella, 2010).

The physical decomposition achieved through this approach uses the accuracy of the CFD code in the *near field* e.g. the region close to the fire source, and takes advantage of the low computational cost of the 1-D model in the region where gradients in the transversal direction are negligible. Several approaches have been proposed for coupling 1D and 3D domains, in general classifiable as direct and indirect. In the case of direct coupling, 1D and CFD simulations run simultaneously according to such iterative algorithm for the convergence and they exchange the boundary conditions during the simulations. In the indirect coupling, they run separately applying different boundary conditions on the CFD for calculating characteristic curves to use on the 1D model as boundary conditions. The innovative tool for the multiscale modelling proposed in this thesis, is given by the full integration of a 1D continuity, momentum, energy and mass transport equation in the open source CFD FDS modifying its source codes. Chapter 4 offers a

literature review as well as a wide description of multiscale simulator here proposed. As will be discussed in this Chapter, the developed tool differs from the approaches available in literature being based on a direct coupling of the complete 1D network model and the 3D code. The result is an open tool accessible for all the scientific community which applicability covers several fields: in addition to those shown in *Figure 1.3*, it can be used to analyse smoke diffusion and temperature distribution in all the systems which geometry presents a prevalent dimension, e.g. metro stations, tunnels skyscrapers.

1.2 Test cases

In order to clarify what has been previously said and to provide a guide for the test cases, *Figure 1.4* summarizes the innovative modelling strategies proposed in this PhD thesis. Two techniques can be distinguished i.e. proper orthogonal decomposition and multiscale modelling, both aimed to the achievement of a compact model.

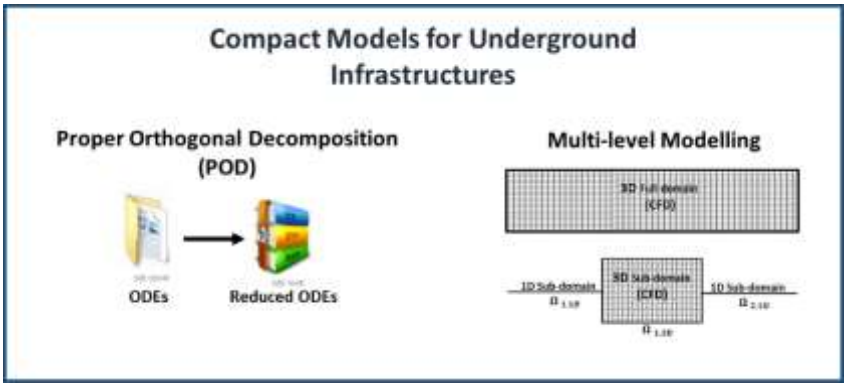

Figure 1.4: *The proposed modelling strategies*.

The modelling methodologies have been applied to study the performance of real underground infrastructures. In some cases, the applications have also been extended to other complex systems as ground heat exchangers and boreholes thermal energy storage systems to demonstrate the flexibility of the proposed modelling strategies in several fields. In the case of ground heat exchangers, the phenomenon of heat exchange with the soil is similar to that occurring in sub-way stations or mines and so it can be analysed with a network model. In the case of boreholes thermal energy storage systems, the application of POD for optimization, real time simulations and control of the thermal storage systems has allowed to confirm its several advantages.
In most of cases the proposed models have been validated with experimental campaigns to assess their accuracy.

1.2.1 The Frejus tunnel

In Chapter 2, the 1D network model is applied on the Frejus tunnel to simulate its fluid-dynamic behaviour.
The Frejus tunnel is a two-way tunnel of 12870 m with a slope of 0.5365 % and a cross section of 47 m^2 located between Italy and France. The ventilation system is fully transverse and it is operated by means of full length supply and exhaust duct located over the tunnel ceiling. The sanitary ventilation is operated by introducing fresh air along the tunnel through 6 U-shaped fresh air ducts and the relative openings installed each 5 m. In emergency conditions, ventilation is operated using both the fresh air and extraction ducts. The latters are the 3 U-shaped ducts connected to extraction dumpers installed each about 125 m. The adopted ventilation strategy depends on the fire position and on the pressure difference between the two portals. A more detailed description of the Frejus tunnel including the emergency strategies of ventilation is given in Chapter 2. Experimental data will

be used to validate the 1D network model in normal operating condition. A fire scenario of 30 MW will be simulated considering the failure mode of a fan with consequent activation of the closed loop algorithm, recently installed to increase the safety conditions in case of anomalies.

1.2.2 Ground heat exchangers

In Chapter 2, the 1D network model is applied on the ground heat exchangers (GHEs) to simulate the heat transfer phenomenon between the fluid and the surrounding soil and to optimize the operating conditions. A GHE with two vertical boreholes is considered and the model is tested through a comparison between experimental data. A more detailed description of the GHE system is presented in Chapter 2.

During the installation and the operation, these systems can be affected by anomalies such as ovalization, variations in the heat transfer between borehole and ground due to fouling, different installation depth etc. The selection of the optimal operation allows to reduce the irreversibilies caused by anomalies with a consequent benefit for the performance of these systems. An optimization analysis based on the Entropy Generation Minimization is performed in different operating conditions reproduced through the 1D model.

1.2.3 The Padornelo tunnel

In Chapter 3 the proper orthogonal decomposition technique is applied on the sanitary ventilation of the Padornelo tunnel during the excavation phase. This is located in the high speed rail line Madrid-Galicia and it will be long 5.971 km with a cross section of 60 m^2. Given the several sources of pollutant due to the

construction phases (drilling, excavation, explosion etc.) and the used machines, the sanitary ventilation must ensure an adequate air quality reducing as much as possible the electricity costs. The model order reduction technique is proposed for this scope. In particular, the POD method is applied on the non-dimensional form of the 1D mass transport equation for pollutant giving a reduced model flexible, accurate and fast. The description of this procedure is explained in Chapter 3. A Fuzzy control algorithm has been developed on the basis of an optimization strategy aimed to minimize the energy consumption and the NO_x level. The training of the control algorithm and the optimization analysis is conducted with the POD model.

1.2.4 Boreholes thermal energy storage systems

In Chapter 3 the proper orthogonal decomposition technique is applied on the boreholes thermal energy storage (BTES) systems to test the flexibility of this modelling technique in other applications. The performance of these systems is affected by the boreholes configurations and ground temperature at which heat is stored. The selection of the optimal design based on the exergy and thermo-economic analysis allows to achieve high efficiency and affordable investment costs. To conduct this analysis, a multi-objective optimization (MOP) strategy is proposed for a BTES system connected with a cogeneration system. Three different stages of operation can be distinguished: charging time to achieve the design temperature in the ground; discharging time i.e. the effective operation to supply energy demand of domestic users; recharging time between two winter seasons. The operation of the plant during a long period is analyzed using the reduced model. This latter is obtained by the non-dimensional form of the 1D thermal model. In Chapter 3, all steps of this procedure are explained.

Once the system is designed, the selection of the optimal operation allows an improvement in the storage efficiency and an economic profit for the plant. The

POD model is implemented in an optimization algorithm in order to discover the optimal times for storing and retrieving additional thermal energy during the operation. This latter is an example of POD application for the real-time simulation and control.

1.2.5 The Monte Cuneo tunnel

In Chapter 4, the multiscale simulator is applied to the Monte Cuneo road tunnel in case of fire. This is located in Avigliana (west of Torino). The tunnel is 1906 m with a cross section of 66 m^2. It presents a semi-transversal ventilation system with accelerators and dumpers for the air extraction. The multiscale approach is used to test the performance of the current ventilation system. The information about the localization of the interfaces between 1D and 3D domain and of the boundary conditions are described in Chapter 4. The multiscale model is validated with experimental data corresponding with emergency configurations, even if without fire. Simulation of a 30 MW fire scenario with the current configuration of the ventilation system shows that the smoke might not be fully confined. For this reason the re-design of the ventilation system with larger extraction dumpers and proper deflectors on the jet fans located is proposed. The results of the simulation with the re-designed ventilation system confirm a significant improvement in terms of safety conditions thanks to the smoke control in the extraction area.

1.3 Main achievements

The main achievements obtained in this thesis can be summarized as follows:

- development of a POD based Fuzzy logic control algorithm for the design and control of the sanitary ventilation and application to a tunnel under construction;

- development of a POD based methodology for the optimization of the design and operation of ground thermal energy storage systems;
- development of the multiscale simulator for the direct 1D-3D coupling obtained integrating the one dimensional code in FDS for the solution of heat and mass transfer;
- application of the multiscale simulator to the Monte Cuneo tunnel for the re-design of the ventilation system.

Chapter 2

1D Modelling

2.1 Introduction

The one dimensional (1D) modelling is particular advantageous for the analysis of complex energy systems characterized by a symmetry so that the phenomena of interest mainly take place with one dimensional evolution. 1D numerical models are obtained by discretizing the partial derivative equations with numerical schemes as finite elements or finite differences. These models allow to simplify complex geometries and to provide fast answers on fluid dynamics such as flow rates, pressure changes, and temperature fluctuations with reduced CPU costs. Therefore they can be used for design and operation optimization purpose.

The mathematical formulation of the 1D models depends on the analysed system and on the relative phenomena. In this chapter the 1D network modelling for systems as tunnels, mines and subway station is discussed starting from the governing equations. Its fluid-dynamic application to the Frejus tunnel is presented as validation and test for the ventilation system.

In the second part of this section, the analysis of the 1D thermal model is presented. As a validation, the application to ground heat exchangers is proposed. The use in a design optimization based on the entropy generation analysis is also discussed in order to present the model features.

2.2 Network modelling

Fluid systems as metro systems, district heating networks, pipelines, blood circulation, tunnels, mines, ventilation systems present one dimension prevailing to a great extent over the others. These complex systems can be described by a compact mathematical representation of the topology through one dimensional network models.

This type of representation is based on the graph theory (Chandrashekar & Wong, 1982; Deo, 2004). A graph represents a set of elements called *nodes* usually corresponding to inlet/outlet, cross sections or junctions and a set of elements called *branches* usually corresponding to a component as a duct or a channel. These elements are together with a relation of incidence which associates each branch with a pair of nodes, called its ends. The interconnections between nodes and branches describes a flow network: the state properties as pressure and temperature, are identified in the nodes; velocity, mass flow rate, geometrical and physical properties as length, cross section, heat transfer rate are associated to the branch bounded by two nodes. After the assignment of the conventional flow direction for each branch in order to establish that inlet and outlet nodes, the interconnections between the nodes and branches, is expresses by the *incidence matrix A*. The convention used in this work, assign a negative value to a flow from outlet node to inlet one. The number of rows of the incident matrix is equal to the total number of nodes while the number of columns matrix is equal to the number of branches. According to the

adopted sing convention, a general element, *Aij*, is 1 if the *i*-th node is the inlet node of the *j*-th branch, while it is -1 if the *i*-th node is the outlet node of the *j*-th branch and it is 0 in all other cases.

Figure 2.1 and *Figure 2.2* report an example of a simple network layout and its relative incident matrix respectively.

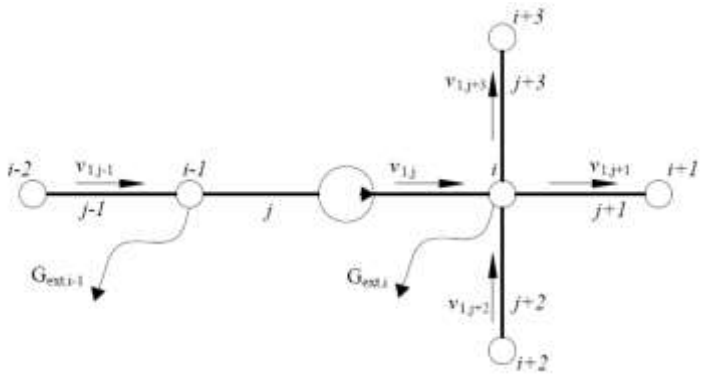

Figure 2.1: *Example of network representation by means of nodes and branches* **(Sciacovelli, et al., 2013)**.

$$\mathbf{A} = \begin{array}{c|ccccc} & j-1 & j & j+1 & j+2 & j+3 \\ \hline i-2 & +1 & 0 & 0 & 0 & 0 \\ i-1 & -1 & +1 & 0 & 0 & 0 \\ i & 0 & -1 & +1 & -1 & +1 \\ i+1 & 0 & 0 & -1 & 0 & 0 \\ i+2 & 0 & 0 & 0 & +1 & 0 \\ i+3 & 0 & 0 & 0 & 0 & -1 \end{array}$$

Figure 2.2: *Incident matrix of the example network system* **(Sciacovelli, et al., 2013)**.

2.2.1 Fluid dynamics model

The fluid dynamic of a flow system is governed by the continuity equation (Eq. 2.1) and the momentum equation (Eq. 2.2). Continuity equations expresses the fact that the rate of flow into a volume must be equal to the rate of change of mass within the volume. Momentum equation establishes that the rate of change in the fluid momentum is equal to the sum of forces acting on it. Both equations are considered in the form of Navier-Stokes equations for a time dependent three dimensional fluid flow (Quartaroni, 2008; Versteeg & Malalasekera, 2007):

$$\frac{\partial \rho}{\partial t} + \nabla \cdot \rho \boldsymbol{v} = 0 \tag{2.1}$$

$$\frac{\partial \rho \boldsymbol{v}}{\partial t} + \nabla \cdot (\rho \boldsymbol{v}\boldsymbol{v}) = -\nabla p + \nabla \cdot \boldsymbol{\tau} + \sum \boldsymbol{F} \tag{2.2}$$

where ρ is the fluid density, t the temporal coordinate, $\boldsymbol{v}$ the velocity vector, p the static pressure, $\boldsymbol{\tau}$ is the stress tensor and $\boldsymbol{F}$ is a momentum source term that also includes the gravity term ρg.

For network systems in Cartesian coordinates *(x,y,z),* the one-dimensional modelling allows to simplify the *y* and *z* spatial dependences. Concerning the viscous term in one dimension, the mathematical formulation of $\boldsymbol{\tau}$ involves partial derivatives with respect to the directions orthogonal to *x,* that have been neglected. This means that viscous stress tensor $\boldsymbol{\tau}$ loses significance in the case of a one-dimensional formulation (Sciacovelli, et al., 2013). In order to take viscous forces into account, a friction term evaluated on the basis of semi-empirical correlations will be introduced, as following explained. According to these assumptions, the continuity and momentum equations can be rewritten in the following forms:

$$\cdot \frac{\partial \rho}{\partial t} + \frac{\partial \rho u}{\partial x} = 0 \tag{2.3}$$

$$\rho \frac{\partial u}{\partial t} + \rho u \frac{\partial u}{\partial x} = -\frac{\partial p}{\partial x} + \sum F_x \tag{2.4}$$

where u is the longitudinal velocity and F_x is the longitudinal momentum source term that includes the term associated with viscous forces, the effects of local fluid dynamic resistance due to valves or junctions, and the effects of pressure rise due to pumps or fans.

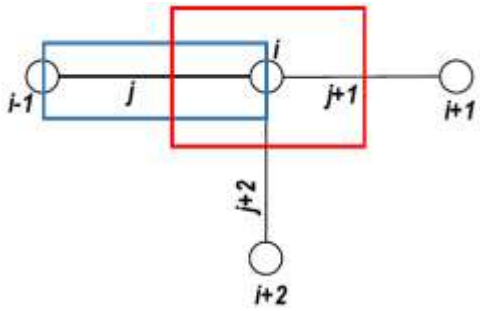

Figure 2.3: *Example of control volumes in network modelling for continuity and momentum equations.*

In network modelling, the domain is discretized in nodes and branches as explained in Section 2.2. The momentum equation is solved in a branch centred control volume while the continuity equation (as well as energy and mass transport equations which will be dealt with in the following sections) is solved in a node centred volume including only half of the length of the branches connected to it.
The generalized Bernoulli formulation for transient flows is given by the integration of equation (2.4) along a branch j bounded by node *i-1* and by node *i* (control volume in blue of *Figure 2.3*)*:*

$$\int_{i-1}^{i} \frac{\partial u}{\partial t} dx + \frac{u_i^2 - u_{i-1}^2}{2} = -\int_{i-1}^{i} \frac{\partial p}{\rho} - g(z_i - z_{i-1}) + \int_{i-1}^{i} \frac{1}{\rho} \sum F_x \, dx \quad (2.5)$$

In Equation (2.5) the buoyancy term has been considered in which *z* represents the vertical elevation and *g* the gravity acceleration.

Considering the total pressure *P* given by the sum of the kinetic, pressure and gravity terms, and explicating all the sources of momentum in to the fan action (ΔP_{fan}), the piston effect (ΔP_{pist}) and the friction (ΔP_{frict}), the Bernoulli formulation of equation (2.5) can be rearranged in the final form for the generic branch *j:*

$$\rho_j \frac{du_j}{dt} L_j + (P_i - P_{i-1}) + \Delta P_{fan,j} + \Delta P_{pist,j} - \Delta P_{frict,j} = 0 \quad (2.6)$$

where L_j is the branch length. The pressure rise ΔP_{fan} due to fans, is usually expressed by a characteristic curve that is approximated by a polynomial function whose coefficients *a,b*, and *c* are obtained empirically (Sciacovelli, et al., 2013) or by Equations (2.8) and (2.9) (Colella, 2010):

$$\Delta P_{fan,j} = a u_j{}^2 + b u_j + c \quad (2.7)$$

$$\Delta P_{fan,j} = n_j \rho_j \frac{A_f}{A_j} K_j u_f (u_f - u_j) \quad (2.8)$$

$$\Delta P_{fan,j} = \eta_j \frac{P_e}{A_j} u_j \quad (2.9)$$

In equation (2.8), *n*, A_f, A_j, u_f and *K* are the number of operating fans, the fan discharging area, the cross section of the generic interconnected branch *j*. the fan discharging velocity and the pressure rise coefficient while in equation (2.9), η, P_e are the fan efficiency and the fan electric power (Colella, 2010).

The evaluation of ΔP_{pist} i.e. the piston effect depends on the type of application considered (tunnels, subway stations, mines) and on the type of vehicles (cars, trains etc.). *PIARC Committee on Road Tunnels* has proposed a formulation for the piston effect for tunnel applications that takes into account the characteristics of the vehicles and the air velocity (PIARC Committee on Road Tunnels, 1995)

Friction losses ΔP_{frict} are given by distributed and local losses (ASHRAE, 2013):

$$\Delta P_{frict,j} = \frac{1}{2}\left(f_j \frac{L_j}{D_{h,j}} + \sum \beta_j\right) \rho_j u_j^2 \tag{2.10}$$

where f_j the branch friction coefficient, β_j the minor loss coefficient, and $D_{h,j}$ the branch hydraulic diameter,

In the case of steady state problems, the time dependence derivative that appears in eq. (2.6) is null and the momentum equation, integrated along a generic branch *j*, is already in its final form.

Now considering the continuity equation in 1D form and its integration in a node centred control volume (red volume in *Figure 2.3*) equation (2.3) becomes:

$$\int_{CV} \frac{\partial \rho}{\partial t} dV + \int_{CV} \frac{\partial \rho u}{\partial x} dV = 0 \tag{2.11}$$

Applying the Gauss's divergence theorem on the second control volume integral of eq. 2.11, for the generic node *i* the continuity equation is given by:

$$\int_{CV} \frac{\partial \rho}{\partial t} dV + \sum_j u_j A_j \rho_j = 0 \tag{2.12}$$

Continuity equation (2.12) can be modified in order to consider a possible extraction of fluid from a node to the external ambient:

$$\int_{CV} \frac{\partial \rho}{\partial t} dV + \sum_j u_j A_j \rho_j + G_{ext,i} = 0 \tag{2.13}$$

The extraction of fluid from the node to the external ambient is given by a positive value of G_{ext}, while its injection into the node from the external ambient is given by a negative value.
For steady state problems, the first term of eq. (2.13) disappears and the continuity equation as obtained affirms that the sum of the mass flow rates entering a generic node of the network must be equal to the sum of the mass flow rate exiting the node.

2.2.2 Thermal model

The thermal model involves in the solution of the energy equation that, in the case of systems with negligible compressibility effects and viscous heating, is given by eq. (2.14):

$$\rho c \frac{\partial T}{\partial t} + \rho c \boldsymbol{v} \cdot \nabla T = \nabla \cdot k \nabla T + \varphi_e \tag{2.14}$$

where T is the temperature, c the fluid heat capacity, k the fluid conductivity, $\boldsymbol{v}$ the vector velocity, and φ_e is the volumetric heat sources.
For network systems in Cartesian coordinates (x,y,z), the energy equation in the longitudinal coordinate x can be rewrite in the following way:

$$\rho c \frac{\partial T}{\partial t} + \rho c u \frac{\partial T}{\partial x} = k \frac{\partial^2 T}{\partial x^2} + \varphi_e \tag{2.15}$$

The volumetric heat source φ_e that appears in the previous equation can be split in φ_v that takes into account the heat generated within the system and into φ_l that considers the heat losses through walls:

$$\varphi_e = \varphi_v - \varphi_l \tag{2.16}$$

Integrating eq. (2.15) in the control volume, the energy balance becomes:

$$\int_{CV} \rho c \frac{dT}{dt} dV + \int_A \rho c u T dA = \int_A k \frac{dT}{dx} dA + \int_{CV} \varphi_v dV - \int_{CV} \varphi_l dV \tag{2.17}$$

Using the discretization of the domain in nodes and branches and considering the node centred CV (red volume in *Figure 2.3*), the generic algebraic equation for a node *i* is given by eq. (2.18):

$$\int_{CV} \rho c \frac{\partial T}{\partial t} dV + \sum_j \rho_j c_j u_j A_j T_j = \sum_j k_j \left.\frac{dT}{dx}\right|_j A_j + \Phi_{v,i} - \Phi_{l,i} \tag{2.18}$$

The net rate of energy transfer due to heat conduction is usually negligible, since the convective contribution is dominant in the heat transfer of systems such as tunnels, subway stations and mines.

The volumetric source term $\Phi_{v,i}$ considered in this work, is due to fire whose analysis is a crucial point for the 1D models due to cannot provide any accurate result for a such complex phenomena. Generally the fire growth curve is obtained by experimental data, by guidelines or standards. For more details description about this argument, we refer the reader to book by *Ingason and co-workers* (Ingason, et

al., 2014) where mathematical representations of design fire curves are presented and discussed

The term $\Phi_{l,i}$ considers the total heat through the walls of the branches belonging to the red control volume reported in *Figure 2.3*. This term is formulated according to the following heat transfer correlation:

$$\Phi_{l,i} = \sum_j \frac{L_j}{2} U_j \Omega_j (T_i - T_{\infty,j}) \tag{2.19}$$

where U_j is the global heat transfer coefficient, Ω_j the perimeter of the j-th branch, and T_∞ is a fixed known temperature (for example the ground or the rock temperature).

The evaluation of T_j (temperature of branch j) that appears in eq. (2.18) requires some care because temperature is defined in the node and not in the branch. A first order upwind scheme is used in order to calculate the temperature at the boundary of the control volume considered (Versteeg & Malalasekera, 2007). The value of T at the boundary is assumed equal to the temperature of the upstream node taking into account the flow direction in the control volume considered. We refer the reader to the section 2.2.5 for a specific description.

For steady state problems, the first term in the LHS of eq. (2.18) can be simplified obtaining the energy equation for a generic node *i*.

2.2.3 Mass transport model

The movement of contaminant in the environment is due to the advective transport as a result of passive movement along with air, and due to the dispersive/diffusive transport to account for diffusion and small-scale variations in the flow velocity. The mass transport phenomena of pollutants in the form of the advection-diffusion PDE (eq. 2.20), combines the Fick theory according which the concentration turbulent fluxes are proportional to the mean concentration gradient, and the continuity equation:

$$\frac{\partial C}{\partial t} + \nabla \cdot (\boldsymbol{v}C) = \nabla \cdot \boldsymbol{D}\nabla C + S_p \tag{2.20}$$

where $\boldsymbol{v}$ is the velocity vector, C the mass concentration (or density) of a pollutant, $\boldsymbol{D}$ the diffusor tensor and S_p is the source term of the contaminant mass flux.

For network systems in Cartesian coordinates *(x,y,z)*, the mass transport equation in the longitudinal coordinate x can be rewritten in the following way:

$$\frac{\partial C}{\partial t} + u\frac{\partial C}{\partial x} = D\frac{\partial^2 C}{\partial x^2} + S_p \tag{2.21}$$

Integrating eq. (2.21) in the control volume, the mass transport equation is given by:

$$\int_{CV} \frac{dC}{dt} dV + \int_A uC dA = \int_A D\frac{dC}{dx} dA + \int_{CV} S_p dV \tag{2.22}$$

Using the discretization of the domain in nodes and branches and considering the node centred CV (red volume in *Figure 2.3*), the generic algebraic equation for a node *i* is given by eq. (2.23):

$$\int_{CV} \frac{\partial C}{\partial t} dV + \sum_j u_j A_j C_j = \sum_j D_j \frac{{C_i}^t - {C_j}^t}{L_j} A_j + S_{p,i} \quad (2.23)$$

The contaminant sources S_p due to vehicles emissions or combustions products can be modelled as a delta distribution or as a line source (Nagendra. & Khare., 2002). More details on the assumption of S_p form will be given in the following.

Similarly to temperature in the energy equation, the evaluation of C_j (concentration of branch *j*) that appears in eq. (2.23) requires some care because concentration is defined in the node and not in the branch. A first order upwind scheme is used in order to calculate the concentration at the boundary of the control volume considered (Versteeg & Malalasekera, 2007). The value of C at the boundary is assumed equal to the concentration of the upstream node taking into account the flow direction in the control volume considered and an adiabatic boundary condition is prescribed at the same CV. We refer the reader to the section 2.2.6 for a specific description.
For steady state problems, the first term in the LHS of eq. (2.23) can be simplified obtaining the mass transport equation for a generic node *i*.

2.2.4 Time dependent problem

In the case of transient operating conditions as a fire event in a tunnel, velocities, pressures, temperatures and concentrations are time dependent variables which time derivatives of equations (2.6), (2.13), (2.18) and (2.23) must be introduced in the network modelling through the integration over a finite time step Δt. The hypothesis of incompressible flow allows to neglect the time derivative of the density in the continuity equation. The discretized equations are in the following form:

$$0 = -\int_t^{t+\Delta}\left[\sum_j u_j A_j \rho_j\right]dt \tag{2.24}$$

$$\int_t^{t+\Delta t}\left[\rho_j \frac{du_j}{dt} L_j\right] dt = -\int_t^{t+\Delta t}\left[(P_i - P_{i-1}) - \Delta P_{fan,j} - \Delta P_{pist,j} + \Delta P_{frict,j}\right]dt \tag{2.25}$$

$$\int_t^{t+\Delta t}\left[\int_{CV} \rho c \frac{\partial T}{\partial t} dV\right] dt = -\int_t^{t+\Delta t}\left[\sum_j \rho_j c_j u_j A_j T_j\right]dt + \int_t^{t+\Delta t}\left[\sum_j k_j \left.\frac{dT}{dx}\right|_j A_j\right] dt + \int_t^{t+\Delta t}\left[\Phi_{e,i}\right]dt - \int_t^{t+t\Delta}\left[\Phi_{l,i}\right]dt + \int_t^{t+t\Delta}\left[\Phi_{v,i}\right]dt \tag{2.26}$$

$$\int_t^{t+\Delta t}\left[\int_{CV} \frac{\partial C}{\partial t} dV\right] dt = -\int_t^{t+\Delta t}\left[\sum_j u_j A_j C_j\right]dt + \int_t^{t+\Delta t}\left[\sum_j D_j \left.\frac{dC}{dx}\right|_j A_j\right] dt + \int_t^{t+\Delta t}\left[\mathrm{S}_{p,i}\right] dt \tag{2.27}$$

A backward Euler method that is first order accurate but unconditionally stable for any time (Quartaroni, 2008), is applied for the temporal discretization. The variable under the time derivative in the LHS of equations (2.24-2.27) are considered prevalent over the whole control volumes, in order to write them as following:

$$0 = (\rho_i{}^t - \rho_i{}^{t-\Delta t})\Delta V_i \tag{2.28}$$

$$\int_t^{t+\Delta t}\left[\rho_j \frac{du_j}{dt} L_j\right] dt = \rho_j\left(u_j{}^t - u_j{}^{t-\Delta t}\right)L_j \tag{2.29}$$

$$\int_t^{t+\Delta t}\left[\int_{CV} \rho c \frac{\partial T}{\partial t} dV\right] dt = \rho_i c_i\left(T_i{}^t - T_i{}^{t-\Delta t}\right)\Delta V_i \tag{2.30}$$

$$\int_t^{t+\Delta t}\left[\int_{CV}\ \frac{\partial C}{\partial t}dV\right]dt = \left({C_i}^t - {C_i}^{t-\Delta t}\right)\Delta V_i \tag{2.31}$$

The use of an implicit formulation i.e. the backward Euler; means that the variables are the ones of the next time step. After performing the double integration and after some rearrangements, equations (2.24-2.27) can be rewritten in the final forms:

$$\sum_j {u_j}^t {A_j}^t {\rho_j}^t + G_{ext,i}^t = 0 \tag{2.32}$$

$$\rho_j \frac{({u_j}^t - {u_j}^{t-\Delta t})}{\Delta t} L_j + ({P^t}_i - {P^t}_{i-1}) + \Delta {P^t}_{fan,j} + \Delta {P^t}_{pist,j} - \Delta {P^t}_{frict,j} = 0 \tag{2.33}$$

$$\rho_i c_i \frac{({T_i}^t - {T_i}^{t-\Delta t})}{\Delta t} + \sum_j {\rho^t}_j {c_j}^t {u_j}^t {A_j}^t {T_j}^t = \sum_j k_j \left.\frac{d{T^t}}{dx}\right|_j A_j - {\Phi^t}_{l,i} + {\Phi^t}_{v,i} \tag{2.34}$$

$$\frac{({C_i}^t - {C_i}^{t-\Delta t})}{\Delta t} + \sum_j {u^t}_j A_j {C_j}^t = \sum_j D_j \frac{{C_i}^t - {C_j}^t}{L_j} A_j + {S_{p,i}}^t \tag{2.35}$$

In order to explain the proposed algorithm for the solution of one dimensional network modelling, the continuity, momentum, energy and mass transport equations must be rearranged in a matrix form. The following two sections show the numerical discretization proposed for the 1D heat transfer and mass transport equation and the numerical procedure to solve the fluid-dynamic equations.

2.2.5 The SIMPLE algorithm

First of all, the continuity and momentum equations must be rewritten in the matrix form. Let's indicate m_n the total number of nodes, m_b the total number of branches

and $G_j=u_j\rho_j A_j$ the mass flow rate in the branch *j*. The continuity equation for all the nodes of the network can be obtained introducing the incidence matrix $\boldsymbol{A}$ (m_n x m_b):

$$\boldsymbol{A}\boldsymbol{G}^{\boldsymbol{t}} + \boldsymbol{G}_{\boldsymbol{ext}}^{\boldsymbol{t}} = 0 \tag{2.36}$$

where $\boldsymbol{G}$ is a column vector whose elements are the mass flow rates that flow in the branches, $\boldsymbol{G_{ext}}$ is the m_n vector in whiche the *i-th* element is the mass flow rate extracted or injected, at the *i-th* node. The matrix form of the momentum equation is given by:

$$\boldsymbol{A}^{\boldsymbol{T}}\boldsymbol{P}^{\boldsymbol{t}} = \boldsymbol{Y}^{\boldsymbol{t}}\boldsymbol{G}^{\boldsymbol{t}} + \boldsymbol{t}^{\boldsymbol{t}} \tag{2.37}$$

where $\boldsymbol{Y}^{\boldsymbol{t}}$ is a ($m_b \times m_b$) matrix containing the term $\frac{1}{2}\left(f_j \frac{L_j}{D_{h,j}} + \sum \beta_j\right)\frac{A_j^2}{\rho_j{}^t} G_j{}^{2\,t} + \frac{L_j}{A_j \Delta t}$ on the diagonal and $\boldsymbol{t}^{\boldsymbol{t}}$ is a vector containing the rest of the terms contained in eq. (2.33) i.e. the pressure gain due to the piston effect and the fans, the transient term $\frac{L_j}{A_j \Delta t} G_j^{t-\Delta t}$ and the buoyancy term $g z_j(\rho_{ref} - \rho_j^{t-\Delta t})$.

The pressure gains due to the piston effect or fan action are treated explicitly by the model.

Two issues are related to the direct solution of the fluid-dynamic equations (2.36) and (2.37): both the momentum equation and the continuity equation are coupled, as the vector $\boldsymbol{G}$ presented in both equations; the term $\boldsymbol{Y}^{\boldsymbol{t}}$ that appears in the momentum equation Eq. (2.37) is not linear due to the $G_j{}^t$ term.

The Semi-Implicit Method for Pressure-Linked Equations (SIMPLE), is the algorithm originally proposed to solve incompressible fluid flows (Patancar, 1980). This method is an iterative solution strategy based on a "guess and correct" procedure.

Considering $\mathbf{P}^*$ and $\mathbf{G}^*$ the guess values of respective quantities, we can define the pressure correction and the mass correction as following:

$$\boldsymbol{P'} = \boldsymbol{P} - \boldsymbol{P}^* \tag{2.38}$$

$$\boldsymbol{G'} = \boldsymbol{G} - \boldsymbol{G}^* \tag{2.39}$$

At the first iteration, the guess $\boldsymbol{P}^*$ is set in the Eq. (2.37) that is so solved for $\boldsymbol{G}^*$. Pressure and mass flow rate corrections are solved according to the equations (2.38) and (2.39). $\boldsymbol{P}'$ is used in the momentum equation, substituting the $\boldsymbol{G}$ value with the continuity equation (2.36):

$$(\boldsymbol{A}\boldsymbol{Y}^{-1}\boldsymbol{A}^{\boldsymbol{T}})\boldsymbol{P'} = -\boldsymbol{G}_{\boldsymbol{ext}} - \boldsymbol{A}\boldsymbol{G}^* \tag{2.40}$$

The pressure correction given by Eq. (2.40) is used to update $\boldsymbol{P}$ and $\boldsymbol{G}$ at each iteration step. The converge to the exact solution is achieved thanks to the under-relaxation step. This is used at each iteration evaluating the new update P and G through relaxation factors. The scaled values of the residuals are monitored for the convergence check.

.

2.2.5 The Upwind scheme

The temperature and the concentration are defined at nodes, as previously explained. However they are computed using quantities defined in the branch, respectively the temperatures *Tj* (see eq. 2.34) and the concentration C_j (see eq. 2.35). The first order upwind scheme is proposed for evaluating the temperatures and concentrations at the boundary, on the basis of the corresponding values at the nodes.

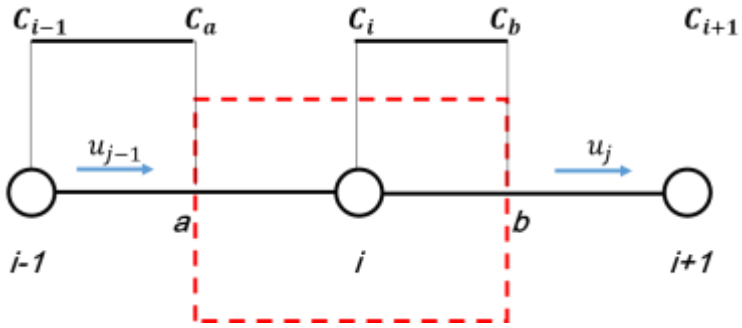

Figure 2.4: *The Upwind scheme for the positive flow direction.*

The upwind scheme takes into account the flow direction when the boundaries temperature and concentration of the control volume (dashed red line of *Figure 2.4*) are determined. The values of *T* and *C* at the boundaries are assumed respectively equal to the temperature and the concentration of the *upstream* nodes. In order to clarify this concept, consider the application of the Upwind scheme for the concentration evaluation in the case of example reported in *Figure 2.4*. A generic node *i*, on which the concentration must be calculated, is connected to two branches and a fluid moves in the positive direction (left to right).The concentration C_a on the left surface of the control volume (*a*) is that of the upstream node C_{i-1}. Similarly, node *i* is the upstream node for the right surface (*b*) and C_b is equal to C_i. The same goes for the temperature evaluation. The application of the Upwind scheme to each node, allows to assemble the energy and mass transport equations in the matrix form.

The energy equation in the form of Eq. (2.34), becomes in the matrix form:

$$(\boldsymbol{M^t} + \boldsymbol{K^t})\boldsymbol{T^t} = \boldsymbol{f^t} + \boldsymbol{M^{t-\Delta t}T^{t-\Delta t}} \tag{2.41}$$

$\boldsymbol{K^t}$ is the stiffness matrix containing in the row the expansion of term $\sum_j c_j {G_j}^t$ according to the up-wind scheme applied to each node, $\boldsymbol{M^t}$ is s matrix with the term

$\frac{\rho_i^t c_i}{\Delta t}$ on the diagonal and $\boldsymbol{f^t}$ is the vector of the known terms. For more details about the assembling procedure of the stiffness matrix, we refer the reader to (Sciacovelli, et al., 2013).

The mass transport equation in matrix form very similar to Eq. (2.41):

$$\left(\boldsymbol{M_c}^{\boldsymbol{t}} + \boldsymbol{K_c}^{\boldsymbol{t}}\right)\boldsymbol{C^t} = \boldsymbol{f_c}^{\boldsymbol{t}} + \boldsymbol{S_p}^{\boldsymbol{t}} + \boldsymbol{M_c}^{\boldsymbol{t-\Delta t}}\boldsymbol{C^{t-\Delta t}} \tag{2.42}$$

$\boldsymbol{K^t_c}$ is the stiffness matrix containing in the row the expansion of summations term of Eq. (2.35) according to the up-wind scheme applied to each node, $\boldsymbol{M^t_c}$ is s matrix with the term $\frac{1}{\Delta t}$ on the diagonal and $\boldsymbol{f^t_c}$ is the vector of the known terms $\boldsymbol{S_p}^{\boldsymbol{t}}$ is a column vector of m_n dimension, containing the source term of pollutant $S_{p,i}$ for each node.

The main steps of the proposed method to solve the complete 1D network model, are summarized below:

a. Set the guess value $\mathbf{P}^*$
b. Solve the momentum Eq. (2.37) to calculate the guess value $\mathbf{G}^*$
c. Solve the pressure correction Eq. (2.38)to calculate $\mathbf{P}'$
d. Update the new **P** and **G** according to the under relaxation
e. Solve Eq. (2.41) to calculate **T** and update density for the buoyancy term that is included in Eq. (2.37).
f. Iterate step *b* to *e* until to the convergence is achieved.
g. Solve Eq. (2.42) with the exact value of velocity to calculate concentration **C.**

The next two sections describe the fluid-dynamic application of the 1D network model for the ventilation system of the Frejus tunnel and the thermal application for ground heat exchangers. In this last case, the thermal problem is similar to that occurs for sanitary ventilation systems in underground infrastructures.

2.3 Validation and application of the 1D fluid-dynamic model for the ventilation system in the Frejus tunnel

The 1D network model has been used to simulate the fluid-dynamic behaviour of the ventilation system in the Frejus tunnel.

The Frejus is a two-way tunnel of 12870 m with a slope of 0.5365 % and a cross section of 47 m^2 (*Figure 2.5(b)*), located between Italy and France. The ventilation system is fully transversal and its representation is reported in *Figure 2.5(a)*. Four ventilation stations (VS) with 6 groups of fresh air fans and the six groups of extraction fans, ensure the longitudinal air control. Sanitary ventilation is operated by introducing fresh air along the tunnel through 6 U-shaped fresh air ducts and the relative openings installed each 5 m. In emergency condition, ventilation is operated using both the fresh air and extraction ducts. Latters are the 3 U-shaped ducts connected to extraction dumpers installed each about 125 m. The adopted ventilation strategy depends on the fire position and on the pressure difference between the two portals. The pressure difference is assumed positive when inducing the air flowing from the French portal towards the Italian portal and it can reach values of several hundreds pascal. The current ventilation algorithm called *control matrix* covers a range of ± 750 Pa as pressure difference and considers 11 fire position.

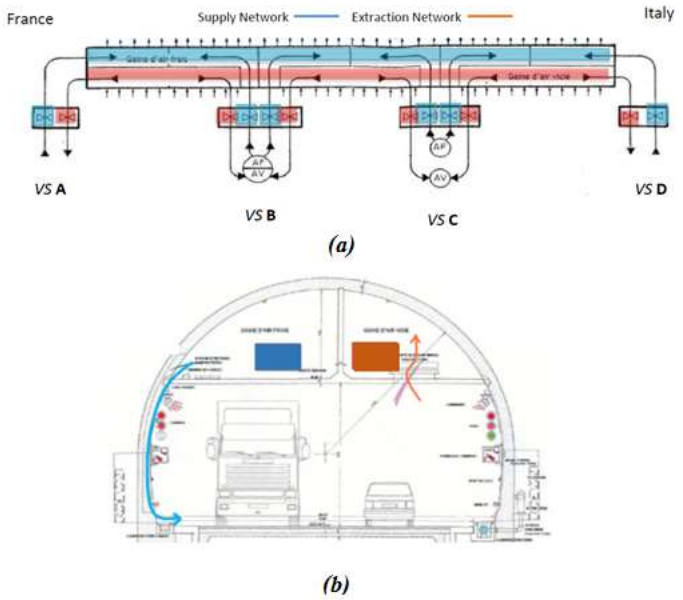

Figure 2.5: *Ventilation system (a) and cross section (b) of the Frejus tunnel.*

In the case of fire, 4 dumpers, 2 located upstream the fire position and 2 downstream, are opened in order to control and extract the smoke. The strategy proposes the confinement of the smoke among the 4 dumpers with a point of zero velocity obtained thanks to a positive velocity (France to Italy) left side of the fire and a negative velocity on the right side. Depending on the fire position and the pressure difference, the only extraction above the fire is not sufficient to stop the smoke propagation along the tunnel.

In this case, the control matrix prescribes to supply fresh air downstream of the fire to enhance smoke confinement *(opposite supply strategy)* and/or to extract air in another point of the tunnel contrasting the effect of pressure difference between the portals *(opposite extraction strategy).*

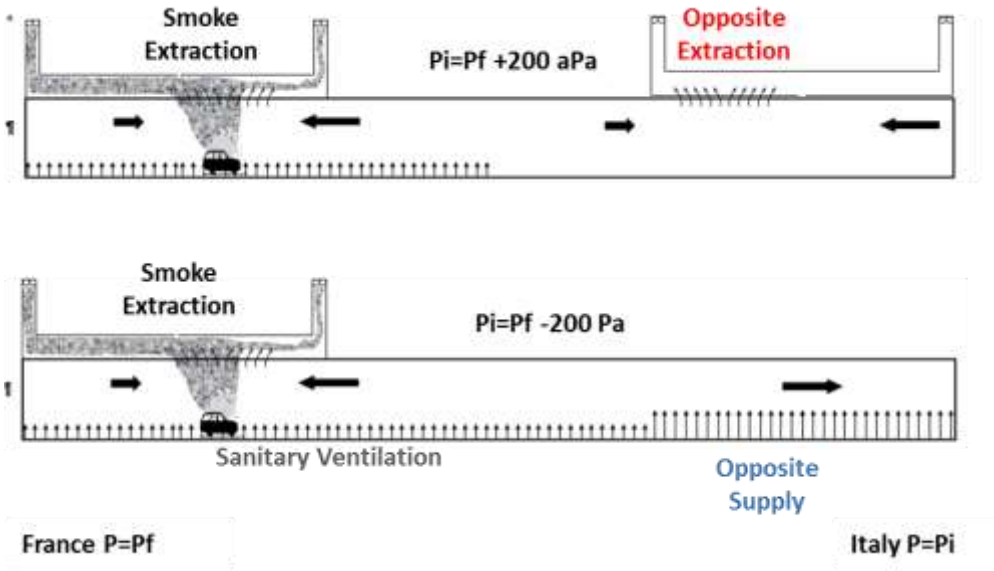

Figure 2.6: *Smoke extraction controlled by (top) opposite extraction and (bottom) opposite supply strategies.*

Figure 2.6 reports an illustrative example of the ventilation system for a fire near the French portal. In the case of negative pressure gain that corresponds to an introduction of air flow from Italy to France (top of the *Figure 2.6*), an opposite extraction is applied near the Italian portal; on the contrary, for positive pressure gain (bottom of the *Figure 2.6*), an opposite supply strategy is adopted in near the Italian portal. Recently, a closed loop algorithm has been installed on the control matrix for the optimization the control of longitudinal velocity both in nominal (all the fans operating) and failure modes (one or more ventilations unavailable).

During August 2016 a test of the ventilation performance, the closed loop algorithm has been activated for a failure mode of a fan in the ventilation station *C.* The aim of the test was to verify the correct activation of the ventilation system and to measure the longitudinal velocity with anemometers located near the dumpers along the tunnel. The operating condition presented a pressure difference of +77 Pa for a simulated fire located at 9510 m. Under these condition and after the activation

of the closed loop algorithm, the control matrix have prescribed the supply fans operating at 30% of full charge, the opposite extraction at 3957 m and 8654 m with the 100% and 65% of the full charge respectively. The experimental results have been compared with that given by the 1D network composed by 425 branches and 328 nodes.

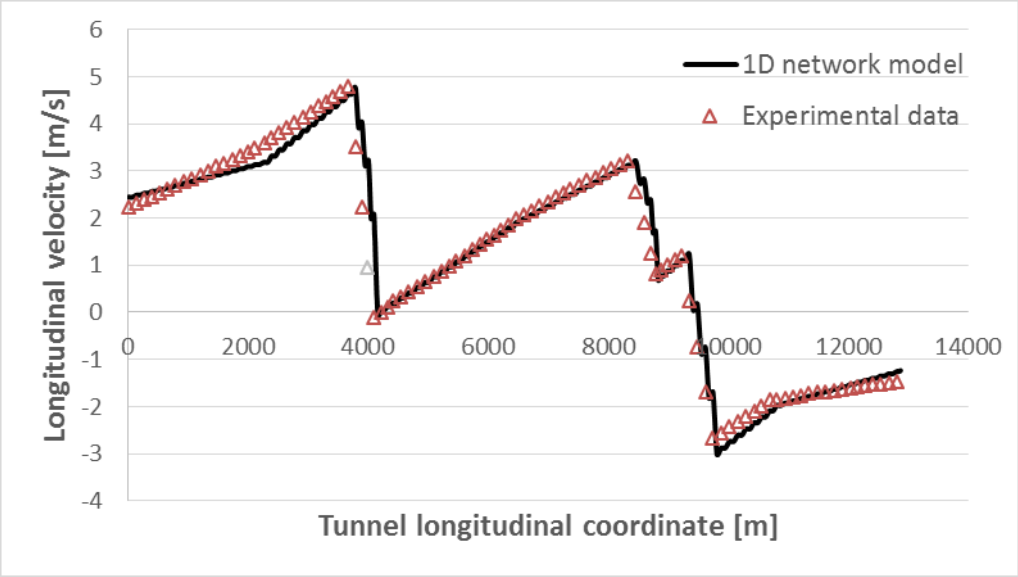

Figure 2.7: *Longitudinal velocity in steady state condition.*

The volumetric flow rates of the axial fans at full charge range between 260÷320 m3/s and 105÷110 m3/s for supply and extraction units according to the measurements campaigns.

The comparison between numerical simulation and experimental data relative to a steady state scenario, is plotted in *Figure 2.7* where the achievement of a quite accurate match between numerical and experimental data can be observed.

In case of fire, the failure mode of a fan and the activation of the closed loop algorithm can cause a delay in the extraction smoke allowing the propagation. For these reasons, an emergency case has been analysed with the 1D network model

considering the same condition of the test (pressure difference on the portal, fire position, sanitary ventilation before the accident etc.). The fire source is 30 MW which heat release rate is plotted in *Figure 2.8* according to the French regulation (CETU, Centre d'études des tunnels, 2003). A delay of 4 minutes for the activation of the ventilation system has been considered and a time of 30 second for the full operation.

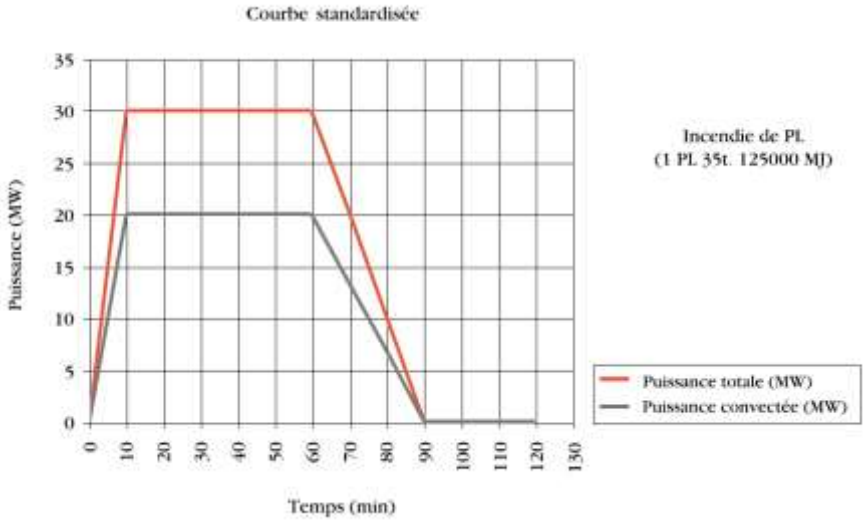

Figure 2.8: *Heat release rate for a fire of 30 MW* **(CETU, Centre d'études des tunnels, 2003)**.

The analysis of the smoke front upstream and downstream of the fire, allows to understand which portion of tunnel is occupied by the smoke and to quantify the time needed to confine it in the extraction zone. As shown in *Figure 2.9*, during the first 4 minutes of fire, the left front of smoke moves for 500 m (300 of which beyond the extraction zone); when fans are activated, the smoke inverts the direction of propagation and after about 240 s and it returns in the extraction area. The right front remains in the same position i.e. above the fire zone for all the time.

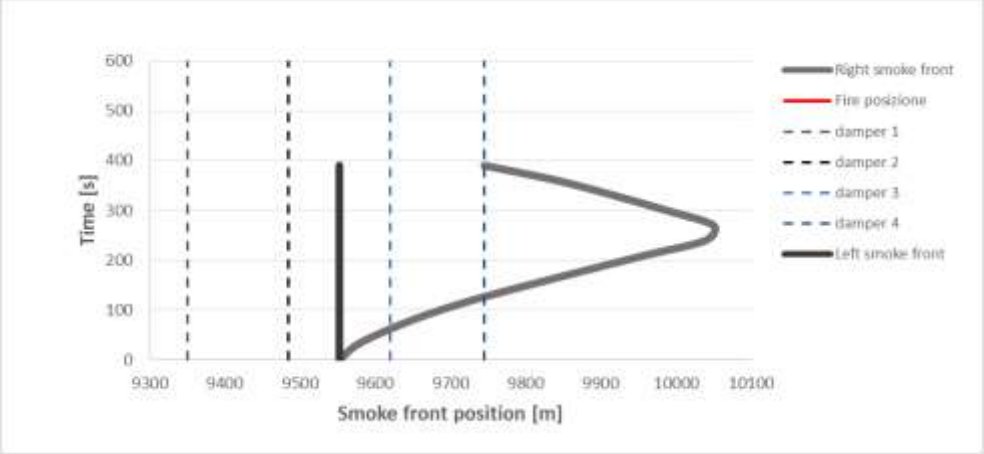

Figure 2.9: *Smoke front position.*

During the first 4 minutes, the direction of propagation is established by the pressure difference between the portals and by the sanitary ventilation.

As shown in *Figure 2.10*, at t=0 s the air flows from the French portal (x=0 m) to the Italian one (x=1285 m). After 4 minutes, the ventilation system has been activated and the dumpers are opened. This causes a changing in the flow profile (t =240 s) until to the its total inversion with a zero velocity among the four dampers, when fans are full operating (t=270 s).The control of the smoke is ensured for all the time of propagation of the fire at the maximum power (t= 2400 s).

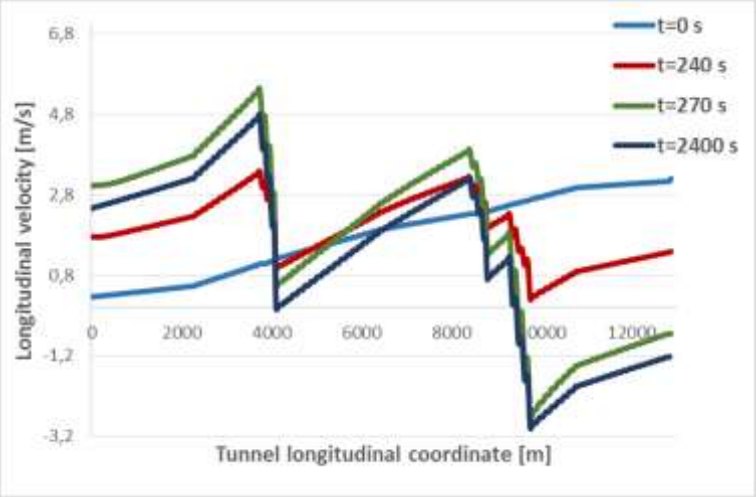

Figure 2.10: *Longitudinal velocity at 4 different times.*

The simulation allows to establish the reliability of the closed loop algorithm, when a failure of a fan occurs in emergency condition. Nowadays the Frejus tunnel is subjected to studies for the failure modes of the fans. The new tunnel adjacent to the Frejus is under construction. The project includes the links through bypass of the respective ventilation ducts and the progressive substitution of the fans in the current tunnel. During these working phases, the ventilation system of the Frejus operates in failure mode and the simulations of the emergency conditions are needed to understand the limit of the ventilation system in term of control and confinement of the smoke.

2.4 Validation and application of the 1D thermal model for the optimal operation of Ground Heat Exchangers

Ground heat exchangers (GHE) belong to the category of geothermal applications in which a heat transfer fluid exchanges heat with surrounding soil. The ground sensible heat can be directly used by linking the GHE with a heat pump. In this

case, the ground coupled heat pump (GCHP) system is constituted by a closed loop circuit buried in the ground where a process fluid, usually glycol water, transfers heat with the ground and with the evaporator or the condenser of a heat pump in heating or cooling mode, respectively. When heating mode is considered, the ground can be also used as storage medium in which sensible heat is stored as internal energy increasing the soil temperature. In this case, underground thermal energy storage (UTES) provides large-scale seasonal storage of cold and heat in natural underground sites (Gao, et al., 2008; Nordell, et al., 2007).

Typically the GHE are vertical boreholes with one or more U-tubes (Yang, et al., 2010). The heat transfer process may usually be investigated in two separated regions. One is the solid soil/rock outside the borehole, where the heat conduction can be treated as a transient process (Zeng, et al., 2003) Since the borehole is much longer than its diameter, this process is often formulated by the one-dimensional line-source or cylindrical-source theory (Bandos, et al., 2009). A transient two-dimensional implicit finite volume model has been used to develop non-dimensional short time-step temperature response factors in vertically ground-coupled heat exchangers (Li & Lai, 2015). A two-dimensional model of the finite line-source has also been proposed in order to consider the axial heat flow in the ground for longer durations (Zen., et al., 2002; Atam & Helsen, 2016). The other region is the volume inside the borehole, including the backfilling, the U-tubes and the circulating fluid inside the pipes. The heat transfer in this region is generally assumed to be in steady-state due to the much smaller dimensions and thermal capacity. Because diameters are smaller than lengths, the borehole has been often treated as one-dimensional pipe heat exchanger neglecting the heat transfer in the direction of the borehole axis (Wołoszyn & Gołas, 2013). An expression of the equivalent diameter is proposed for the heat transfer of a vertical U-tube heat exchanger and the thermal processes in the borehole has been represented by a

single borehole resistance (Florides & Kalogirou, 2007; Gu & O'Neal, 1998). A response-test method has been used for the determination of borehole thermal resistance (Claesson & Eskilson, 1988).

In this work, the vertical U-tube GHE is discretized in branches e nodes along the installation depth L_d. The control volume around the node *i* represents a cylindrical coaxial heat exchanger and it is analyzed using a one-dimensional model in radial coordinates. The 1-D model includes fluid core, an equivalent convective resistance layer, tube layer, grout layer that is surrounded by the ground. Consequently, four radiuses are identified: r_i (inner u-tube radius), r_{ex} (outer u-tube radius), r_g (borehole radius) and r_s (ground). The ground radius is chosen sufficiently large to consider the corresponding temperature equal to the unperturbed one. *Figure 2.11* shows the domain and the various radiuses (Cosentino, et al., 2016).

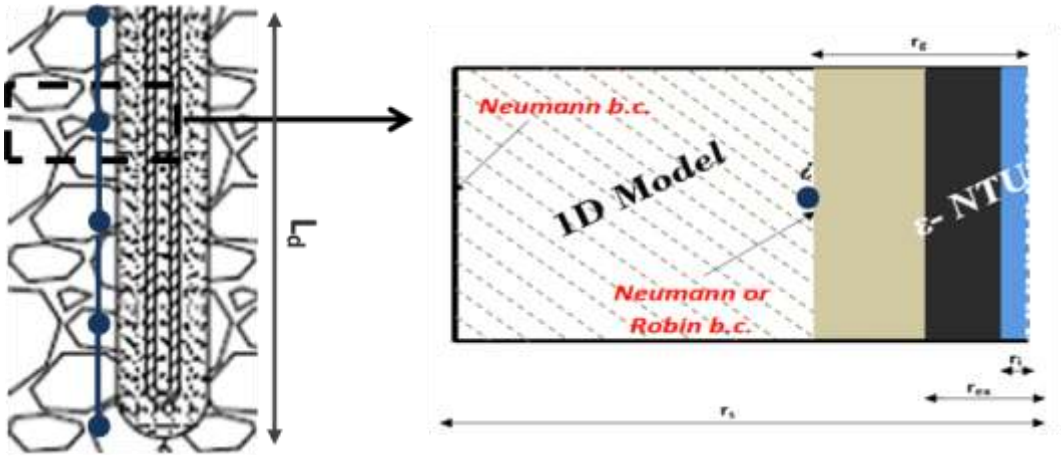

***Figure 2.11**: Schematic representation of the GHE* **(Cosentino, et al., 2016)**.

The temperature distribution in the soil around the vertical U-tube GHE is given by the solution of the energy equation (2.42) in 1-D cylindrical coordinates considering only the conductivity contribution:

$$\rho_s c_{ps} \frac{\partial T}{\partial t} = \frac{1}{r} \frac{\partial}{\partial r} (k_s r \frac{\partial T}{\partial r}) \tag{2.42}$$

where r is the radial coordinate while ρ_s, c_{ps} and k_s are the soil proprieties. Moreover, as illustrated in *Figure 2.11*, the U-tube GHE is discretized along its entire length (equal to twice the borehole depth) and Eq. 2.42 is solved for each element of the discretization. This approach allows one to account for the variation of the fluid temperature along the GHE. As a consequence of this assumption, heat transfer in the axial direction occurring at the bottom of the borehole is neglected, but this contribution is roughly less than 2.5% of the total (Cosentino, et al., 2016). Central finite difference is used to discretize the spatial derivatives while implicit backward Euler scheme is adopted for time integration.

The initial condition is given by undisturbed soil temperature:

$$T(0, r\ ) = T_s \tag{2.43}$$

On the inner surface ($r=r_g$) the boundary condition depends on the operation. Robin boundary condition is prescribed during the effective operation i.e. the energy requirement (eq. (2.44a)):

$$k_s \left.\frac{\partial T(t,r)}{\partial r}\right|_{r=r_g} = h_w (T - T_{av}) \tag{2.44a}$$

$$k_s \left.\frac{\partial T(t,r)}{\partial r}\right|_{r=r_g} = 0 \tag{2.44b}$$

where h_w is the convective heat transfer coefficient and the mean temperature T_{av} refer to the heat transfer fluid that flows in the vertical U-tube GHE.

In the case of no energy requirement the system is considered adiabatic and the relative boundary condition is given by Neumann boundary condition (eq. (2.44b))

On the outer surface ($r=r_s$), unperturbed temperature is prescribed (eq. (2.45)):

$$\mathrm{T}(\mathrm{t}, \mathrm{r_s}) = \mathrm{T_s} \tag{2.45}$$

Figure 2.11 also shows where boundary conditions are applied. The time distribution of soil temperature at borehole interface (node *i*) evaluated using Eq. 2.42. This value represents the source temperature, with infinity heat capacity, that exchanges heat with the inlet fluid in the borehole. Temporal evolution of outlet fluid temperature in borehole is calculated by relating the heat flux with a logarithmic temperature difference between ground (at radius r_s) and process fluid. This implies the fact that transient behaviour of the borehole is neglected, which is

a reasonable approach considering that the characteristic time here is of the order of few minutes and much smaller than the characteristic time in the ground and the timeline adopted for the analysis. Such approach allows one to reduce the computational efforts but it is not suitable for applications such as control system design (see for example [31]). The heat transfer coefficient referred to inner tube surface is expressed as (Cosentino, et al., 2016):

$$U = \frac{1}{\frac{1}{h_w} + ln(\frac{r_{ex}}{r_i})\frac{r_i}{k_p} + ln(\frac{r_g}{r_{ex}})\frac{r_i}{k_g} + ln(\frac{r_s}{r_g})\frac{r_i}{k_s}} \tag{2.46}$$

The model has been tested through a comparison between experimental data and calculated data with the model itself. The available experimental data refer to a plant with 51 geothermal boreholes of 100 m (double U De32 mm) divided into 3 circuits each one with 17 boreholes. The measurements relate to the inlet temperature and outlet temperature of the fluid circulating in the plant and the mass flow rates of each circuit (Cosentino, et al., 2016). These measures are available every hour during the winter heating season for the winter season 2012-2013. The thermal model has been used to calculate the temperature of the fluid at the outlet of one of the 17 boreholes belonging to the first circuit.

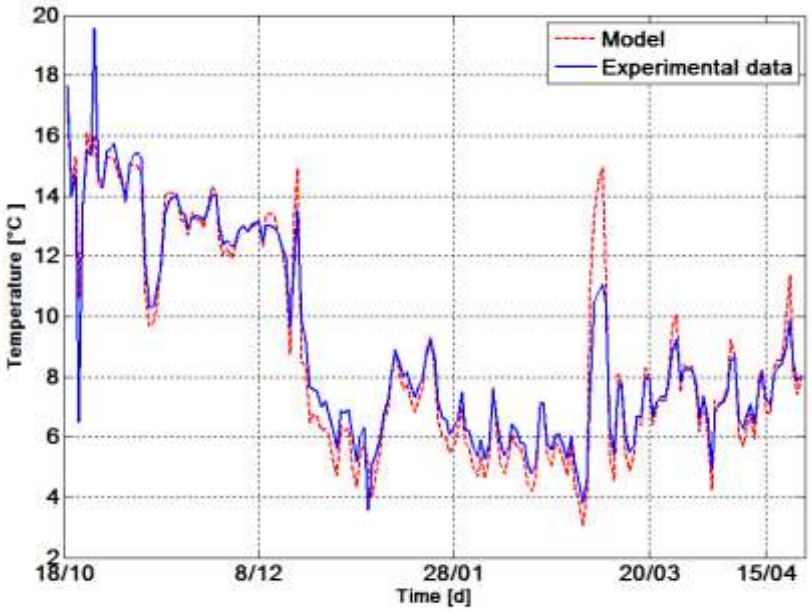

***Figure 2.12**: Temperature of the outlet fluid from the Boreholes* **(Cosentino, et al., 2016)**.

Figure 2.12 reports the data computed by the model and the experimental data. The comparison between the two curves confirms a good accuracy of the model.

The 1D model has been presented in two works (Cosentino, et al., June 25–27, 2014.; Cosentino, et al., 2016) for the optimization of the operating conditions of small GCHP systems constituted by two vertical boreholes. During the installation and the operation, these systems can be affected by anomalies such as ovalization, variations in the heat transfer between borehole and ground due to fouling, different installation depth etc. The selection of the optimal operation allows to reduce the irreversibilies caused by anomalies with a consequent benefit for the performance of these systems. The Entropy Generation Minimization is the selected method for this aim. A complete description of its application for the cases studied is available

in (Cosentino, et al., 2016; Cosentino, et al., June 25–27, 2014.). The proposed parametric analysis aims to identify the minimum of entropy generation in various scenario, considering the mass flow rate distribution between the two boreholes as the unconstrained operating variable. Results show that, when no design anomalies affect the system, the minimum entropy generation is achieved by a mass flow rate equally distributed between the two vertical U-tubes. In contrast, when design or operational anomalies occur, an optimal adjustment of the mass flow rate allows one recovering a significant amount of the exergy losses. As example, the results of EGM analysis in term of the optimal mass flow rate distribution (μ) between the two boreholes are reported in *Figure 2.13*.*Figure 2.13*(a) for different installation depths (λ is the ratio between the two boreholes).*Figure 2.13* (b) shows the corresponding entropy generation distinguish the different contributes (friction losses and heat transfer).

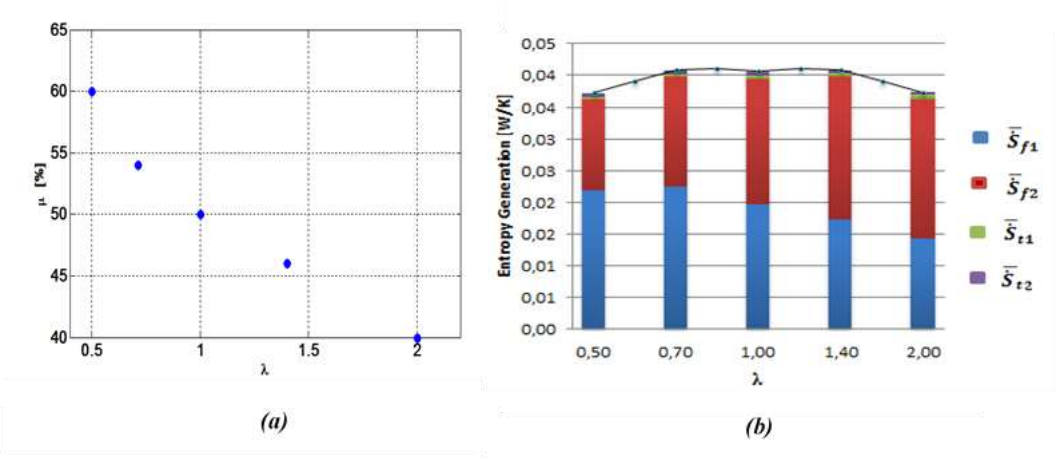

Figure 2.13: *Results of the optimization analysis for different installations depths; (a) the optimal mass flow rate distribution and (b) the relative entropy generation.*

For more details and for the other results, we refer the reader to (Cosentino, et al., June 25–27, 2014.; Cosentino, et al., 2016).

Chapter 3

Model Order Reduction

3.1 Introduction

Model order reduction (MOR) is a technique to simplify the simulation of dynamical systems described by differential equations. The idea is to project the original, high-dimensional, state-space onto a properly chosen low-dimensional subspace to arrive at a (much) smaller system having properties similar to the original system. The mainly diffused MOR techniques are meta-models, response surface method, and proper orthogonal decomposition (POD) (Buljak, 2012). All of these techniques are *a posteriori* reduction methods because they extract the essential information from a pre-existing full model of the interested problem and reduce it to a compact model that is properly the reduced order model. Consequentially computational costs are significantly reduced while preserving the accuracy. In order to mainly clarify this concept, the MOR techniques are comparable with the creation of a compressed file that occupies a reduced memory (see *Figure 3.1*).

Figure 3.1: *Analogy of MOR techniques.*

The application of POD has been proposed in several fields as the images processing (Rosenfeld & Kak, 2014) analysis of turbulent fluid and multiphase flows (Berkooz, et al., 1993; Brenner, et al., 2012), unsteady aerodynamic flows (Dowell, et al., 2006), unsteady two-dimensional flows (Bangia, et al., 1997) and many others. As modelling technique for complex energy systems, POD has been applied to model the transient behaviour of a sensible thermal energy storage system (Sciacovelli, 2016), to the optimal operation of a district heating network both in a parametric analysis investigating various operating conditions (Cosentino, et al., 2014) and in an optimization algorithm for the minimization of the pumping costs (Cosentino, et al., 2015). POD has also been applied to a wildfire prediction model for the investigation of fire propagation over a flat ground (Guelpa, et al., 2016).

In this thesis, the POD method based on *snapshots* is proposed to modelling complex energy systems for their optimal design, operation and control. The modelling methodology consist in the application of the MOR techniques to non-dimensional form of equations that describe the studied energy systems. This allows to obtain flexible, computationally efficient and accurate reduced models.

In this chapter, after a general description of the POD method, its applications to tunnels ventilation and to underground thermal energy storage systems are discussed.

3.2 POD technique

POD model is constructed following the method of snapshots, as proposed by Sirovich (Sirovich, 1987), for determining the coefficients of a "proper" eigenfunctions expansion. The method, provides a parametric fit of a set of given multidimensional data by constructing an appropriate expansion series and its coefficients. POD extracts both the interpolating functions and the coefficients from the information contained in the data set. The procedure explained in this sections, refers to transient systems which proprieties changes with the time.

A snapshot is a vector $\boldsymbol{u}$ of *M* relevant physical quantities that identify the behaviour of the system (i.e. temperature, pressure, concentration, etc.) obtained by experiment or simulation at the time instant t_i.

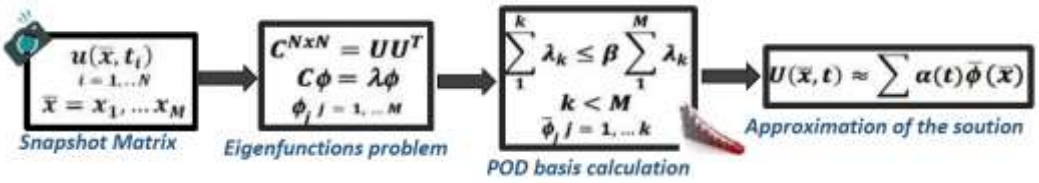

Figure 3.2: *POD procedure.*

The collection of snapshots for *N* time steps, is stored in the so called *snapshot matrix* $\boldsymbol{U_{MxN}}$. POD aims to construct the set of orthonormal vectors, resembling the original snapshots matrix in an optimal way.

The covariance matrix ***C*** of the snapshot matrix, is used to solve an eigenvalues and eigenvectors problems as defined:

$$C\phi = \lambda\phi \tag{3.1}$$

where $\boldsymbol{\phi_j}\ j = 1, \ldots M$ is the eigenvector and λ_j the corresponding eigenvalue. The eigenvalues are first ranked and then pruned by discarding those that are negligible by some norm with respect to the others:

$$\sum_1^k \lambda_k \leq \beta \sum_1^M \lambda_k \tag{3.2}$$

This is achieved by applying an "energy" method based on a linear algebra theorem which states that the energy of the k^{th} mode scales with the corresponding eigenvalue λ_k. The truncation of the POD basis is accomplished by deciding which fraction β of the global energy we wish to include in further calculations, and this leads to the search for the mode number K that fulfils the Eq. (3.2).

The resulting truncated POD $\bar{\boldsymbol{\Phi}}$ basis consists of $K<M$ vectors of length N and it can be demonstrated that there is no other orthogonal basis that transfers more energy within the same number of modes (Ostrowsky, et al., 2005). An arbitrary snapshot $U^a(\bar{x},t_i)$ at a certain time instant can be approximated as:

$$U^a(\bar{x}, t_i) \approx \bar{\Phi}(\bar{x}) \cdot \bar{\alpha}^a(t_i) \tag{3.3}$$

where $\bar{\alpha}^a$ is the amplitude vector associated with snapshot $\boldsymbol{U^a}$ and the corresponding amplitude matrix $\bar{\boldsymbol{A}}$ can be calculated as:

$$\bar{A} = \bar{\Phi}^T \cdot U \tag{3.4}$$

The original snapshots matrix is given by the following approximations:

$$U(\bar{x}, t) \approx \sum_{i=1}^{K} \overline{\Phi}(\bar{x}) \cdot \bar{\alpha}^{a}(t_i) \tag{3.5}$$

3.3 Application of POD technique to the design and operation of sanitary ventilation in the Padornelo tunnel

The control of air quality in infrastructures such as road tunnels, mines and subways is crucial both during the excavation phase and during the effective operation. In particular, the construction of underground infrastructures is essential yet dangerous activities. Appropriate security measures for workers must be adopted because they work under reduced light conditions, with difficult or limited access and egress and with the potential for exposure to air contaminants. NOx, CO, exhausted from passing vehicles, silica dust, diesel particulate, fog and fumes are due to the working machines, to drilling and explosions stages. The concentration of these contaminants can be effectively reduced by using various control technologies along with adequate air quantities and proper ventilation method. The installation of sensors allows to measure the pollutants concentration and to send this information to an opportune control algorithm for the ventilation system. The scope of this latter is to ensure a good quality of air according with the regulations and to minimize electrical power consumption for cost effectiveness. The most used control algorithm for the ventilation of underground infrastructure is the *Fuzzy Logic Control* (FLC). Literature offers several applications and examples of FLC. A control method based on the prediction of a number of jet-fans and the fuzzy control of pollutant levels has been proposed for longitudinal ventilation of road tunnels (Bogdan, et al., 2008). A fuzzy logic control model for tunnel ventilation has been coupled with a dynamic equation describing the concentration of air

pollution (Chen, et al., 1998). A genetic algorithm with the aim to maintain an adequate level of the pollutants and to minimize the power consumption has been integrated in FLC (Chu, et al., 2008).

The application proposed in this thesis regards the development of a FLG for real tunnel during the excavation phase with the aim to ensure an acceptable NO_x level and to minimize the electricity costs. The descriptive part of the FLC is not included in this work. We refer the reader to (Ragot & Lamotte, 1993) for more details. The POD method is applied to model pollutant concentration in order to optimize the crisps value depending on the tunnel dimensions.

3.3.1 Tunnel description and POD model

The FLC algorithm has been developed for the Padornelo tunnel in the high speed rail line Madrid-Galicia (Ferrovial, 2017,). The research project *Etúnel-aire* proposed by *Ferrovial* is focused on the improvement of the safety and health conditions of workers in underground infrastructures of new construction (Ferrovial Agroman, 2013). The main steps of this project are:

1. Installation of gas sensors to monitor the air quality;

2. Development of a technology that allows the detection and dilution of the pollutant automatically.

3. Development of an optimization control algorithm that regulates the system velocity according to air quality parameters and energy efficiency criteria.

4. Installation and test of the control algorithm in the Padornelo tunnel.

5. Generalization of the control algorithm for further application to any other underground construction (Ferrovial Agroman, 2013).

The limit for pollutant as CO, NO_x, CO_2, SH_2 and SO_2 are established by Spanish and European regulations for mines (Ferrovial Agroman, 2013).

Figure 3.3: *Excavation phase of the Padornelo Tunnel.*

During the excavation, the pollutants are diluted thanks the air flow of the ventilation duct (see *Figure 3.3*). The proposed model for studying pollutants has been developed for NO_x but it can be extended to any others. The mass transport equation for NOx concentration is described by eq. (2.21) that in non-dimensional form becomes:

$$\frac{\partial C^*}{\partial t^*} = \frac{1}{Pe}\frac{\partial^2 C^*}{\partial x^{*2}} - \frac{\partial C^*}{\partial x^*} + S_p{}^* \tag{3.6}$$

where:

-$C^* = \frac{C - C_{min}}{C_{max} - C_{min}}$ is the non-dimensional form of the concentration, C_{max}-C_{min} is the range concentration from 5 ppm to 50 ppm;

-$x^* = \frac{x}{L}$ is the non-dimensional form of longitudinal coordinate with L corresponding to the tunnel length;

-$t^* = t\frac{u}{L}$ is the non-dimensional form of the time with u corresponding to the longitudinal air velocity due to the forced air flow;

-*Pe* is the Peclet numbers;

-$S_p{}^* = \frac{S_p * L}{\Delta C * u}$ is the non-dimensional form of the pollutants source.

The emission sources are related to the construction phases (drilling, excavation, explosion etc.) and the used machines (loaders, excavators, trucks etc.) during a typical working day. They have been approximated as functions of space (Gaussian distribution) and time (step or sinusoidal trend).

The initial condition is given by average NO_x concentration in the air (5 ppm):

$$C^*(0, x^*) = C^*{}_{in} \tag{3.7}$$

where $C^*{}_{in} = \frac{C_{air} - C_{min}}{C_{max} - C_{min}}$

On the external portal (x=0) the Direchlet b.c. is prescribed (eq. (3.8)) while on the working surface (x=L), the adiabatic condition is prescribed (eq. (3.9)).

$$C^*|_{x=0} = C_{air}{}^* \tag{3.8}$$

$$\left.\frac{\partial C^*}{\partial x^*}\right|_{x=L} = 0 \tag{3.9}$$

Central finite difference is used to discretize spatial derivatives while implicit backward Euler scheme is adopted for time integration.

The 1D model has been validated with experimental measurements given by NO_x sensors located every 130 m when the tunnel excavation was at 500 m. The

comparison is plotted in *Figure 3.4* considering the average value of concentration during a typical working day.

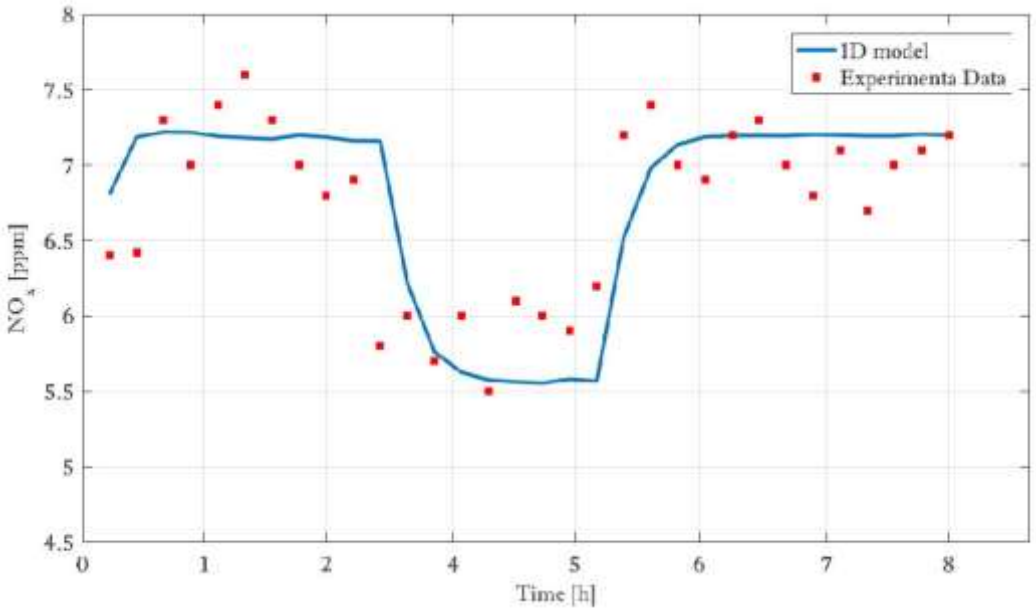

Figure 3.4: *Comparison of 1D model and experimental measurements.*

The POD method is applied on the snapshots matrix that is obtained simulating a working day of 8 hours with eq. (3.6).The comparison between the full model and the reduce model during two different excavation phases, are plotted in *Figure 3.5*.

.

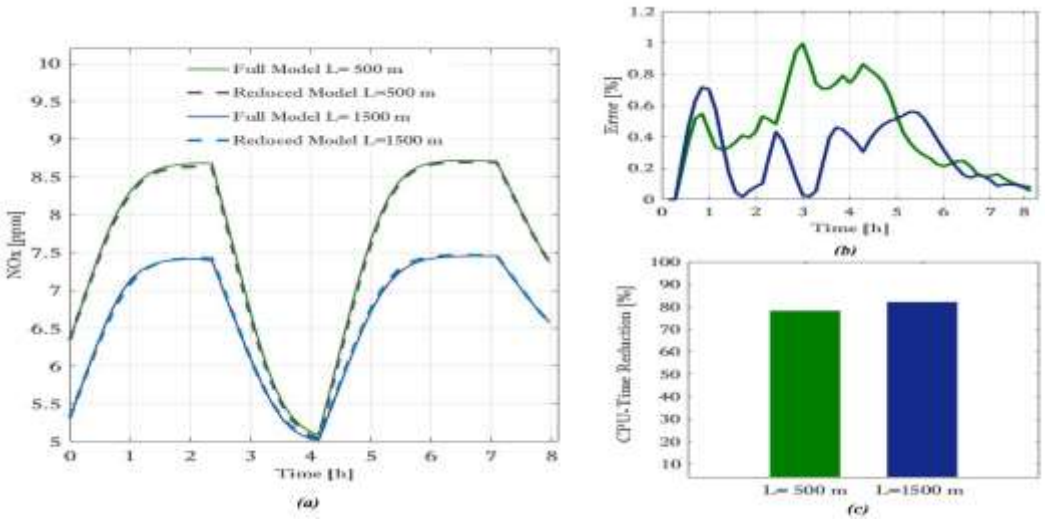

Figure 3.5: *Full model VS POD model for two tunnel lengths: (a) Average NOx diffusion simulation; (b) Relative error between the full and the reduced model; (c) CPU-Time reduction respects with the full model.*

The flexibility of the POD model is confirmed by its application to different excavation phases i.e. 500 m and 1500 m of length (*Figure 3.5*(a)). The development of the percentage error maintains low and negligible for all the simulation time (*Figure 3.5*(b)). The reduction of CPU-time is significant especially in larger CFD domain where it achieves the 82% (*Figure 3.5*(c)).

3.3.2 Fuzzy Logic Control for the fans regulation

The proposed FLC algorithm is schematically reported in *Figure 3.6*. The *linguistic variables* (Ragot & Lamotte, 1993) of the two inputs are the NOx concentration measured by sensors and the time of the last fan regulation. This latter has been chosen to prevent abrupt variations of the fans in short time and to take into account the transients of NOx diffusion. The *membership functions* (Ragot & Lamotte, 1993) selected for the inputs are Gaussian. The *linguistic variables* of the output is the fan velocity which *membership functions* is triangular.

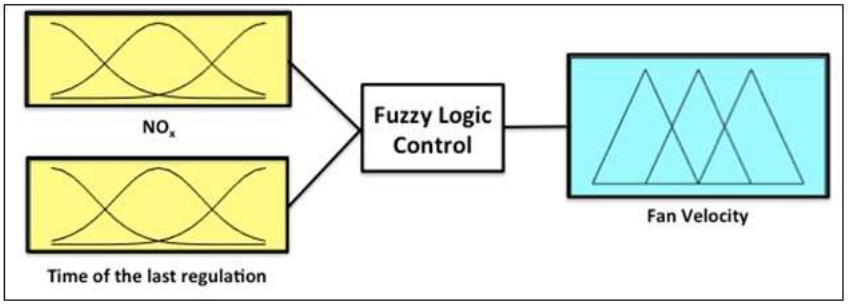

Figure 3.6: *FLC algorithm for the studied case.*

The definition of *crisp values* is based on optimization process to find the minimum of the following objective function:

$$min\big(\boldsymbol{F}(u)\big) = \min\big(\Delta P_{tot}(u) + r * P(C_{NO_x}(u))\big) \tag{3.10}$$

where ΔP_{tot} the total pressure losses in the tunnel and in the ventilation duct and it is directly linked with the electricity consumptions; *r* is the penalty coefficient and $P\left(C_{NO_x}(u)\right) = \max\left(0; C_{NO_x}(u)\right)^2$ is the penalty function in the quadratic form. The longitudinal air velocity *u* due to fan is the decision variable which variability range is imposed by the minimum and the maximum fan velocity. The optimization is performed simulation the NO_x diffusion with POD model. In order to adjust the crisp values depending on the tunnel size, a parametric analysis has been proposed exploring different cross sections and tunnel lengths. For each design equation 3.10 coupled with the POD model, has been solved for the selections of the best crisp values. An example of the results given by the parametric analysis in shown in *Figure 3.7* for a crisp value.

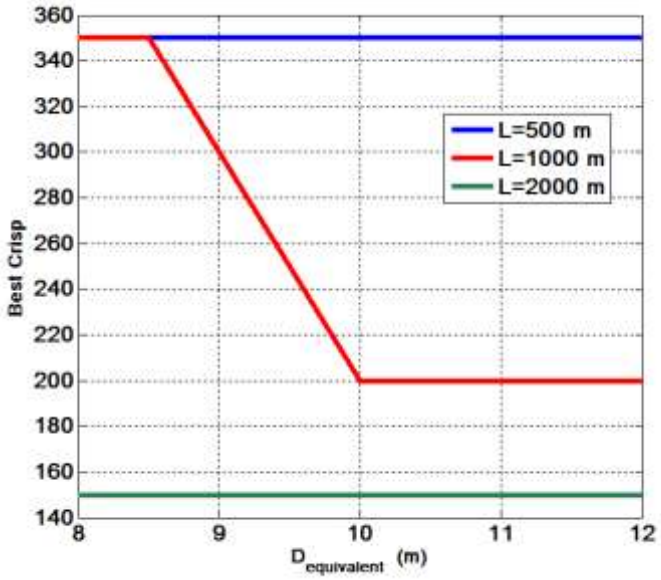

***Figure 3.7**: Characteristic map for the selection of crisp value.*

This approach allows to define a characteristic map for the application of the FLC for different tunnel designs.

A comparison between the fan operation at constant velocity (1052 rpm) and the operation regulated by the FLC algorithm, is shown in *Figure 3.8* for the excavation phase at 1500 m of length. The simulation has been performed for a typical working day. Assuming a fan efficiency of about 72%, the energy consumption is about 258 kWh in the case of operation at constant velocity. The use of the FLC algorithm allows to reduce it of about 24% maintaining NO_x within the acceptable limits for human health.

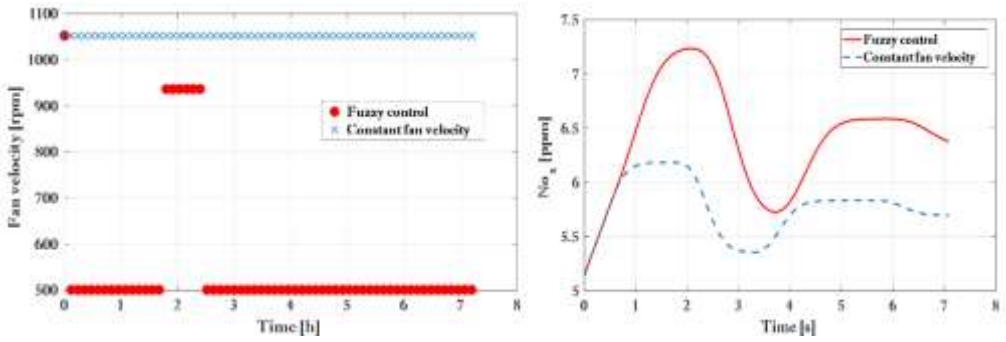

(a) ***(b)***

Figure 3.8*: Fan velocity (a) and NO_x production (b) during a work day with and without Fuzzy control.*

The proposed algorithm has been installed in the Padornelo tunnel. Several tests have been conducted confirming an optimal control of the air quality with a significant reduction of the energy consumptions.

3.4 Application of POD technique to the design and operation of BTES

Boreholes thermal energy storage (BTES) systems are a particular application of underground thermal energy storage (UTES) where heat is stored in dry rocks by circulating a fluid through a borehole. The common BTESs are low temperature systems, usually linked with a ground source heat pump in which the working fluid absorbs heat circulating in the borehole heat exchanger (Wu, et al., 2014; Zhai & Yang, 2011).Recently, various analytical and numerical studies have been conducted about BTES systems, mostly concerning with the modelling of pipe configurations, investigation of heat transfer characteristics, thermal response tests

of different types of boreholes, materials to increase the thermal conductivity etc. (Zen., et al., 2002; Bernier, 1986; Florides & Kalogirou, 2007; Sharqawy, et al., 2009; Zhai & Yang, 2011) The performance of these systems is affected by the configurations of the boreholes and the temperature of ground at which the heat is stored. Several studies about the design and the performance of BTES are based on energetic and exergetic analysis for determining improvement potentials of BTES and for studying the effects of the operating conditions on energy and exergy efficiencies of these plants on order to maximize the performance (Ozgener, et al., 2005; Kizilkan & Dincer, 2015; Lundh & Dalenback, 2008; Sibbitt, et al., 2012). Most of these works do not present a specific reference to the charge stage required by BTES systems that can represent an issue if it is too long. In fact BTES systems with high performances at high temperature can present a drawback in the case of large charging time before achieving the design temperature (Lundh & Dalenback, 2008). This disadvantage can be reduced by selecting an optimal design that ensures a high value of the efficiency. However BTES systems with high efficiency are affected by another drawback linked with the large investment costs of the borehole exchangers (materials and drilling works) and of additional ground works (excavation and refilling). The high installation expense of borehole heat exchangers and complex excavation work are the main obstruction to development to some extent. The needed to have systems with high performance and reduced costs is on the basis of the modern energy systems (Bejan, et al., 1996)

The increase in efficiency and the decrease of investment costs are two conflicting objectives that must be considered in the design stage to select the best configuration. The thermoeconomic approach represents a tool to account for both aspects and obtain an appropriate combination of exergetic and economic analysis (Tsatsaronis, 1993). Thermoeconomics allows to rationally assess costs depending on the quality (exergy) of the energy flows that are exchanged. In the field of the

thermal storage, the thermoeconomic analysis has been applied for describing the complete charging-discharging cycle of sensible heat, for researching the minimum total cost of owning, maintaining, and operating (Domańsk & Fellah, 1998), for studying the irreversible losses in a sensible heat-storage system (Zubair, et al., 1993). The results have shown the advantages of adopting such an approach for designing and operating thermal energy storage units.

We propose a multi-objective optimization (MOP) strategy for the optimal design of a BTES system supplied by a district heating network. Three different stages of operation can be distinguished: charging time to achieve the design temperature in the ground; discharging time i.e. the effective operation to supply energy demand of domestic users; recharging time between two winter seasons. The operation of the plant during a long period has been analyzed using the reduced model.

Once the system is designed, the selection of the optimal operation allows an improvement in the storage efficiency and an economic profit for the cogeneration plant. The POD model has been implemented in an optimization algorithm in order to discover the optimal times for storing and retrieving additional thermal energy during the operation.

3.4.1 Description of BTES system and POD model

Each borehole is a single U-tube, in polyethylene with an inner diameter of 0.029 m and an outer diameter of 0.033 m and k=0.33 W/(m K). The borehole is in saturated sand with a diameter of 0.1 m and k=1.8 W/(m K). The mass flow rate in each borehole is 0.9 kg/s. The soil has been considered with a thermal conductivity of 2.5 W/(m K). For the charge and recharge stages, the inlet water has been considered at 90°C, from district heating network.

The design of BTES system is defined by the pitch between two boreholes and the installation depth as shown in *Figure 3.9*(a). The layout of the boreholes for the installation is in concentric circles in order to maintain constant the pitch between the tubes (see *Figure 3.9*(b)).

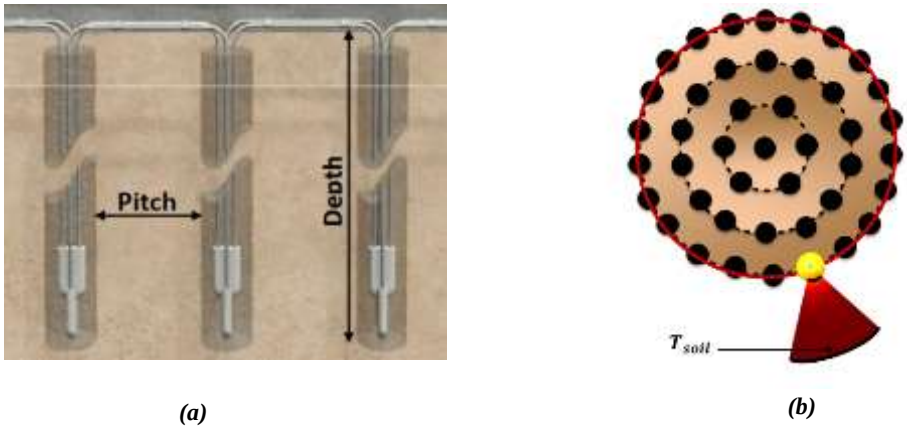

***Figure 3.9**: BTES system (a) design variable and (b) layout.*

Each borehole is modelled as explained in Section 2.4 and the heat transfer with the soil is studied with Eq. (2.42), that in non-dimensional form becomes:

$$\frac{\partial \theta}{\partial t^*} = \frac{\partial^2 \theta}{\partial r^{*2}} + \frac{1}{r^*}\frac{\partial \theta}{\partial r^*} \tag{3.11}$$

where $\theta = \frac{T - T_{min}}{T_{max} - T_{min}}$ is the non-dimensional form of the temperature with T_{max} - T_{min} representing the operating temperatures range from 90°C to 15°C, $r^* = \frac{r}{p}$ is the non-dimensional form of radial coordinate and $t^* = t\frac{\alpha}{p^2}$ of the time. The parameter

p represent the pitch between two boreholes and α is the diffusion coefficient. The initial condition is given by average soil temperature in the mid-season (15°C):

$$\vartheta(0, r^*) = \theta_{in} \tag{3.12}$$

where $\theta_{in} = \frac{T_{in} - T_{min}}{T_{max} - T_{min}}$

On the inner surface ($r=r_g$) the Robin (eq. (3.13)) or Neumann (eq. (3.14)) boundary condition is considered depending of the operation condition. On the outer surface ($r=r_s$), the adiabatic condition is prescribed.

$$\left(1 + \frac{h_w A}{2\dot{m} c_p}\right) \frac{d\theta}{dr^*} = Bi(\theta - \vartheta_{bc}) \tag{3.13}$$

$$\frac{d\theta}{dr^*} = 0 \tag{3.14}$$

where A is the exchange surface, Bi the *Biot* number and $\vartheta_{bc} = \frac{T_{av} - T_{min}}{T_{max} - T_{min}}$ with T_{av} equal to the mean temperature of the heat transfer fluid that flows in the vertical U-tube.

In order to generalize as much as possible the application of POD, Neumann b.c. is prescribed in a form of Robin b.c. with a convective heat transfer coefficient $h_w = 10^{-6}$ W/m^2 K.

The boreholes installed in the external perimeter cannot be assumed as adiabatic. A 2-D CFD model is used to model the external boreholes and to estimate the correction factor to apply on the thermal power produced by these latters. The 2-D CFD model presents a new external radius so far from the previous one on which the undisturbed soil temperature is prescribed as b.c. (*Figure 3.9*(b)). The correction factor obtained simulation the operation is 0.19 and allows analyzing the system with the 1-D model.

Central finite difference is used to discretize spatial derivatives while implicit backward Euler scheme is adopted for time integration.

The POD method is applied on the snapshots matrix that is obtained simulating a charge stage of 28 days with eq. (3.11). Six eigenvalues has been identified on the basis of eq. (3.2). The normalized POD functions that appears in eq. (3.5) are plotted in *Figure 3.10*.

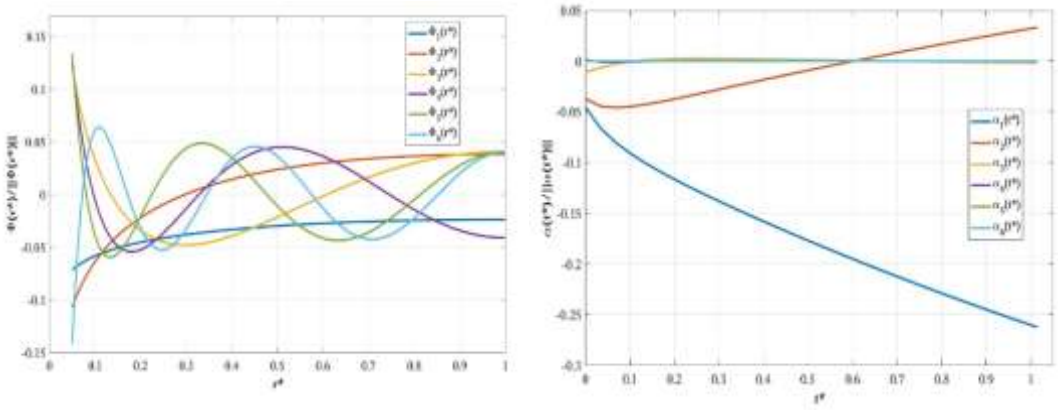

Figure 3.10: *Normalized POD functions.*

A comparison between the full model, previously validated in section 2.4., and the reduced model (*Figure 3.11*) a different time steps, shows the accuracy of the POD model which presents an average percentage error less than 0.01% and a reduction of the CPU time of about 99.5%.

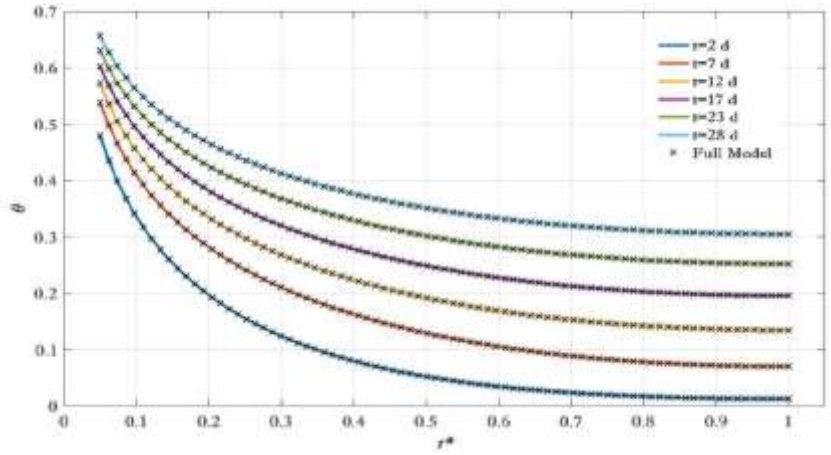

Figure 3.11: *Simulation of BTE systems with POD model and full model.*

3.4.2 Multi-objective optimization for the BTES system design

The multi-objective optimization (MOP) strategy starts from results of a previous energy, exergy and thermoeconomic analysis (Cosentino, et al., 2015; Cosentino, et al., November 13-19, 2015,). An energy and exergy parametric analysis has been proposed in order to investigate the optimal time required by BTES to charge the ground to the design temperature and to maintain the internal energy in the ground constant after each year (Cosentino, et al., 2015). The parametric study has been performed in different operating conditions as different installation depths and different distances between boreholes. The range of pitches is 3-7 m with a space step of 1 and the range of installation depths is 25-125 m with a space step of 25. The various combinations of pitch-depth selected for the analysis result in 25 different BTES configurations, each one with a proper length and a proper thermal extraction capacity. Results have shown that the optimal charging time significantly depends on the design parameters. It varies from 30 to 86 days for boreholes with pitch of 3 m at the installation depth gradually increasing. The optimal charging

time reaches the value of 994 days for the design with deepest and furthest boreholes. A summer recharging time of about 20 days is necessary for all designs to guarantee constant internal energy in the soil between two equal operation seasons (Cosentino, et al., 2015). *Figure 3.12* clarifies the concept of constant internal energy showing two different operating conditions for the same system in term of recharging time. The first operating condition (dashed blue line) is performed with a non-optimal recharge stage with a consequent internal energy U_2 (at the end of the second year of operation) lower than U_1. In the second operating condition (red line), the optimal recharging time ensures an internal energy U'_2 approximately equal to that of the previous year.

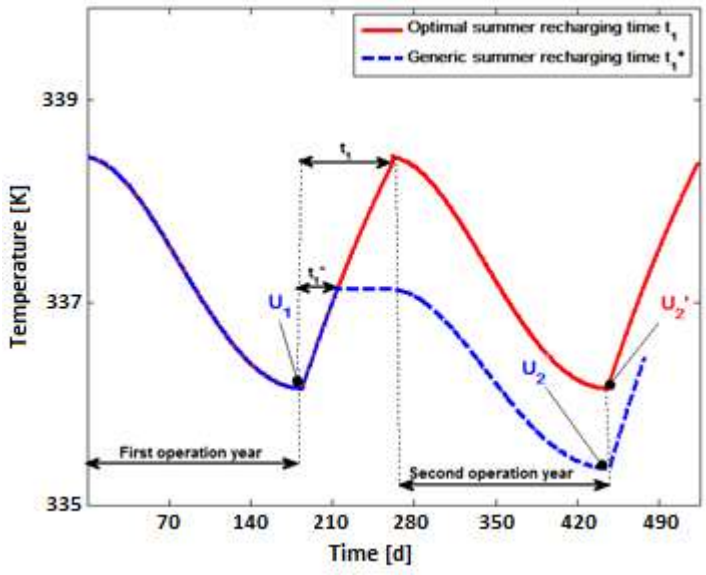

Figure 3.12: *Average Ground Temperature with two different summer recharging time* **(Cosentino, et al., 2015)**.

Energy and exergy efficiencies have been calculated considering 10 years and 20 years of operation. The exergy efficiency or second law efficiency has been evaluated according with the following equation:

$$\varepsilon_{II} = \frac{\sum_{i=1}^{N_{seasons}} Ex_{Ext,i}}{Ex_{I,Ch} + \sum_{i=1}^{N_{season}-1} Ex_{\mathrm{Re}ch,i}} \tag{3.15}$$

where $Ex_{Ext,i}$ is exergy extracted at each season of operation, $Ex_{I,Ch}$ is the exergy associated to the first charge stage (needed to achieved the design temperature in the ground) and $Ex_{Rech,i}$ is the exergy associated to each recharge stage (needed to maintain constant the internal energy in the ground between two consecutive seasons of operation).

For each design both efficiencies increase with increasing operation time. This means that the amount of energetic (or exergergetic) resource stored in the charge stage is used and so exploited during the operation. A system with shallow and near boreholes is characterized by an efficiency of about 36% after 10 years and about 40% after 20 years of operation. These values decrease with increasing depth and pitch up to about 15% after 20 operation years (Cosentino, et al., 2015). These results allow to conclude that BTES plants with small size result more advantage in term of charging time and efficiency, especially for a long period of plant operation. The efficiency value for long operation period and the relative charging time can be considered two new indicators to take into account for selecting the type of plant during the design. The logic to maintain the internal energy in the ground constant during the years of operation can also represented a tool of optimization that maximizes the efficiency.

This approach needs to be combined with an economic analysis. Installation costs depend on the number of perforations more than depth. From an economic point of view, this would lead to prefer a reduced number of boreholes but deeper

contrasting the parametric analysis results. In addition, installation of boreholes at large depth and small pitch is technically difficult to perform, with high risk of drill crossing (Cosentino, et al., 2015).

For these reasons, the thermoeconomic analysis has been developed in (Cosentino, et al., November 13-19, 2015,) for the selections of BTES configuration. Boreholes are designed to charge the ground to the design temperature and to supply heat to an underfloor heating system directly connected with the users without any heat pump. The underfloor heating system provides a constant thermal power of 100 kW through water that flows in the BTES at 35°C until to achieve 38 °C. The same configurations of (Cosentino, et al., 2015) are explored but two possible levels of storage temperature (45°C and 55°C) are proposed in order to investigate about the influence of the ground temperature on the performance (Cosentino, et al., November 13-19, 2015,). The exergy analysis is needed to compare the two scenarios at different temperatures of operation. Also in this case, for each configuration the charging time is evaluated to ensure a constant internal energy of the ground during the operation and the first and second law efficiencies are calculated for 20 years of operation. The efficiency is resulted higher for installation in reduced volume of the ground. Furthermore the efficiencies have proved to be greater in the case of storage and installation of the plant in the ground at higher temperature (55°C) (Cosentino, et al., November 13-19, 2015,). The trend of unit exergetic costs has confirmed the results obtained by the energy and exergy analysis i.e the most efficient configurations are characterized by the lower value of the exergetic cost. The unit exergoeconomic cost is resulted high for the most performance configurations and it seems to be particularly influenced by the unit exergoeconomic cost of the resource (Cosentino, et al., November 13-19, 2015,). Although storing energy in larger ground volume needs a reduced number of boreholes, the increase of the exergetic resource that follows, influences so the unit

cost as causes its increase. The unit exergoeconomic cost has turned out to be lower in the case of storage at high temperature. This last result suggests that a better exploitation of the energy stored in the charge stage occurs when the storage is at higher temperature. Although the storage at higher temperature involves longer charging time and higher initial costs, these are amortized in the years of operation (Cosentino, et al., November 13-19, 2015,).

The proposed methodology for the design of BTES system has been presented at ASME 2015 conference and it has been awarded with the *prestigious ASME Edward F. Obert Award*.

The MOP considers the results presented in (Cosentino, et al., November 13-19, 2015,) to define the competing objectives, the decision variables and the relative constrains. The unit exergoeconomic cost c_p and the exergetic efficiency ε_{II} are selected as function to optimize. The productive structures in term of resources and products are explained in detail in (Cosentino, et al., November 13-19, 2015,). The decision variables are the design parameters i.e. the pitch p and the installation depth L_d. The MOP problem can be summarized as follows:

$$min\left(\boldsymbol{F}(p, L_d)\right) = \min\left(\boldsymbol{c_p}(p, L_d), -\boldsymbol{\varepsilon_{II}}(p, L_d)\right) \tag{3.16}$$

$$\textit{subject to} \begin{cases} 3m \leq\ p \leq 6m \\ 100m \leq\ L_d \leq 125m \end{cases}$$

The multi-objective genetic algorithm function *gamultiobj* of *Matlab* tool has been used to solve Eq. (3.16).

For each possible design solution (p, L_d) the *population* given by Matlab function, the unit exergoeconomic cost c_p and the exergetic efficiency ε_{II} (*fitness functions*)

are evaluated according with a complex procedure which schematic representation is reported by *Figure 3.13*.

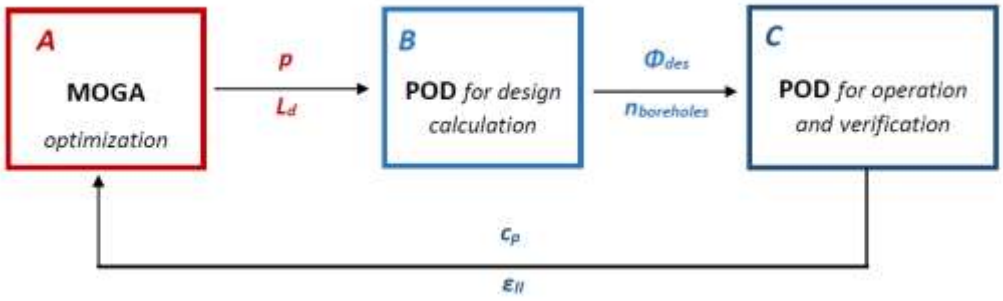

Figure 3.13: *Multi-objective strategy with POD modelling.*

Each design point (p and L_d) is characterized by a proper heating extraction capacity and by the corresponding number of boreholes. In order to evaluate them, an iterative process (block *B*) has been proposed, as illustrated in *Figure 3.14*.

The design condition corresponds to minimum external temperature in the winter season, during which the thermal power is required for 18 hours. For a possible plant located in Turin, the minimum design temperature is -8°C and the indoor design temperature is 20°C.

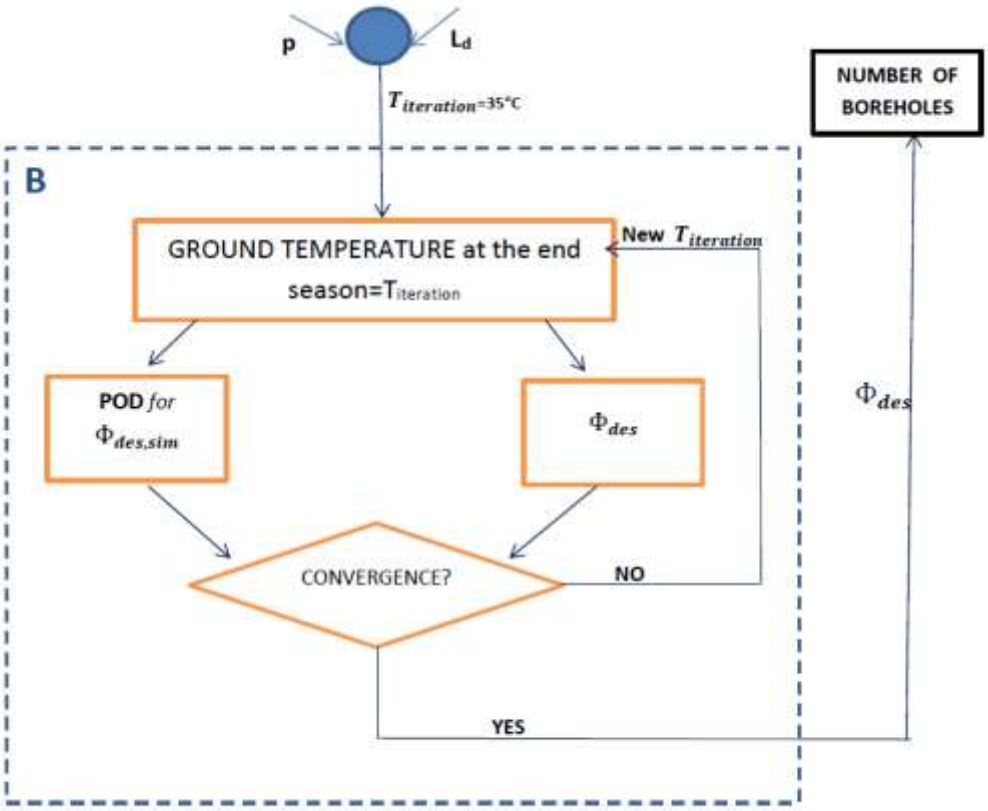

Figure 3.14: *Iterative process to the thermal power calculation in the design condition.*

Assuming that the design condition occurs exactly at mid-season, the heating extraction capacity Φ_{des}can be calculated using the degree-day theory (Cosentino, et al., November 13-19, 2015,) and compared with the heating extraction capacity $\Phi_{des,sim}$ given by the POD model.

The output of the procedure *B* is the input for simulating the operation (block *C*) with the reduced model (see *Figure 3.15*). The energy analysis downstream the discharge stage allows establishing if the configuration is suitable for providing the daily energy in the winter season. The energy demand is calculated according with

the average daily outside temperature. A configuration is unsuitable if it requires more than 24 h to satisfy the heating requirement of one day.

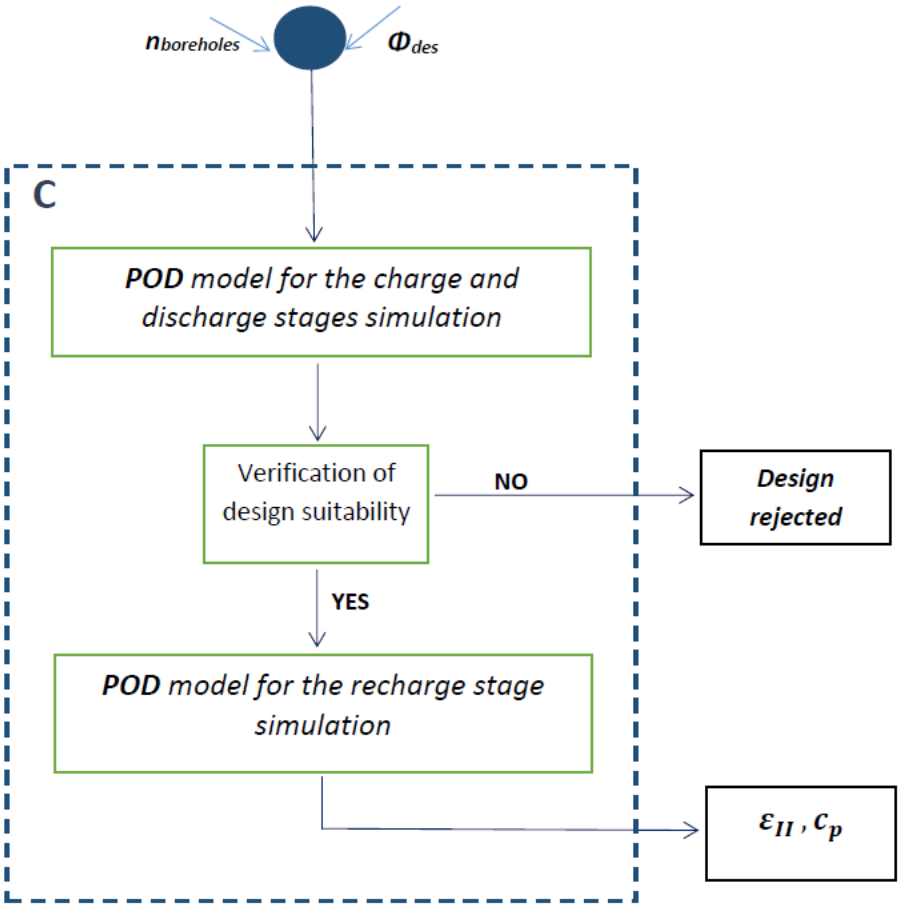

Figure 3.15: *Verification and simulation of BTES operation with POD model.*

For the suitable configurations, the charging time for bringing the design ground temperature and the relative amount of energy and exergy storage in that period, are evaluated. A constant internal energy between two consecutive seasons of

operation can be guaranteed thanks to a recharging stage at the end of the winter season. The recharge is obtained using the district heating network. The evaluation of recharging time and relative energy and exergy stored are performed considering that the two consecutive heating seasons are the same.

For each configuration, the second-law efficiency and the unit exergoeconomic cost are evaluated considering 20 operation years, under the hypothesis that the winter seasons repeat themselves without changing.

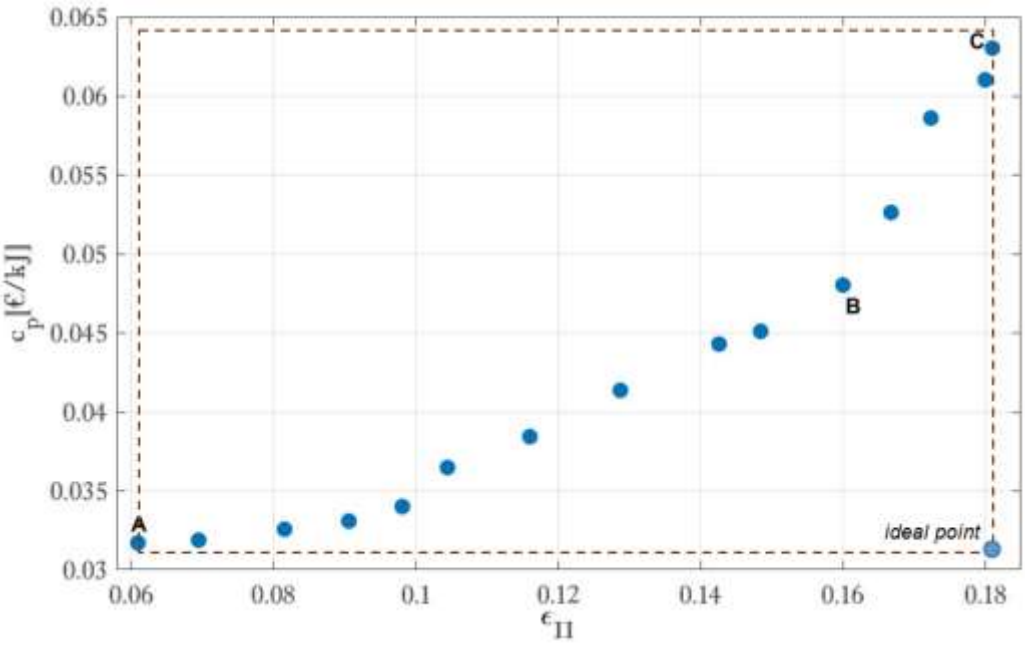

Figure 3.16: *Pareto front of MOGA optimization for the BTES system.*

The Pareto front of the MOP strategy is reported in *Figure 3.16*. The Pareto front is the objective space where the values of objective functions related to each optimal solution are plotted. A solution is Pareto-optimal if it is not dominated by any other

solution in decision variable space and the set of all these solutions is called the Pareto-optimal or non-dominated set.

The unit exergoeconomic cost increases moderately of about 52.2% as the exergecit efficiency increases of about 38.6%. As shown in *Figure 3.16*, the maximum exergetic efficiency exists at design point *C* (18.2%), which the greatest exergoeconomic cost corresponds (0.064 €/kJ). On the other hand, the minimum value for the c_p occurs at design point *A* which is about 0.031 €/kJ. Design point *A* is the optimal situation when the unit exergoeconomic cost is the only objective function, while design point *C* is the optimum point when exergetic efficiency is the only objective function. In multi-objective optimization, a process of decision-making for selection of the final optimal solution from the available solutions is required. The process of decision-making is usually performed with the aid of a hypothetical point in *Figure 3.16*(the ideal point), at which both objectives have their optimal values independent of the other objectives. The ideal point is not a solution located on the Pareto frontier because it is impossible to have both objectives at their optimum point simultaneously, as shown in *Figure 3.16*. The closest point of the Pareto frontier to the ideal point might be considered as a desirable final solution.

Note that in multi-objective optimization and the Pareto solution, each point is a optimized point. Therefore, the selection of the optimum solution depends on the preferences and criteria of the decision maker, suggesting that each may select a different point as for the optimum solution depending on the needs. A good trade off in term of efficiency and cost could be given by the design point B for which p=3 m and L_d = 120 m and the correspondent efficiency and unitexergoeconomic cost are 16% and 0.048 €/kJ respectively.

3.4.3 Optimization of the BTES system operation

The operating conditions of this system is mainly subjected to the thermal energy demand of buildings, to the state of charge, to the availability of additional energy to store and to the energy market. An optimization algorithm has been proposed for a real time optimization of the BTES system operation supplied by a cogeneration plant. A schematic representation of the procedure is reported in *Figure 3.17*.

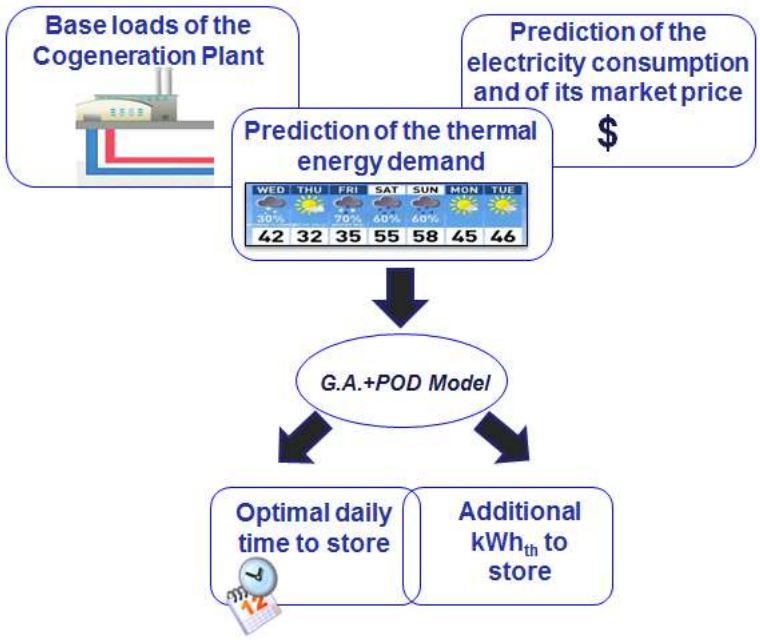

Figure 3.17: *Optimization algorithm per the BTES system operation supplied by a cogeneration plant.*

The base loads of the cogeneration plant, the prediction of electricity and thermal energy consumptions (for example blue and red line of *Figure 3.18*) and the

prediction of the electricity market price (*Figure 3.18)* are the input for the proposed optimization strategy. The genetic algorithm is used to discover the optimal times for storing and retrieving additional thermal energy during the operation, eventually changing the base loads of the CHP. The optimization is performed daily considering the time for the additional storage t_{ad} as the decision variable. The objective functions are the exergetic efficiency of BTES system and the economic profit *$* of the cogeneration plant. The problem can be formulated in the following way:

$$max\big(\boldsymbol{F}(t_{ad})\big) = \max(\$(t_{ad}), \boldsymbol{\varepsilon_{II}}(t_{ad})) \tag{3.17}$$

$$\textit{subject to } \{0\ h \leq t_{ad} \leq t_{BTES,daily}$$

where $t_{BTES,daily}$ is the number of operation hours of BTES system expected for that day.

The POD model performs fast and accurate simulation of the BTES system operation in order to evaluate the second law efficiency.

The result of the proposed algorithm is the identification of the interval time during which storing extra thermal energy.

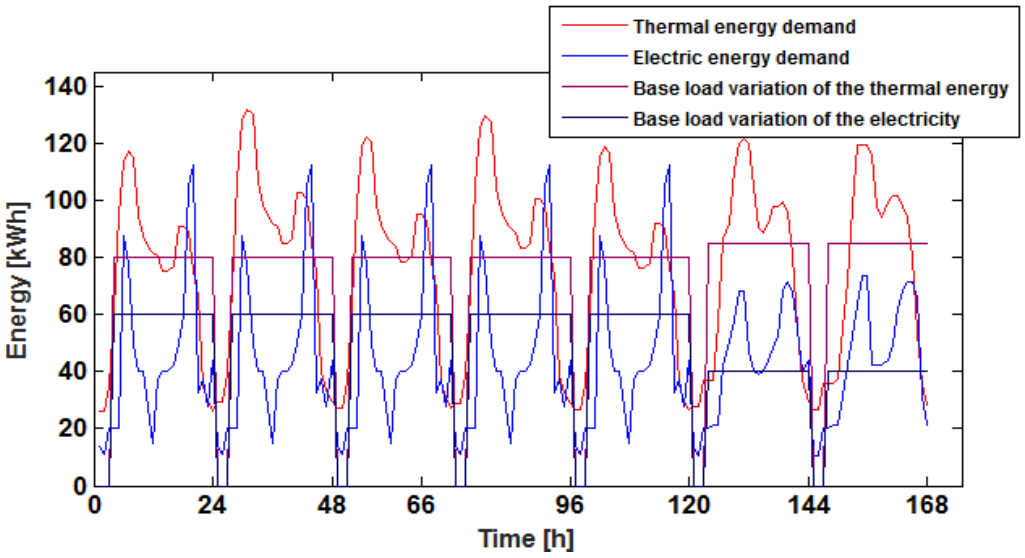

Figure 3.18: *Loads prediction for 7 days.*

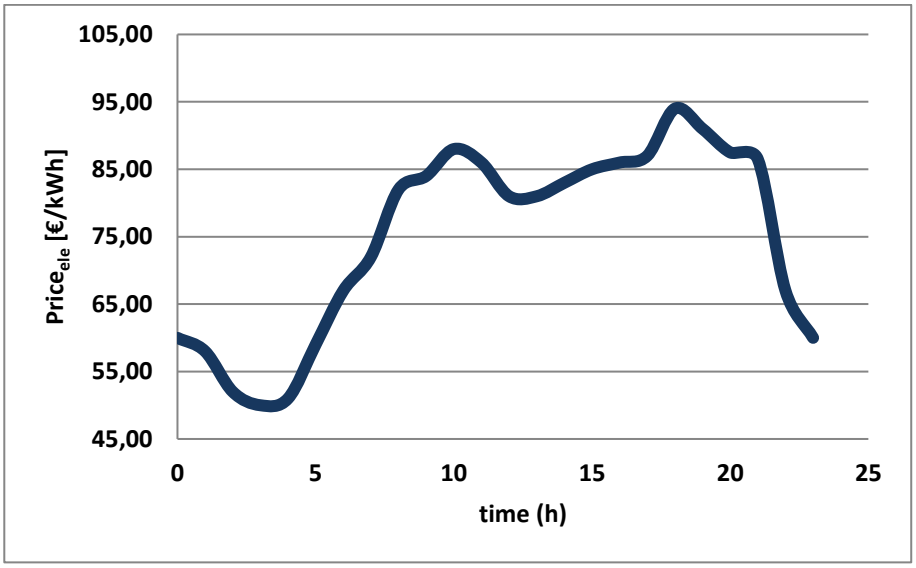

Figure 3.19: *Daily market price of electricity.*

Referring to the same one week of operation (*Figure 3.18*), the second law efficiency and the economic profit have been compared for three different cases:

- Case *A* in which the operation is optimized by the proposed algorithm;
- Case *B* in which the operation is characterized by prefixed daily time for the additional storage (2 hours per day);
- Case *C* in which the operation does not consider any daily storage.

For the cogeneration plant, the production costs of thermal and electricity energy are 0.1 €/kWh and 0.07 €/kWh respectively.

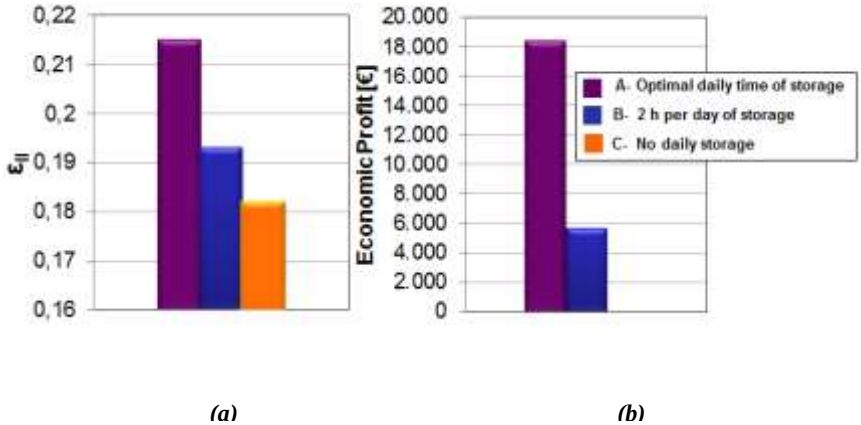

Figure 3.20: *(a) Second law efficiency and (b) economic profit for 3 different scenarios.*

The results in *Figure 3.20*(a) show that a significant improvement of the second law efficient is achieved for Case *A* with an increase of about 18.8% respects with the Case *C*. For Case *B* the improvement is only of 5.5%. The economic profits for the cogeneration plant are significantly higher for the optimized case (*A*) as shown by *Figure 3.20*(b).

Chapter 4

Multiscale Approach

4.1 Introduction

The design and the operation of ventilation systems is of large importance for underground infrastructures such as road tunnels, mines, metro stations etc. In this framework, Computational Fluid Dynamics (CFD) is largely used as an engineering tool for the analysis of both normal operating conditions and emergence conditions i.e. in the case of fire (Teodosiu, et al., 2016) (Zhu, et al., 2016) (Adjiski, et al., 2015).

CFD is the analysis of systems by means of computer-based simulations involving fluid flow, heat transfer and/or associated phenomena such as a chemical reactions (Versteeg & Malalasekera, 2007).In the considered systems, CFD simulations are based on the solution of the three-dimensional unsteady form of the Navier-Stokes equations asserting the conservation of mass, momentum and energy either in transient or steady state forms. This set of partial differential equations is solved numerically leading to detailed predictions of velocity and temperature fields, species concentration, heat fluxes mapping and so forth. The computational domain

is numerically discretized thus generating a large number of control volumes in which the conservation laws are enforced and solved.
Commercial codes as FLUENT (Inc., ANSYS, 2013), Flow3D and STAR-CD or open source codes as Fire Dynamic Simulator (FDS) (McGrattan, et al., 2013), OpenFoam (Greenshields, 2016) and SMARTFIRE (Taylor, et al., 1997) have been largely tested in term of accuracy for the prediction of air flow and fire. The accuracy of CFD in the prediction of local flow field data i.e. velocity and temperature fields, is affected by the mesh size used for the domain discretization. The grid independent solutions can be achieved only for large mesh density with consequent unsuitable computational costs for vast domains. CFD becomes unsuitable for the design and the operation of ventilation systems and for the analysis of smoke propagation in network infrastructures several kilometre long. For this reason, in most of the applications, the computational domain is limited to a small region i.e. close to the fire and the velocity and temperature profiles in the rest of the domain are assumed known.

The use of 1D model for complex network systems solves the problem of high computational costs of CFD thanks to complete and compact description of the system of interest. In the last three decades, several models have been developed by national institutions: MFIRE (U.S., Bureau of Mines, 1995), ROADTUN (Dai & Vardy, 6-8 July,1994; West, et al., 28-30 Nov 1994), RABIT and SPRINT (Riess, et al., November 2000), Express'AIR and SES (NTIS, 1990). In the 1D modelling, the flow is assumed homogeneous in each cross section making 1D models unsuitable to simulate the fluid behaviour in regions at high temperature gradients i.e. close to the fire or in region at velocity gradients near the jet fans, at the nose and tail of the trains, at tunnel junctions, near the subway stations. Proper corrections and empirical correlations must be introduced to account for the tri-dimensional behaviour of flow in such regions. Nevertheless the results of 1D

models for fire scenario are affected by large uncertainties especially, for smoke propagation and temperature profiles.

In order to make the analysis and optimization of these systems possible and more accurate but in a reasonable time, the adoption of multiscale methods based on hybrid 1D-3D computational techniques has been proposed. The multiscale approaches consist in a physical decomposition of the domain in sub-regions assigning to each one a model of different complexity, i.e. 1D and 3D. The simultaneous use of a complex modelling as computational fluid dynamics (CFD) and of a compact modelling as 1D ensures the accuracy of results in the field with temperature and velocity gradient, and the low computational cost of the 1-D model in the region where gradients in the transversal direction are negligible. In the last decade this type of approach has been used in tunnel ventilations field and it has been developed through a direct-indirect coupling of the commercial CFD code Fluent and a 1D network model (Colella, et al., 2009; Colella, et al., 2010; Colella, et al., 2011; Colella, et al., 2011). The 1D network is applied on the tunnel regions where the flow is fully developed *(far field*), while CFD on the regions where flow conditions require 3D resolution (*near field*). In (Colella, et al., 2009; Colella, et al., 2010) the direct and indirect multiscale methodologies are used to simulate the velocity field generated by an operating pair of jet fans both in normal and emergency ventilation conditions in real tunnels. A comparison between numerical results and experimental data demonstrated how the developed methodology can be used as a valid design tool for any tunnel ventilation system. The same approach is tested in (Colella, et al., 2011) to study the transient flow interaction between a growing fire and a ramping-up ventilation system in a modern tunnel, investigating several ventilation scenarios. Authors show that this method is a reliable tool to conduct accurate simulations in long tunnel domains, when the limitations of the computational cost becomes too restrictive. In case of fire in steady state conditions

(Colella, et al., 2011), the comparison of multiscale model with the full CFD solution shows that the maximum flow field variation is less than few percents, with a reduction of two orders of magnitude in computational time. Possible limitations in the development of multiscale approach presented in (Colella, et al., 2009; Colella, et al., 2010; Colella, et al., 2011; Colella, et al., 2011) are due to the use of a commercial CFD code as Fluent that must be interconnected by an external routine with the one-dimensional model. This limits the physical and geometrical complexity of the portion modelled by 1D model. The application is in fact limited to simple geometry and does not include mass transport. Recently the possibility to use an unique open source code for the multiscale modelling has been investigated in (Ang, et al., 2016). Authors propose the use of the open-source code FDS 6.1.1 (McGrattan, et al., 2013) and of its 1D model HVAC (Heating, Ventilation and Air Conditioning) feature for predicting the flow conditions in a real tunnel. The jet fans are modelled by the HVAC routine and the numerical results are compared with the full CFD and with experimental measurements. The multiscale modelling in FDS6 results as accurate as full CFD but up to 2.2 times faster and that computational savings increase with the length of the tunnel (Ang, et al., 2016). The fire scenario for the same tunnel studied in (Colella, et al., 2011), has been investigated with the multiscale modelling based on FDS and HVAC routine (Vermesi, et al., 2017). The multiscale implementation consisted of placing a 30 MW fire in the centre of a 400 m long 3D domain, along with two 400 m long 1D ducts on each side of it, that were again bounded by two nodes each. The feasibility analysis showed a difference of only 2% in temperature results from the published reference work that was performed with Ansys Fluent (Colella, et al., 2011). The reduction in simulation time was significantly larger when using multiscale modelling than when performing multiple processor calculation (Vermesi, et al., 2017). The current version of the HVAC routine implemented in FDS is characterized by two major limitations for the multiscale modelling of complex

systems. These limitations are linked with the original scope of the HVAC routine i.e. heating, ventilation and air conditions end not to modelling of large portions of the domain as tunnels, mines and subway stations. First limitation in this sense is due to the absence of 1D mass transport for the different species (McGrattan, et al., 2013). In the case of the exhaust gas propagation from the CFD domain and the corresponding back layering of smoke, it would calculate the concentration in the 1D domain and reproduce appropriately the backflow. Second limitation is due to the energy conservation form that does not include the heat losses through the walls and does not allow one to analyzing the temperature evolution along a duct (McGrattan, et al., 2013), which is very interesting in the case of semi-transversal ventilation.

This chapter describes an innovative tool for the multiscale modelling given by the fully integration of a 1D continuity, momentum, energy and mass transport equation in FDS modifying its source codes. The new multiscale simulator is an open tool accessible for the entire scientific community. It has been tested for modelling the ventilation system of the Monte Cuneo road tunnel in case of fire. It presents a semi-transversal ventilation system with accelerators and dumpers for the air extraction. In the current configuration of the ventilation system, depending on the traffic and atmospheric conditions at portals, smoke might not be fully confined as shown by simulations. Installation of larger extraction dumpers and of proper deflectors on the jet fans located in the lay-bys, ensures a correct smoke control with, a zero velocity in the fire area and converging velocities on both sides and significant improvements in terms of safety conditions.

4.2 Basis of multiscale approach

The multiscale approach refers to the domain decomposition methods (DDM) applied on any discretization techniques of partial differential equations such as finite volumes, finite differences, finite elements and spectral-element method. DDMs make the algebraic solution of PDEs more efficient on parallel computer platforms, reformulating the boundary-value problem on a part of the computational domain divided into sub-regions.

Figure 4.1: *Example of non-overlapping domain decomposition (left) and overlapping domain decomposition (right).*

This technique is particularly appropriate to solve heterogeneous or multi-physics problems governed by differential equations of different kinds depending on the portion of the considered computational domain. Two possible strategies can be adopted to the subdivision of the computational domain generating overlapping or non- overlapping (disjoint) sub-regions.

In non-overlapping domain decomposition methods, the subdomains Ω_1 and Ω_2 (see *Figure 4.1*) only share the so-called interface Γ. As possible iterative methods, *Dirichlet-Neumann methods* and *Neumann-Neumann methods* are applied for non-overlapping domain decomposition (Quarteroni & Valli, 1999).

In overlapping domain decomposition methods, the subdomains Ω_1 and Ω_2 share a thin Ω_{12} (see *Figure 4.1*) layer with their neighbours Γ_1 *and* Γ_2. In this case, *Dirichlet-Dirichlet* or *Schwarz methods* are applied on the interfaces Γ_1 *and* Γ_2 for the sub-domains Ω_1 and Ω_2 respectively (Quarteroni & Valli, 1999).

Several approaches for domain decomposition have been proposed for the numerical resolution of Navier-Stokes equations on parallel computers as Dirichlet-Neumann and Schwartz methods.
The detailed description of the mathematical theory for domain decomposition method and its applications to Navier-Stokes equations, is not the purpose of this work. We refer the reader to Quarteroni and Valli's book (Quarteroni & Valli, 1999) and also to (Quarteroni, 1994) (Houzeaux & Codina, 2004).

The multiscale approaches based on non-overlapping domain decomposition can be used to model complex systems as the underground infrastructures (tunnels road, mines and sub-way stations) and to study the ventilation systems both in sanitary and emergency conditions. It consists in the splitting of the full domain in sub-regions assigning to each one a model of different complexity, i.e. 1D and 3D. The choice of the dimensionality model for each region depends on the phenomena position. Several studies on the flow fields in underground infrastructures show that in the portion of the domain close to the operating jet fans or to the fire, flow has a complex 3D behaviour with velocity and temperature gradients. This region, which is known as the *near field*, must be modelled in 3 dimensions to ensure the accuracy of the results by using CFD tools. On the other side, in the portion of domain that is far from this region, the temperature and velocity in the longitudinal direction is prevalent with respect to transversal component and the flow becomes 1D. This region so called the *far field* can be described by 1D model.

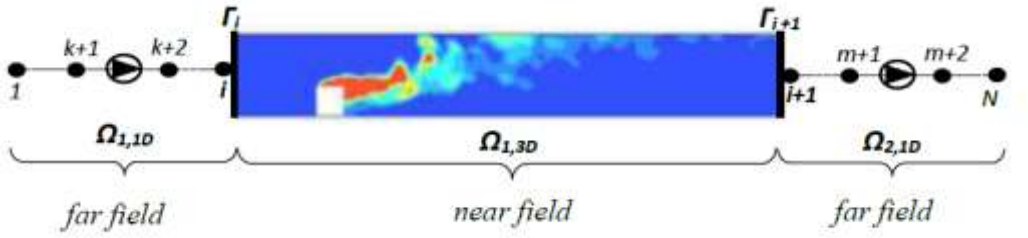

***Figure 4.2**: Schematic representation of a Multiscale modelling for a tunnel ventilation.*

The simultaneous use of a complex modelling as CFD and a compact modelling as 1D ensures the accuracy of results in the *near field* and the low computational cost of the 1-D model in the *far field* thanks to a continuous exchange of information at each 1D-3D interface in a form of boundary conditions.

This exchange of information consists on the Dirichlet-Neumann coupling strategy and it can be performed in indirect or direct way. In Indirect coupling, 1D and CFD simulations run separately. The global system is first analyzed by the 1D model and after identifying the near field, the CFD analysis is conducted prescribed uniform boundary conditions at the interfaces obtained by the previous 1D simulation. In Direct coupling, the 1D model is embedded within the CFD model and they run iteratively together with a constant exchange of information during the solution procedure. The direct coupling algorithm has to perform the operations at each iteration step.

This work proposes a direct coupling strategy that will be detailed analysed in the section 4.4 obtained by a full integration of a 1D network model with the CFD code *FDS.*

4.3 Fire Dynamics Simulator

FDS is an open source CFD model in Fortran 90 of fire-driven fluid flow developed by National Institute of Standard and Technology (NIST) which first version was publicly released in February 2002. This study has been carried out using FDS version 6.5.1 which has been released in June 2016. FDS was developed primarily as a tool for solving practical problems in fire protection Engineering and for studying fundamental fire dynamics and combustion. For these reasons, it is widely used by fire safety scientific community in particular for the design of smoke control and sprinkler activation systems. FDS is used together with *Smokeview*, a 3D rendering software that allows a graphical visualization of results.

The geometry is described in terms of rectangular obstructions and vents from which air or fuel can be either injected into, or drawn from, the flow domain (McGrattan, et al., 2013). The VENT group is used to prescribe planes adjacent to obstructions or external walls and to apply a particular boundary condition to a rectangular patch on a solid surface (McGrattan, et al., 2013). The exterior boundary of the computational domain is identified by the OPEN vent that denotes a passive opening to the outside.

Geometry is discretized by using rectilinear meshes where the government equations are approximated. The hydrodynamic model solves numerically a form of the Navier-Stokes equations appropriate for low-speed ($Ma < 0.3$), thermally-driven flow with an emphasis on smoke and heat transport from fires (McGrattan, et al., 2013). The numerical scheme is an explicit predictor-corrector algorithm with Cartesian grid, characterized by a second order accuracy in space and time. Turbulence is treated by means of Large Eddy Simulation (LES).

The fluid governing equations in FDS model are numerically solved by dividing the domain in a large number of prismatic cells. In each cell, gas properties are assumed to be only function of time: scalar quantities are assigned to the centred of each cell, vector quantities, instead, on the cell faces. Prismatic volumes are none

other than meshes in which FDS domain is divided. The separation between the large resolvable scale and the small modelled scale is archived by applying a spatial filtering operator (McGrattan, et al., 2013). Quantities obtained by this filtering can be physically interpreted as cell means. Roughly, eddies of size larger than filter scale are large eddies, those smaller are small eddies and need to be modelled. For a generic continuous field $\Phi(x_1', x_2', x_3', t)$, the filtered field $\bar{\Phi}(x_1, x_2, x_3, t)$ is obtained using the following formulation (McGrattan, et al., 2013):

$$\bar{\Phi}(x_1, x_2, x_3, t) = \frac{1}{\delta x_1\, \delta x_2\, \delta x_3} \int_{x_1-\frac{\delta x_1}{2}}^{x_1+\frac{\delta x_1}{2}} \int_{x_2-\frac{\delta x_2}{2}}^{x_2+\frac{\delta x_2}{2}} \int_{x_3+\frac{\delta x_3}{2}}^{x_3+\frac{\delta x_3}{2}} \Phi(x_1', x_2', x_3', t)\, dx_1' dx_2' dx_3' \quad (4.1)$$

where (x_1', x_2', x_3') are the continuous coordinates of the domain, and (x_1,x_2,x_3) are the discretized coordinates used to specify the centred of the cells. Using the filter definition, any field can be split up into: a large scale component $\bar{\Phi}$ which is directly simulated and sub-grid scale component Φ' that is modelled.

$$\Phi = \Phi' + \bar{\Phi} \quad (4.2)$$

LES is the default mode of operation (McGrattan, et al., 2013). Details of the mathematical models are thoroughly documented in the FDS Technical Reference Guide (McGrattan, et al., 2013) which we refer the reader for more details.

4.3.1 HVAC routine

FDS is equipped of an HVAC network model from v5.5.This routine allows to specify the topology of an HVAC system along with dampers, fans, forward/reverse flow loss through ducts and fitting. It has been is indirectly coupled with the FDS solver. Details of the HVAC implementation are in the FDS Technical Reference Guide (McGrattan, et al., 2013).

In the HVAC system the network is represented as described in the previous section, by nodes and ducts that are the equivalent of braches. The interface between the CFD domain and the 1D network model is given by nodes for each one the conservation equation of mass energy and momentum are prescribed in the following forms (McGrattan, et al., 2013):

$$\sum_j \rho_j u_j A_j = 0 \tag{4.3}$$

$$\sum_j \rho_j u_j A_j h_j = 0 \tag{4.4}$$

$$L_j \rho_j \frac{du_j}{dt} = P_i - P_k + (\rho g \Delta z)_j + \Delta p_j - \frac{1}{2} K_j \rho_j |u_j| u_j \tag{4.5}$$

where *u* is the duct velocity, *A* is the duct area and *h* is the enthalpy of the fluid in the duct. The subscript *j* refers to a duct, the subscripts *i* and k indicate nodes respectively where one or more ducts join or where a duct terminates in a compartment. Δp is a fixed source of momentum (a fan or blower), *L* is the length of the duct segment, and *K* is the friction continuous loss of the duct segment evaluated as $K = \frac{fL}{D}$, while f is the friction factor (McGrattan, et al., 2013).

The momentum equation (12) is non-linear with respect to velocity due to the loss term and the pressure difference between two nodes in the network is influenced by the pressure change at all nodes connected with the same duct. An iterative scheme is proposed for the solution of the momentum equation and it is described in the FDS guide (McGrattan, et al., 2013)

The HVAC model uses prior time step values as its boundary conditions and provides to FDS wall boundary conditions of temperature, velocity, and species for prediction of the next FDS time step.

Boundary conditions at each node are determined by summing the mass and energy of the gas cells next to node and averaging the pressure (McGrattan, et al., 2013):

$$\bar{\rho}_i = \frac{\sum_j \rho_j A_j}{\sum_j A_j} \tag{4.6}$$

$$\bar{Y}_{\alpha,i} = \frac{\sum_j Y_{\alpha,j} \rho_j A_j}{\sum_j A_j \rho_j} \tag{4.7}$$

$$\bar{P}_i = \frac{\sum_j P_j A_j}{\sum_j A_j} \tag{4.8}$$

The total mass and energy along with the average pressure are then used to determine the average temperature (McGrattan, et al., 2013):

$$\bar{h}_i = \frac{\sum_j c_p(T_j,Y_j) \rho_j A_j}{\sum_j A_j \rho_j} \tag{4.9}$$

$$\bar{T}_i = \frac{\bar{h}_i}{c_p(\bar{T}_i,\bar{Y}_i)} \tag{4.10}$$

For wall cells containing inflow from an HVAC duct that is not leakage flow, the surface temperature, T_w, is set to the value in the connected duct while in the case of leakage flow, T_w is calculated considering the thermal properties of the surface. The other wall boundary conditions in term of density, velocity and gas species are set in the following form (McGrattan, et al., 2013):

$$\dot{m}_\alpha'' = Y_{\alpha,d} \cdot \dot{m}'' \tag{4.11}$$

$$\dot{m}'' = \frac{u_d A_d \rho_d}{A_v} \tag{4.12}$$

$$u_w = \frac{\dot{m}''}{\rho_w} \tag{4.13}$$

$$\rho_w = \frac{p\bar{W}}{RT_w} \tag{4.14}$$

$$Y_{\alpha,w} = \frac{\dot{m}_\alpha'' + \frac{2\rho_w D Y_{\alpha gas}}{\delta n}}{\frac{2\rho_w D}{\delta n} + \rho_w u_w} \tag{4.15}$$

where the *d* refers to the connected duct, A_v is the total area of the vent and *w* represents the wall cells.

4.4 Multiscale modelling

A first version of a 1D network model called Whitesmoke was developed at the Energy Department of Politecnico di Torino. This code has been written in Fortran 90 and includes mass, momentum and energy equations respectively in the form of eq. (2.32), eq. (2.33) and eq. (2.34). *Whitesmoke* has been modified in the present PhD work, in order to include the mass transport equation given by eq. (2.35). This new version of the 1D network model has been fully integrated in FDS resulting in new open source for the multiscale analysis of complex systems. *Figure 4.3* reports the Command Prompt of the new .exe file and a geometrical reproduction of a multiscale model.

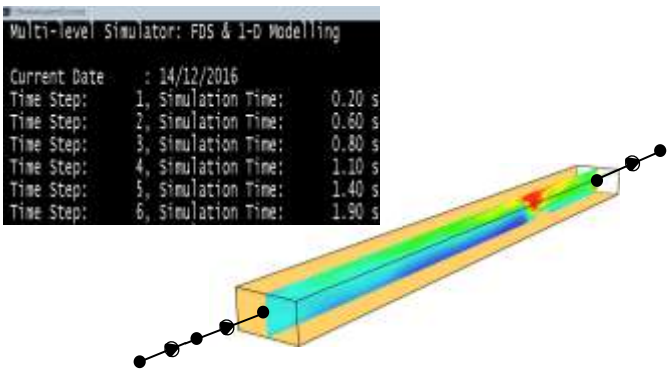

Figure 4.3: *Multiscale Simulator.*

The integration between FDS domain and the 1D network model has been performed using a new special "vent" type called EXCH, which has been introduced in the FDS code. This has been added to the Vent name-list group of the FDS current version and allows to specify the type of 1D-3D boundary condition exchanged. In the case in which the pressure is prescribed on the FDS boundary, this is treated as an OPEN vent. The position of the OPEN and the EXCH vents in the case of fire is influenced by the critical velocity, as it will explained.
The preliminary version of the multiscale simulator allows to couple only two 1D domains with the CFD and it has been tested as following. The current version gives one the possibility to implement several 1D networks but it is still in test phase.

The default background species in FDS is the AIR constituted by N_2, O_2, CO_2, and H_2O (McGrattan, et al., 2013). The default composition has been modified adding the Soot and CO species. They are set equal to zero in absence of combustion phenomena. On the contrary, the mass transport model of FDS evaluates the concentration for all the species. In the case of outlet flow from the CFD domain, the evaluated concentrations become the boundary condition at the interface for the 1D mass transport model. Depending on the operating conditions an inversion velocity can occur and the exhaust gasses that "re-enter" in the CFD domain, cause the back-layering phenomena. In this case, the inlet flow is set with the proper concentration calculated by the network model. This ensures a correct estimation of air quality in emergency condition, allowing to increase the level of security for users. Section 4.4.5 is especially dedicated to this aspect.

4.4.1 Boundary conditions at 1D-3D interfaces: direct coupling

Consider the system reported in *Figure 4.2* in which the full domain Ω is split in two 1D regions *(*$\Omega_{1,1D}$ and $\Omega_{2,1D}$) and in one 3D region ($\Omega_{1,3D}$) using the non-overlapping domain decomposition technique. Two interfaces can be identified corresponding to the pair node *i* of the 1D domain and surface Γ_i of the CFD domain and to the pair node *i+1* and surface Γ_{i+1}. As suggested in (Formaggia, et al., 2001), the continuity of area, velocity, pressure and temperature must be guaranteed at each interface 1D-3D. In nodes i and i+1, the 1D model provides average values for pressure, temperature and mass flow rate that can be applied on the boundary faces of the CFD domain. Analogously, the same quantities can be calculated on the surfaces Γ_i and Γ_{i+1} by performing integral averaging at the CFD boundary faces.

In the case of Navier–Stokes equations with non-overlapping domain decomposition method, Dirichlet–Neumann boundary conditions for fluid flow must be prescribed at each interface (Formaggia, et al., 2001). This approach has been tested in tunnels ventilation field, both in sanitary and emergency conditions (Colella, et al., 2009; Colella, et al., 2011; Colella, et al., 2010; Colella, et al., 2011). A Dirichlet- Dirichlet boundary condition is used for heat transfer and mass transfer.

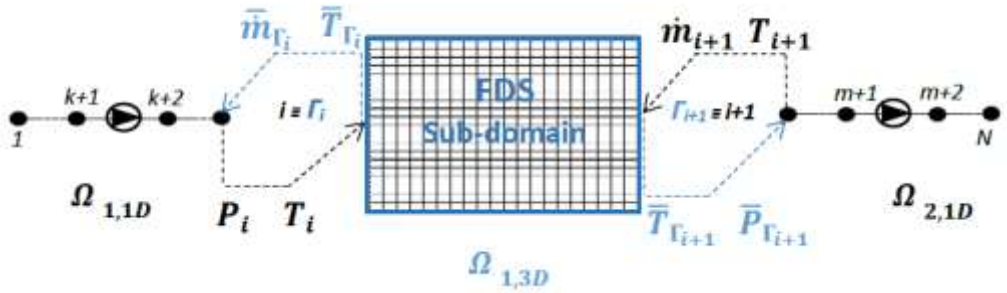

Figure 4.4: *Boundary conditions at 1D-3D interfaces.*

Even if an iterative procedure is possible (i.e. iterative convergence of the 1D and 3D results at boundaries), a time monitoring update has been implemented for the prescription of boundary conditions during the multiscale simulation. The exchange of boundary conditions does not occur at each iteration of FDS calculation but after a prefixed times step (Δt), ensuring a temporal convergence of thermodynamic variables. The value assumed by Δt cab be modified by the user according with his specific needs.

The following explanation refers to a simple case of *Figure 4.4*.

The complete sequence of operations is:

1. *Time = 0 : Δt*

a. Run the 1D model of the *far fields* $\Omega_{1,1D}$ and $\Omega_{2,1D}$ assigning appropriate boundary conditions. for nodes *i* and *i+1;*
b. Evaluate pressure and temperature of the node *i* (P_i and T_i) and mass flow rate and temperature of the node *i+1* ($\dot{m}_{i+1}$and T_{i+1}).

2. *Time =0 : Δt*

c. Run the 3D model of the *near fields* $\Omega_{1,3D}$ assigning P_i, T_i and $\dot{m}_{i+1}$ and T_{i+1} at the surfaces Γ_i and Γ_{i+1} respectively.
d. Evaluate the average mass flow rate and temperature at the surface Γ_i ($\bar{\dot{m}}_{\Gamma_i}$ and $\bar{T}_{\Gamma_i}$) and the average pressure and temperature at the surface Γ_{i+1} ($\bar{P}_{\Gamma_{i+1}}$ and $\bar{T}_{\Gamma_{i+1}}$).

3. *Time = Δt : t+Δt*

e. Run the 1D model of the *far fields* $\Omega_{1,1D}$ and $\Omega_{2,1D}$ assigning $\bar{\dot{m}}_{\Gamma_i}$ and $\bar{T}_{\Gamma_i}$ at node *i* and $\bar{P}_{\Gamma_{i+1}}$ and $\bar{T}_{\Gamma_{i+1}}$ at node *i+1,* of previous time step*;*
f. Evaluate pressure and temperature of the node *i* (P_i and T_i) and mass flow rate and temperature of the node *i+1* ($\dot{m}_{i+1}$ and T_{i+1});
g. Run the 3D model of the *near fields* $\Omega_{1,3D}$ assigning P_i, T_i and $\dot{m}_{i+1}$ and T_{i+1} at the surfaces Γ_i and Γ_{i+1} respectively;
h. Evaluate the average mass flow rate and temperature at the surface Γ_i ($\bar{\dot{m}}_{\Gamma_i}$ and $\bar{T}_{\Gamma_i}$) and the average pressure and temperature at the surface Γ_{i+1} ($\bar{P}_{\Gamma_{i+1}}$ and $\bar{T}_{\Gamma_{i+1}}$).

4.4.2. Pressure boundary condition at the OPEN vent

Pressure boundary condition in FDS can be prescribed if and only if the surface is defined as OPEN vent and in the form of *dynamic pressure* (McGrattan, et al., 2013). This type of boundary condition depends on whether the local flow is incoming or outgoing. In either case, it is assumed that hydrodynamic pressure head

H remains constant along a streamline (McGrattan, et al., 2013) and it is imposed as:

$$H = \begin{cases} {P_{dyn}}/{\rho_\infty} + \frac{|u|^2}{2} & (outgoing) \\ {P_{dyn}}/{\rho_\infty} & (incoming) \end{cases} \tag{4.16}$$

where ρ_∞ is the ambient density and u is the velocity on the boundary.

The first step for the direct coupling 1D-CFD, is to ensure that the exchanged quantities have the same physical meaning. As shown in section 2.2.2, the pressure P of the 1D network model, is the total pressure given by the sum of the kinetic, pressure and gravity terms. During the multiscale simulation, the pressure prescribed by the 1D model to the Open vent of FDS must be in accordance with eq. (4.16). Several tests have been performed in order to compare the input-output pressures of FDS and the corresponding one of the 1D model.

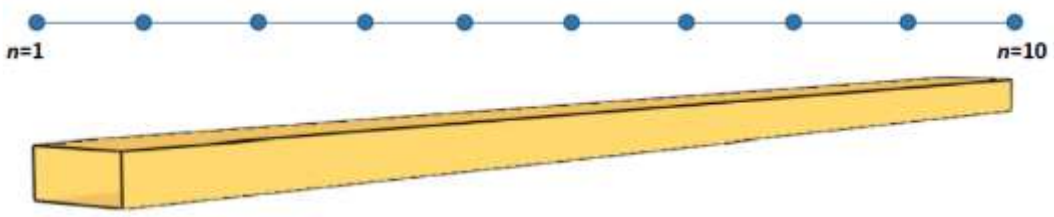

Figure 4.5: *1D and CFD domain for the tests.*

Figure 4.5 shows the horizontal tunnel of 180 m with a cross section of 66 m^2 used for the tests in which no fire phenomena occur. The 1D network consists of 10 nodes and 9 branches. *Table 4.1* summarizes the 4 tests performed in term of b.c. on the portals of the respective models.

Test	1D Network		FDS	
	n01	*n10*	*x=0 m*	*x=180 m*
1	P_{tot}=0 Pa	G_{inlet} =166 m^3/s	*Open Vent* $P_{dyn}=P_{n01}-0.5\rho u^2$	*Surf Vent* v=-2.51 m/s
2	P_{tot}=0 Pa	G_{outlet} =166 m^3/s	*Open Vent* $P_{dyn}=P_{n01}$	*Surf Vent* v=2.51 m/s
3	G_{inlet} =166 m^3/s	P_{tot}=5 Pa	*Surf Vent* v=-2.51 m/s	*Open Vent* $P_{dyn}=P_{n10}-0.5\rho u^2$
4	G_{outlet} =166 m^3/s	P_{tot}=5 Pa	*Surf Vent* v=2.51 m/s	*Open Vent* $P_{dyn}=P_{n10}$

Table 4.1 *Tests for the comparison of 1D and CFD.*

For all the tests, the pressures measured on the portals of the FDS domain are comparable with the corresponding pressures of the network model as demonstrated by *Figure 4.6*. In fact, the error percentage varies between 2.1% and to 9.7%. Results confirm that depending on the local flow is incoming or outgoing, the total pressure given by 1D must be reduced by the kinetic terms. On the contrary, the average pressure calculated on the FDS surf that becomes the b.c. for the interface node, is hydrodynamic pressure $H \cdot \rho$.

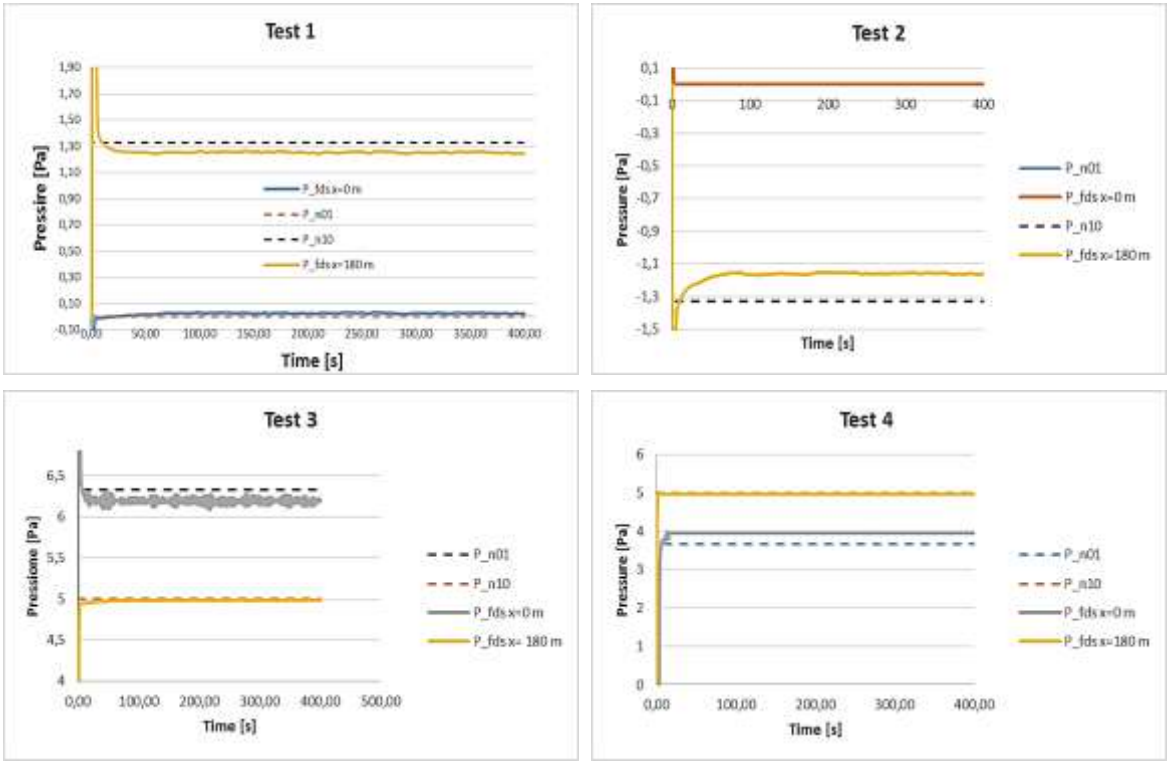

Figure 4.6: *Pressures comparison of 1D and FDS.*

.

4.4.3 EXCH vent position

As previously declared, the evaluation of the air concentration during a fire is fundamental to reproduce the phenomena of back-layering and the multiscale simulator proposed in this work is able to study this phenomena imposing an inlet flow in CFD domain with the correct concentration. The position of the EXCH and OPEN vents as interfaces between the 1D and FDS domain is crucial for this scope to avoid to exclude a portion of the CFD domain occupied by exhausts. The current version of FDS considers the OPEN vent applied to the exterior boundary of the

computational domain. The air composition of ambient that exists beyond the OPEN vent can be modified only before that the simulation starts changing the input parameters *Y_O2_INFTY* and *Y_CO2_INFTY* and it cannot be updated during the simulation.

The inlet flow concentration can be prescribed on the EXCH vent which localization is strictly correlated with the type of ventilation system and with the *critical velocity*. This latter represents the value of the ventilation able to prevent the formation of back-layering. Several derived models are available to calculate the critical ventilation velocity (Thomas, 1968; Danziger & Kennedy, 1982; Oka & Atkinson, 1995; Wu & Bakar, 2000; Kunsch, 2002). These studies are based on the dimensionless velocity and dimensionless heat release rate and they consider the tunnel hydraulic height as the characteristic length in the analysis. The relative expressions of the dimensionless critical velocity are reported in *Table 4.2* (Brahim, et al., 2013).

The back-layering distance L_b is defined as the length of the smoke back-layering upstream of the fire when the ventilation velocity is lower than the critical one (Ingason, 2005). It can be predicted by an experimental correlation that links it with the tunnel geometry, the ventilation velocity U and the fire HRR Q (Ingason, 2009).

Formulae	Remark	Source
$U_c = \left(\frac{gHQ}{\rho_0 T_0 c_p A} \right)^{1/3}$		Thomas (1968)
$U_c = \left(\frac{gHQ}{\rho_0 T_0 c_p A R_{i,c}} \right)^{1/3}$	$R_{i,c} = 4.5$	Danziger & Kennedy (1982)
$Uc^* = 0.35 \left(\frac{\dot{Q}^*}{0.124} \right)^{1/3}$ for $\dot{Q}^* < 0.124$ $Uc^* = 0.35$ for $\dot{Q}^* > 0.124$	$Uc^* = \frac{U}{\sqrt{gH}}$ $\dot{Q}^* = \frac{\dot{Q}}{\rho_0 T_0 c_p g^{1/2} H^{1/2} A}$	Oka & Atkinson (1995)
$U'_c = 0.4 \left(\frac{Q'}{0.20} \right)^{1/3}$ for $Q' \le 0.20$ $U'_c = 0.30$ for $Q' \ge 0.20$	$U'_c = \frac{U_c}{\sqrt{g\bar{H}}}$ $Q' = \frac{Q}{\rho_0 T_0 c_p g^{1/2} \bar{H}^{5/2}}$ $\bar{H} = 4A/P$	Wu & Bakar (2000)
$U_a' = c_1 \frac{\sqrt{1 + c_2 Q_0^{*2/3}}}{1 + 6.13 Q_0^{*2/3}} Q_0^{*1/3}$ $(H/w) = 1, \quad c_1 = 1.44, \quad c_2 = 3.57$ $(H/w) = 0.5, \quad c_1 = 1.48, \quad c_2 = 3.11$	$U_a^* = \frac{U_a}{\sqrt{gH}}$ $Q_0^* = \frac{Q}{\frac{\gamma}{\gamma - 1} p \sqrt{g} H^{5/2}}$	Kunsch (2002)

Table 4.2: *Expressions of the dimensionless critical velocity* **(Brahim, et al., 2013)**.

In the case of longitudinal ventilation systems, if the initial velocity is lower than the critical one the ventilation momentum is not sufficient to push all the smoke backward, downstream of the fire source. Then the smoke can travel upstream as well causing the back-layering (Merci & Beji, 2016) (see *Figure 4.7*). The back-layering length increases with the deviation of the velocity from the critical value. In this case we suggest to put the EXCH vent upstream of the fire and the OPEN vent downstream of its as shown in *Figure 4.7*.

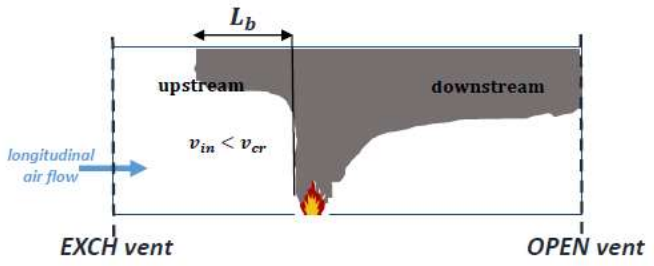

Figure 4.7: *Possible back-layering in the case of longitudinal ventilation.*

In the case of semi-transversal ventilation, smoke control is performed with the effective smoke extraction through the dumpers and the confinement of fire and smoke in the extraction area suppling fresh air flow from both side. In the case of smoke extraction, the longitudinal velocity at the ends of the extraction zone corresponding with critical velocity, can been considered for the system effectiveness (Ingason, 2005). A potential initial scenario for semi-transversal ventilation is reported in *Figure 4.8*. If the initial velocity upstream of the fire is lower than the critical, the back-layering occurs, covering a distance indicated as $L_{b,us}$. Initially, the airflow propagates towards the upstream 1-D–3-D interface and then, when the velocity inverts, crosses it again determining the backflow. In this

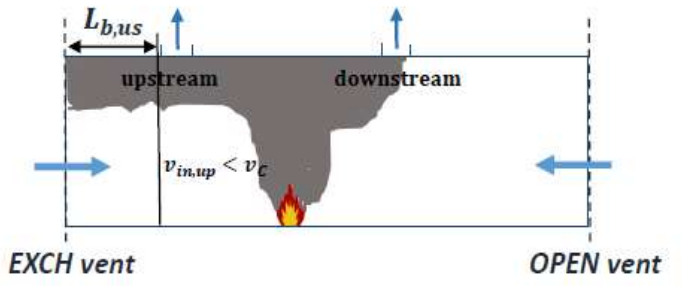

Figure 4.8: *Possible upstream back-layering in the case of semi-transversal ventilation.*

case, we suggest to put the EXCH vent at the upstream of the fire in order to calculate the concentration of the inlet/outlet flow.

In the case the initial velocity (in module) is lower than the critical velocity on both sides, the airflow propagates both the sides.

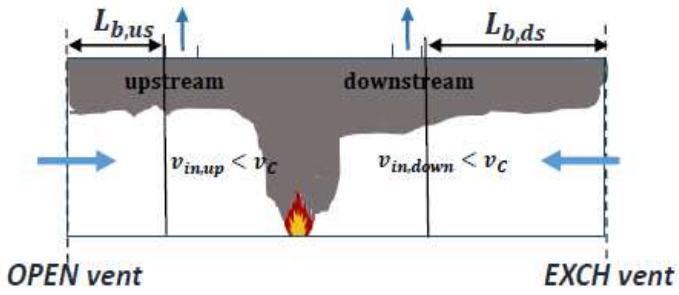

Figure 4.9: *Possible upstream and downstream back-layering in the case of semi-transversal ventilation*

Referring to the scenario of *Figure 4.9*, the velocity downstream the fire is the smallest with a consequent back-layering distance $L_{b,ds}$ greater than that upstream $L_{b,us}$. In this case the EXCH vent can be put downstream of the fire while the CFD domain can be extended upstream for covering the total back-layering distance $L_{b,us}$. Therefore, the EXCH vent can be localized where the initial velocity is the smallest and the CFD domain can be extended on the opposite side. This possible approach allows one to include back-layering from both sides.

4.4.4 Test of the fluid-dynamic behaviour

The test illustrated in this sections, considers a horizontal tunnel of 180 m with a cross section of 66 m^2 in absence of fire modelled both by 1D network and by the multiscale model. The 1D model is formed by 10 nodes and 9 branch (*see Figure 4.10*) while the multiscale model has a CFD domain of 100 m located in the central part of the tunnel and 2 1D networks at its boundaries as shown in *Figure 4.10*. An interface is constituted by node 3 and Γ_3 surface.

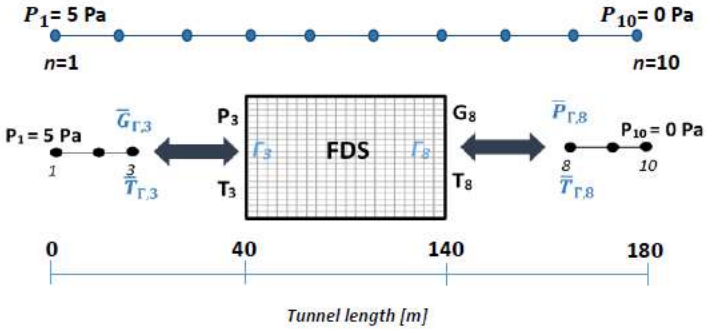

Figure 4.10: *1D model (top) and multiscale model (bottom) for the test case.*

This latter is an OPEN vent in which pressure b.c. given by node 3 is prescribed while the average mass flow rate of the Γ_3 surface is the fluid-dynamic b.c. for the node 3.

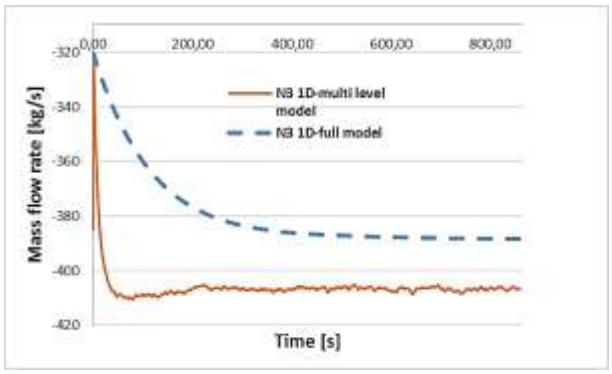

***Figure 4.11**: Mass flow rate in node 3.*

The other interface is represented by node 8 and Γ_8 surface that is an EXCH vent with a mass flux imposed by node 8. On this last one, the average pressure value on Γ_8 surface is applied. On the portals (nodes 1 and 10) the external pressure is applied in order to have a pressure drop of 5 Pa.

The aim of the test is to understand if the two models can be made comparable, as much as possible, including the friction losses. The 1D network considers the friction factors *f* as discussed in section 2.2.1. FDS allows to specify the roughness on the SURF line (McGrattan, et al., 2013) that can be calculated in the Moody diagram on the basis of the Reynolds number and the friction factor.

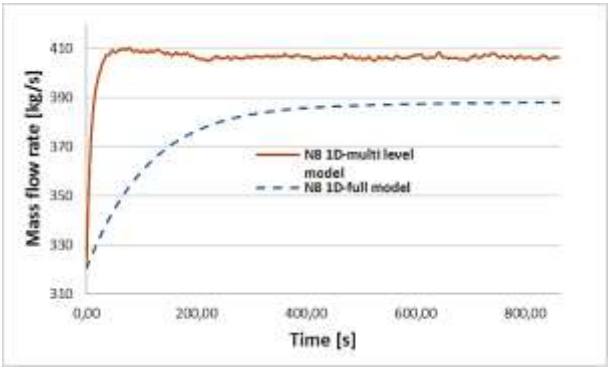

***Figure 4.12**: Mass flow rate in node 8.*

Figure 4.11 and *Figure 4.12* show the mass flow rate at nodes 3 and 8 in the case of simulation with the full 1D model and with the multiscale model described above. Negative and positive values correspond to the sign convention for the 1D network. At the steady state condition, the average percentage error is about of 4.6% with an absolute velocity variation of 0.3 m/s. The trend of the 1D curves (dashed lines) is characterized by a transient phase longer than the multiscale model. This latter achieves the steady state condition after about 40 s with an abrupt variation of slope. These differences are strictly correlated with the corresponding fluid-dynamic models. The evolution of the mass flow rate in the case of the multiscale model is linked with the LES method adopted in FDS and with the incompressibility of the fluid.

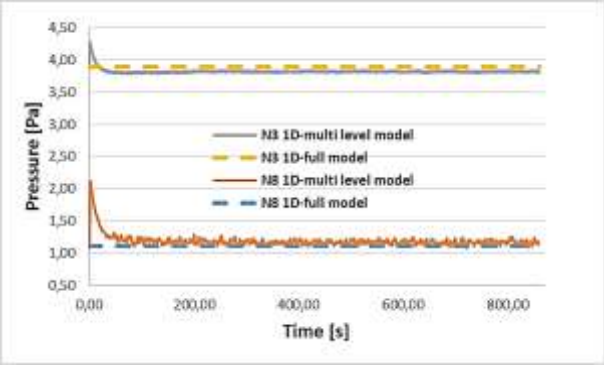

Figure 4.13: *Pressures at nodes 3 and 8.*

The pressure values at the nodes of interface are plotted in *Figure 4.13*: after 40 s, the steady state condition is obtained with a negligible deviation with respect to the full 1D model values.

4.4.5. Test of a fire scenario

The test described in this section compares a fire scenario for the same tunnel of the previous test (see Section 4.4.4) in the case of simulation with FDS and with the multiscale simulator.

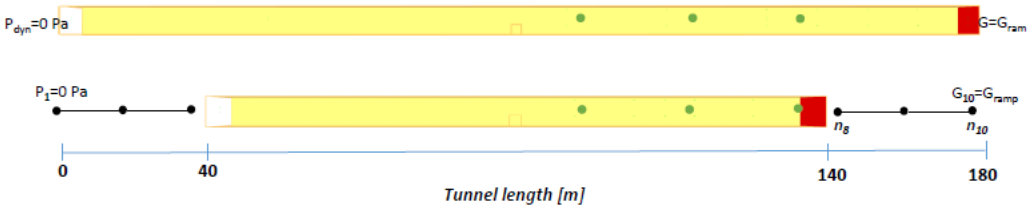

Figure 4.14: *Full model in FDS (top) and Multiscale model (bottom).*

The geometrical representation of the tunnel in FDS and in the multiscale simulator is given by *Figure 4.14*. For the CFD domain, a uniform grid is obtained diving the mesh into 20 cm cubes. The multiscale model is the same as that of the previous test in terms of vents localization and of boundary conditions at the interfaces. The difference consists on a fire source located in the centre of the tunnel in both the models and on the boundary conditions applied on the portals. On the first one (x=0 m), pressure is imposed equal to zero while on the second ones (x=180m) a forced flow is prescribed. The aim is to test the accuracy of the multiscale simulator in case of fire and in particular in the case of smoke back-layering. The condition of last event has been intentionally assumed by inverting the volume flow rate on the second portal. In order to do this, the forced flow is prescribed by a ramp that changes with time (see *Figure 4.15*).

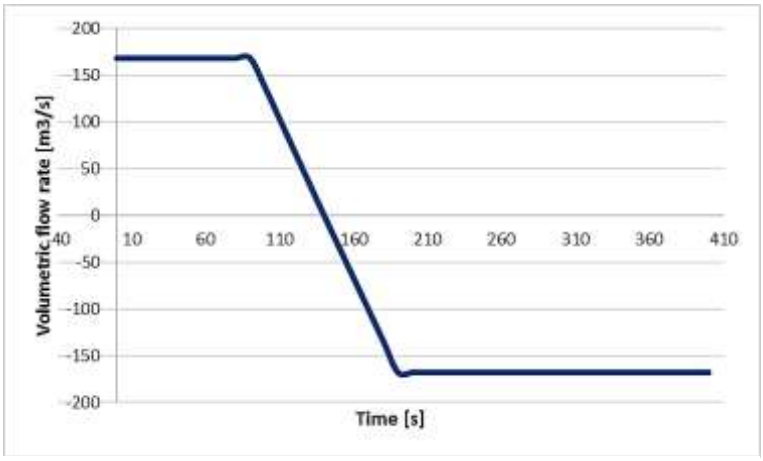

Figure 4.15: *Ramp of the volumetric flow rate at x=180 m.*

A negative value means that the flow is entering while a positive value means that it is extracted from the tunnel. The soot concentration is measured by 3 sensors located at 1.8 m of height in x=100 m, x=120 m and x=140 m. The inversion of velocity covers an interval time between 100s and 200s. The fire source is a vehicle that burns with 4 m^2 of surface and the propane is considered as fuel. In the case of the full FDS model, the concentration of soot during the forced back-layering downstream of the fire will be totally calculated by CFD tool that covers all the domain. In the Multiscale model the concentration is evaluated by 3D-1D mass transport equations, updating the boundary conditions at the interfaces.

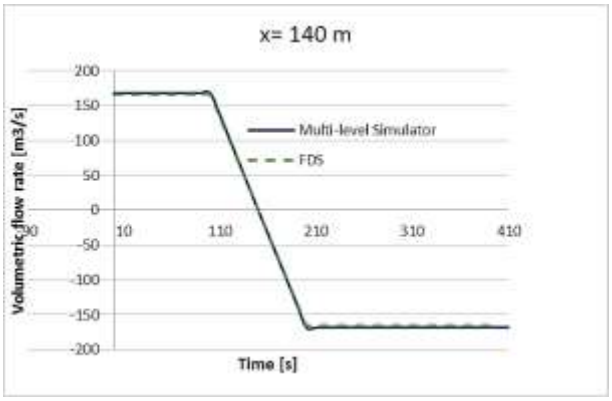

Figure 4.16: *Development of the volumetric flow rate.*

The fluid-dynamic convergence between the two models is confirmed by *Figure 4.16* comparing the volumetric flow rate evolution at x=140 m during the 400 s of simulation.

A snapshot of the smoke propagation in the tunnel is reported in *Figure 4.17*. The time instant considered is 150s when the forced velocity on the second portal is zero. A previous qualitative analysis suggests that in the tunnel section between 40 m and 140 m, the smoke propagation is the same for the two models.

Figure 4.17: *Smoke propagation in the tunnel with FDS (top) and with the Multiscale simulator at t=150 s.*

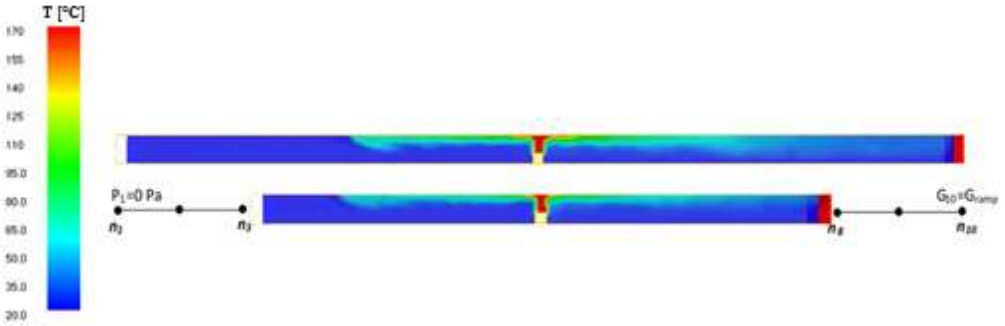

***Figure 4.18**: Temperature distribution in the tunnel with FDS (top) and with the Multiscale simulator at t=150 s.*

The temperature distribution for the same time instant is reported in *Figure 4.18* confirming what has previously said for the smoke propagation.

The three sensors allow to compare the soot concentrations calculated by the two models during 400 s of simulation, as shown in *Figure 4.19*. After 200 s, the soot concentration is null because smoke is pushed in the opposite direction.

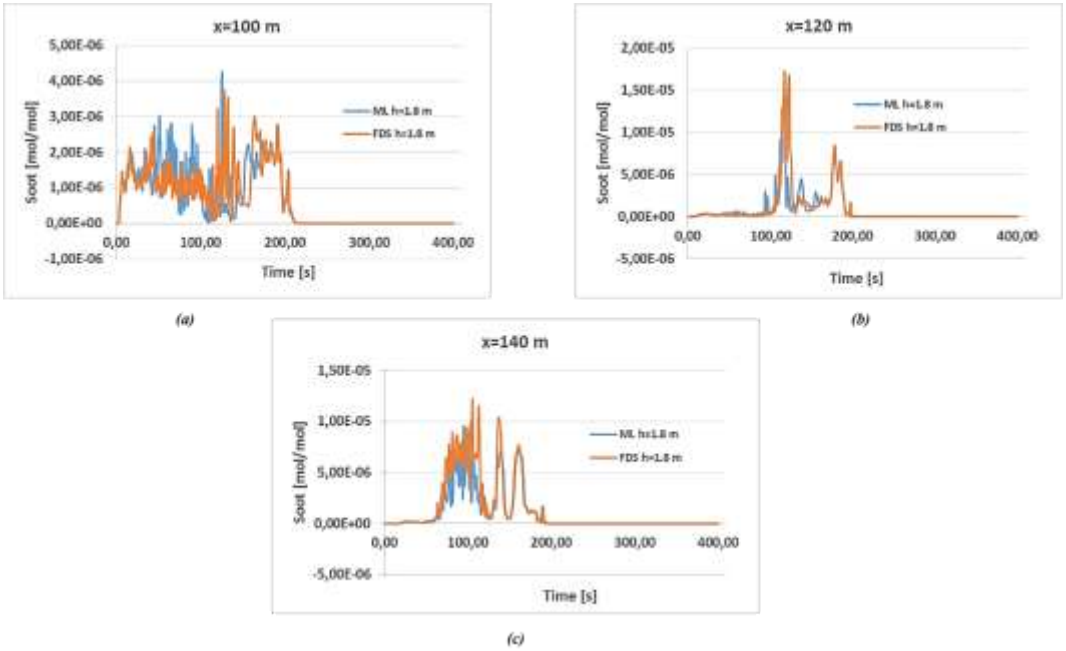

***Figure 4.19:** Evolution of the soot concentrations given by sensors located at x=100 m (a), at x=120 m (b) and at x=140 m (c).*

In order to compare these results, the moving average has been calculated with an interval of 30 considering the first 200 s of simulation. For the sensor located at x=100 m, the average difference is 2.2E-07 mol/mol that corresponds to a percentage variation of about 10.2%; for the second sensor (x=120 m) the average difference is 1.12E-07 mol/mol (7.6%) and for the last sensor is 1.4E-07 mol/mol (8.7%). Results plotted in *Figure 4.20*, show that the trend is approximatively the same with a larger but constant deviation for the nearest sensor to the fire (x=100 m). Anyway, the results of the two model present the same order of magnitude with the advantage to obtain reduction of the CPU time of about 55% in the case of the multiscale model.

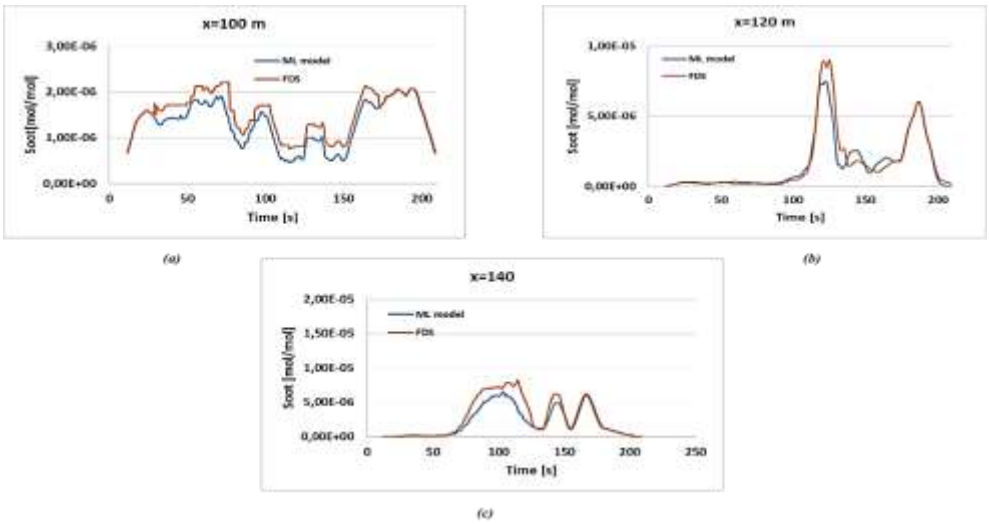

Figure 4.20: *Moving average of the soot concentrations given by sensors located at x=100 m (a), at x=120 m (b) and at x=140 m (c).*

4.5 Application to the ventilation system of Monte Cuneo road tunnel

The Monte Cuneo road tunnel has been considered as the case of study in this thesis: it is located in Avigliana (west of Torino). The tunnel is 1906 m with a cross section

of 66 m^2 and a longitudinal profile with two different splopes (1.79% slope for the first 846 m from North gate and then -2.65% slope for 1060 m) (Musinet Engineering S.p.A., 2011) as shown in *Figure 4.21*.

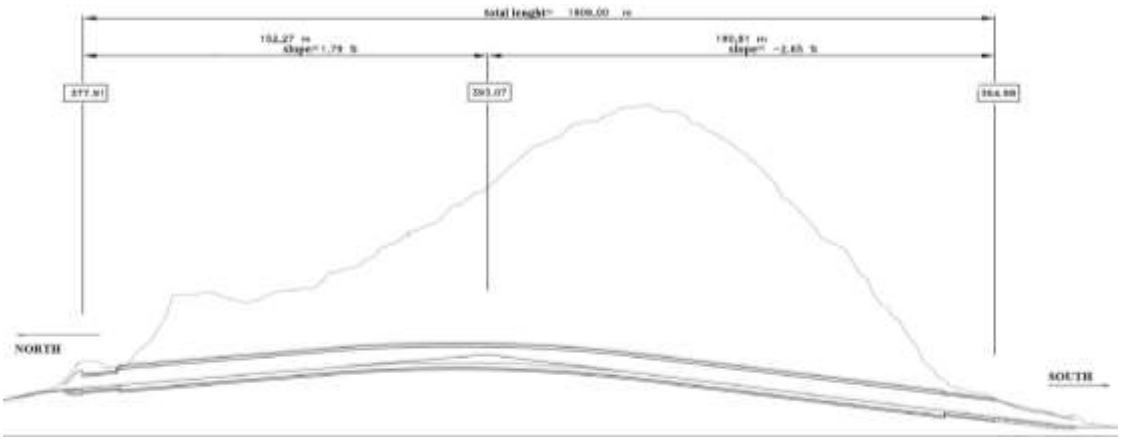

***Figure 4.21**: Longitudinal profile of Monte Cuneo tunnel.*

The current ventilation system in Monte Cuneo has a semi-transversal configuration. A duct for air extraction is installed on the top of the roadway (*Figure 4.22*(a)), and it is connected to the tunnel by mean of 18 remote controlled dampers with sizes 1.2 x 1.66 m^2.

Near the tunnel ends two ventilation rooms (north and south one) are installed: each room is connected to the air duct by means of two dampers *Figure 4.22*(b)). In the case of the north ventilation room, a transversal duct orthogonal to the tunnel axis is installed. In each ventilation room there are two axial fans, a noise attenuator and a damper that connect the room to the external environment.

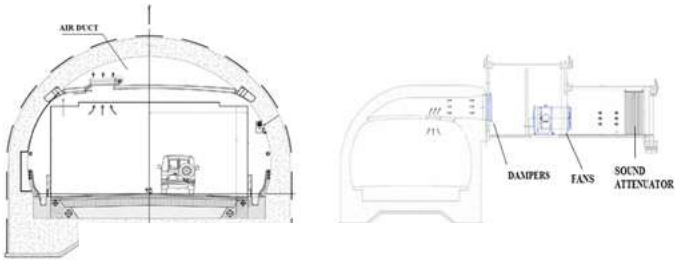

(a) ***(b)***

Figure 4.22: *(a) Tunnel and air duct cross sections and (b) ventilation room junction with the air duct.*

The axial fans have an internal diameter 1800 mm and the following characteristics in the design working point: power 158 kW, pressure gain 1550 Pa and flow rate 65 m^3/s. Four accelerators are installed in order to control more properly the axial air flux in the roadway in case of fire. The accelerators have an internal diameter of 1000 mm and a thrust of 900 N at a density of 1.2 kg/m^3. During normal operating condition, air is extracted by means of the four central dampers while the others are closed. In case of fire, regulation states that only the dampers located at a distance of less than 200 m from to the fire are opened and in addition the velocity of the air flux orthogonal to the dampers should be about 20 m/s (DETEC, Département fédéral de l'environnement des transports de l'énergie de la communication, 2008). Regulation also prescribes that the longitudinal air velocity must be o1.5 m/s at both sides of the extraction zone and directed towards to the fire place in order to ensure smoke control and to limit velocity in the fire zone (DETEC, Département fédéral de l'environnement des transports de l'énergie de la communication, 2008). In order to satisfy this in emergency conditions, the four dampers above the fire are opened.

Inside the Monte Cuneo tunnel anemometers, opacimeters, CO concentration meters and fire detectors are installed: information from these sensors is the base for controlling the ventilation system and guarantee users safety. The control of

ventilation system can be *manual* or *automatic.* The automatic control is obtained through three PID (*Proportional Integral Differential*) control algorithms. The first PID controls the extracted volumetric flow rate relying on the CO concentration; a second PID algorithm still controls the extracted flow rate but on the basis of the opacity. The third PID, instead, controls the number of accelerators to be activate in case of fire in order to guarantee the aerodynamic equilibrium.

4.5.1 Multiscale model for the case study

A schematic representation of the multiscale model and the prescribed boundary conditions is reported in *Figure 4.23*. The full domain of the tunnel has been split in 3 sub-regions: two *far fields* modelled by the network of 9 nodes and 8 branches each one and one *near field* in 3 dimensions. This portion of roadway in FDS is located between 1D model's nodes N09 and N15: it is 369 m long with the fire in the centred position and the four corresponding open dampers. In the 3D model a vehicle burning in the centred of the tunnel has been considered. The vehicle has dimensions 2x4x2 m^3 and it is located in the middle of the FDS domain. To model the fire, on the upper surface of the vehicle (with size 4 m^2) was set the *heat release rate per unit area* (HRRPUA). A heat release rate (HRR) of 30 MW has been considered in the design of tunnel ventilation system (DETEC, Département fédéral de l'environnement des transports de l'énergie de la communication, 2008). Its temporal evolution is plotted in *Figure 4.24: Heat release rate.* on the bases of experimental results (Ingason, 2009).

***Figure 4.23**: 1D-3D model for tunnel studied.*

The air duct and the dampers are not included in the model for the reasons explained in section 4.4, therefore the air extraction is imposed at the dumpers. This limitation has been overcome in the version of the simulation tool currently under testing.

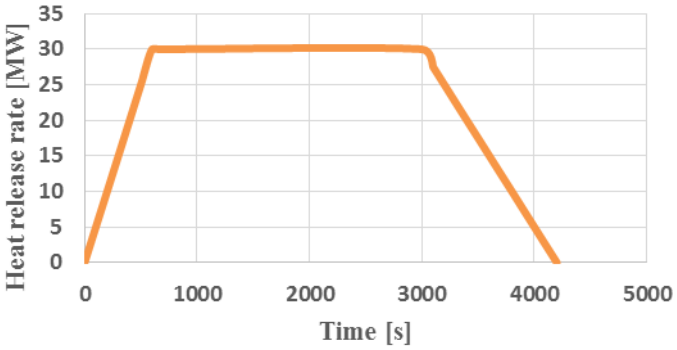

***Figure 4.24:** Heat release rate.*

In order to simulate the air extraction, on the upper part of the roadway four surfaces have been created in correspondence of open dampers. The extracted mass flows have been imposed as b.c. considering the numerical results of 1D complete network model (tunnel+ air duct) which structured is reported in ***Figure 4.25***. The 4 jet fans and the axial fans have been modelled in the full 1D network taking into account their characteristics curves (Musinet Engineering S.p.A., 2011).

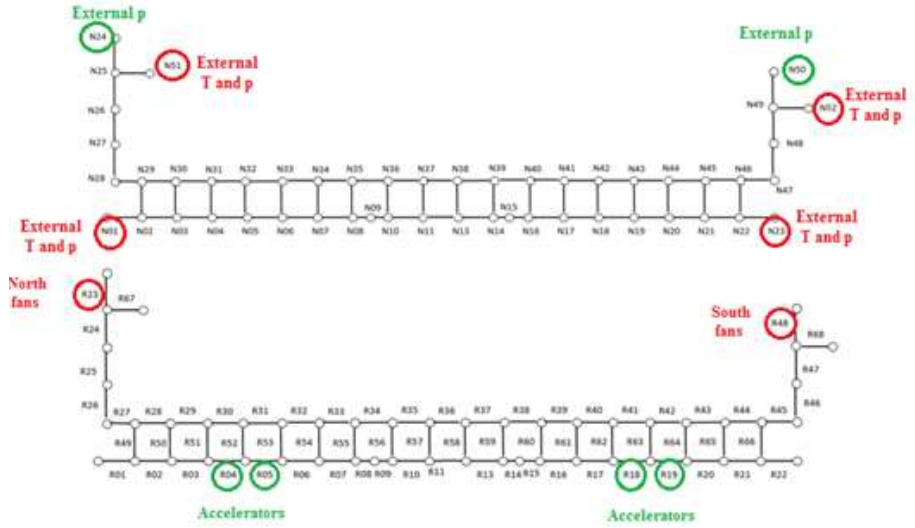

Figure 4.25: *1D network model of the tunnel linked with the air duct: (top) boundary conditions and (bottom) jet fans and axial fans positions***.**

Only the jet fans located in the branches R04, R05, R18 and R19 are included in 1D networks of the multiscale model.

4.5.2 Validation of the multiscale model

The multiscale model has been validated considering experimental tests without fire condition inside the Monte Cuneo tunnel in April 2014 (Musinet Engineering S.p.A., 2011). The tunnel was closed to the traffic and the ventilation system was working in *normal operating condition* with the four central dampers opened. Five anemometers were placed in the roadway at a height of 5 m allowing to estimate the volumetric flow rate of at the north and south gates, in proximity of the 4 dampers and at the two ventilation rooms. *Table 4.3* summarizes the experimental and numerical results.

	Multiscale model [m^3/s]	**Measurements [m^3/s]**	**Error [%]**
north gate	59	55	6.7
south gate	135	130	3.7
open dampers	159	150	5.6

Table 4.3: *Comparison of experimental and numerical results.*

The comparison between numerical predictions and experimental demonstrates the accuracy of the multiscale model for the prediction of air flow with an acceptable relative error.

4.5.3 Performance of the ventilation system with the multiscale simulator

The fire scenario has been simulated for the current ventilation system (dampers with sizes 1.2 x 1.66 m^2 and 4 accelerators). The considered pressure gain at the portals is of 5 Pa and it corresponds to an adverse condition for a short tunnel. The pseudo steady state conditions is achieved after 900 s and they are maintained until the fire is at the maximum HRR i.e. until to t=3000 s. During this phase, the longitudinal velocity profile (e.g. at t=2700 s) is reported in *Figure 4.26*.

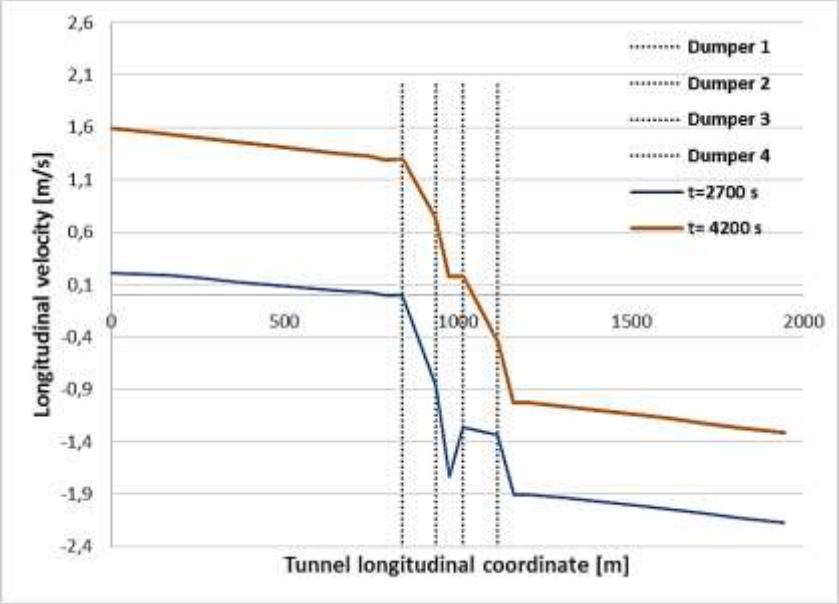

Figure 4.26: *Mean longitudinal velocity in the roadway at two different times.*

Results show the zero velocity takes place outside the extraction area. Therefore smoke is not perfectly confined within the 4 dampers and tends to leave the extraction area. During the first 400 s smoke propagates almost symmetrically with respect to the fire position and concentrated in the upper part of the roadway (*Figure 4.27*). The trend changes at t=600s when the fire reaches its maximum HRR. As shown in *Figure 4.26*, velocity in the south side (x=end) boundary is at higher elevation than north one generating a longitudinal air flow from south to north. The stack effect causes a smoke propagation towards the north portal and then back-layering (see *Figure 4.27* at t= 600 s). The profiles remain similar between 600 s and 3000 s and then smoke is removed by the ventilation system when HRR starts decreasing. The influence of the stack effect is also confirmed by the velocity profile during the fire extinguishing (between 3000 s and 4200 s). In fact, the volume flow from the north gate (x=0) and south gate increases and decreases respectively, achieving a balance form both sides at t=4200 s (see *Figure 4.26*).

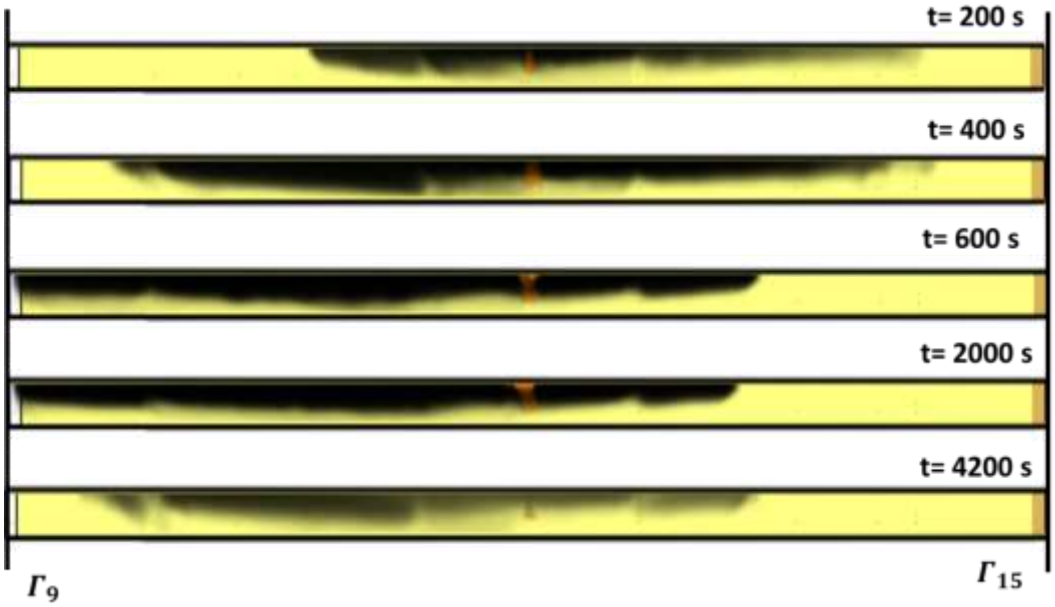

Figure 4.27: *Smoke propagation at different time step in 3D domain.*

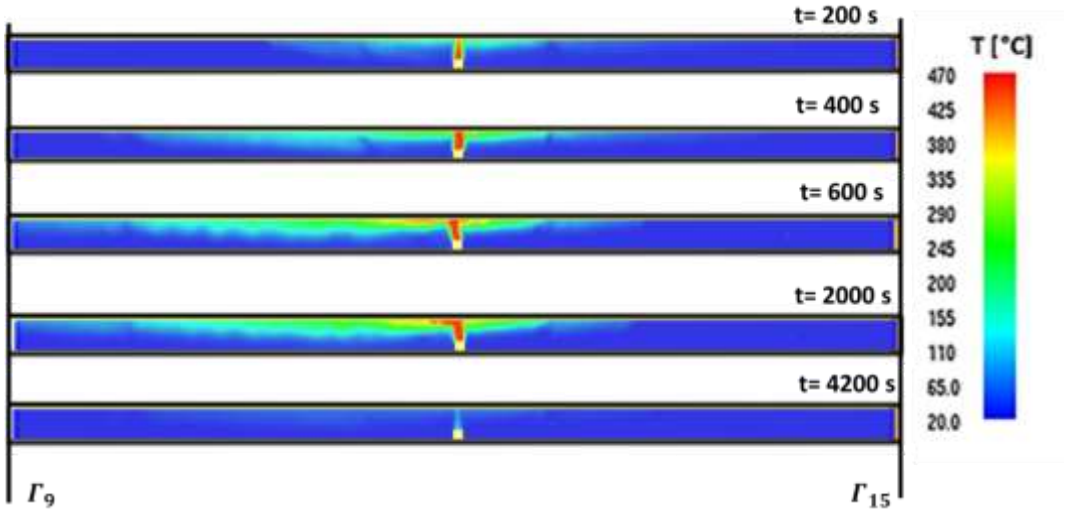

Figure 4.28: *Temperature distribution in the smoke area of 3D.*

In *Figure 4.28.* the temperature fields in the smoke area are plotted. Results are in accordance with the smoke propagation. The longitudinal air flow from south to north after 600 s of the trigger, maintains the temperatures of about 20 °C in the south region of the tunnel while in the north part the hot smoke propagates with a consequent increasing of temperature.

4.5.4 Optimization of the ventilation system with the multiscale simulator

In order to improve the performance of the ventilation system in terms of correct smoke control, the installation of large dumpers and deflectors on the axial fans is studied in this section. A parametric analysis has been performed with the full 1D network model (tunnel + air duct) for the selection of the optimal dumpers area that is resulted of 1.8 x 2.3 m^2. Deflectors are activated only in case of fire. Their installation causes an increase in the pressure rise of each accelerator from about 3.5 Pa to 6 Pa. Thanks to the re-design of the ventilation system, the exaction capacity in case of fire increases of about 16.5% with respect to the current configuration. The following results refer to the same conditions of the previous analysis in terms of fire development and static pressure at the portals.

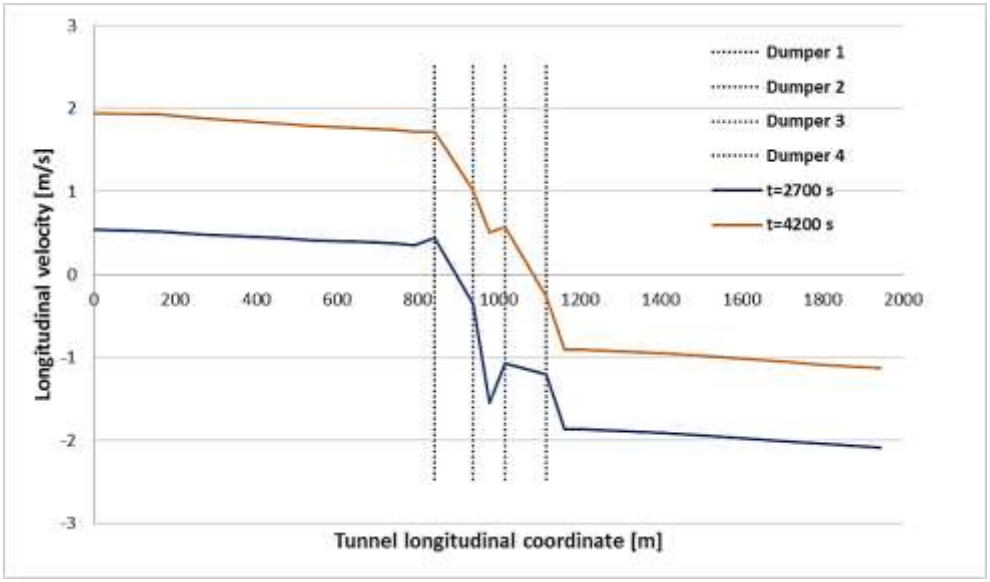

Figure 4.29: *Mean longitudinal velocity in the roadway in the re-designed configuration at two different times.*

The pseudo steady state condition is achieved after 900 s and they are maintained until to 3000 s for all fire duration at the maximum HRR. During this time interval, the longitudinal velocity profile (e.g. at t=2700 s) with this configuration is plotted in *Figure 4.29*. The zero velocity is located in the fire area and converging velocities are achieved on both sides. The volumetric flow rate difference between the two portals decreases thanks to the deflectors that push air in the opposite direction of the longitudinal air flow. The velocity at north gate, which is about zero with current configuration, becomes close to 0.5 m/s with the modified design and it is almost constant in south gate. Although this value of velocity is yet lower than the critical velocity, a sensible improvement has been obtained with the new configuration.

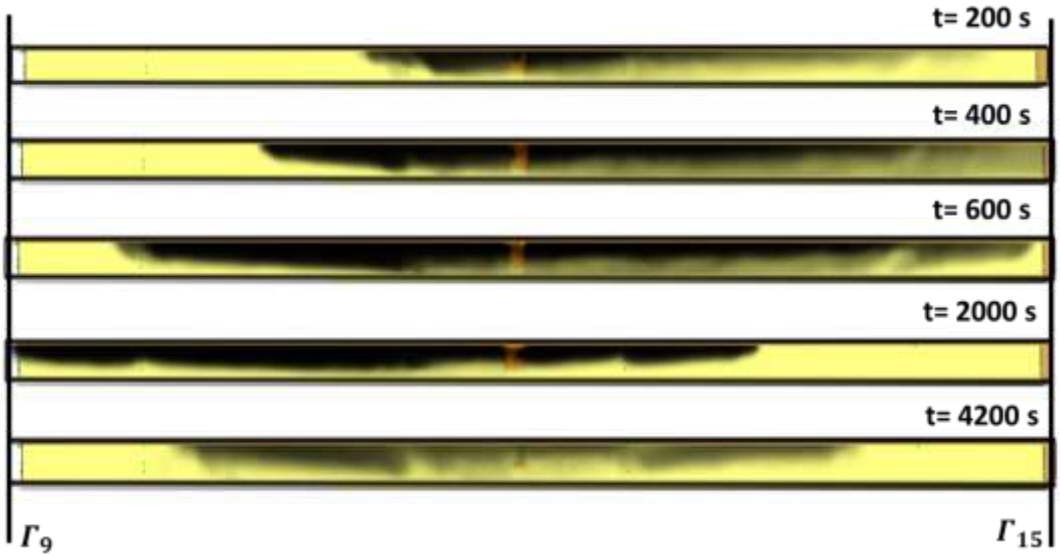

***Figure 4.30**: Smoke propagation at different time step in the re-designed configuration.*

Figure 4.30 shows the smoke propagation at different times. For t < 600 s the smoke occupies almost all the roadway. When the HRR is maximum (between 600s and 3000 s), the smoke is pushed towards the north side due to the stack effect and then back-layering. When the HRR decreases (after 3000 s), smoke is progressively removed by the ventilation system until to be perfectly controlled at t=4200 s.

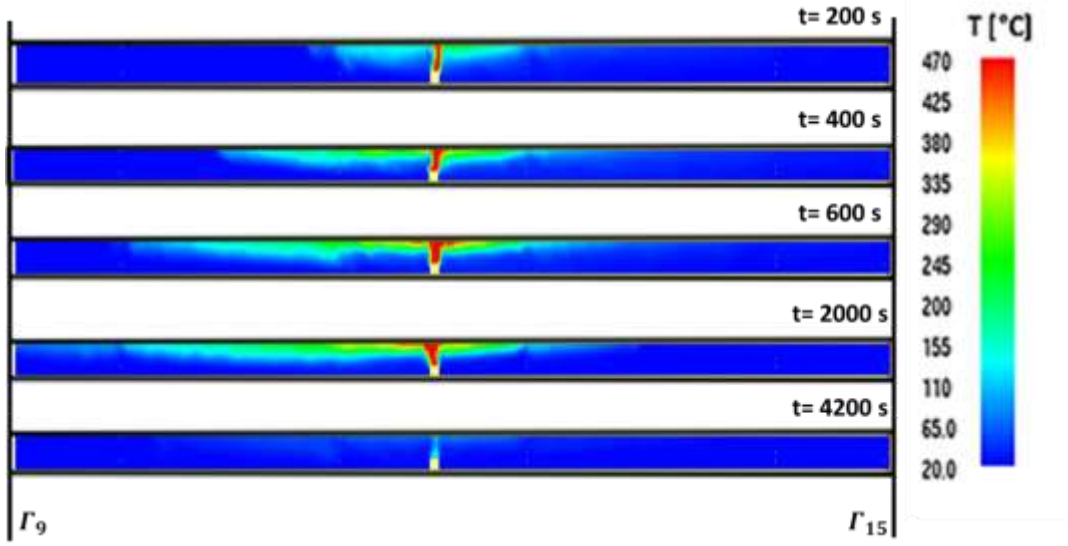

***Figure 4.31**: Temperature distribution in the smoke are in the re-designed configuration.*

Figure 4.31 reports the temperature field in the plane at the centred of the roadway at different time instants. The maximum temperatures near the ceiling decrease with respect to the current configuration and smoke is mainly concentrated in the upper part of the roadway. This effect improves the visibility and the safety conditions for the evacuation. The smoke temperature particularly affects the operation of axial fans, which should be maintained below 250°C for two hours in case of emergency. This limit is exceeded with the current configuration while in the case of optimized configuration the extraction temperature is lower than 240 °C for the entire simulation time confirming the sensible improvement.

The use of the multiscale model has allowed to compare two different configurations of the ventilation system extending the analysis to the all the active ventilation devices and to the whole tunnel layout. Unlike a traditional CFD approach in which a limited region of the tunnel is investigated (e.g. the fire area),

boundary conditions at the portals and flow characteristics in areas far away from the fire region have been taken into account in the model providing an accurate solution of the smoke diffusion and the air flow. This has allowed to appreciate the improvements of the ventilation systems in the re-designed configuration both in term of safety and smoke control.

Chapter 5

Conclusions and Future Works

The work presented in this thesis proposes innovative modelling strategies for the thermal fluid-dynamic analysis of underground infrastructures. The constant requirement of a high safety level both in normal and emergency conditions, makes the design and operation of the ventilation systems particular important. In the thesis, various numerical approaches have been developed and validated against experimental data from real systems including 1D network models, reduced order models and multiscale models.

The proposed 1D network model includes the continuity, momentum, energy and mass transport equations in transient form. It has been applied on the Frejus tunnel to predict the fluid-dynamic behaviour. In normal operating conditions the 1D model has been validated against experimental data demonstrating a great accuracy in the prediction of the ventilation conditions within the tunnel. A particular emergency condition has also been investigated. It refers to a fire of 30 MW during which the failure mode of a fan occurs. The current regulation system is equipped by a closed loop algorithm that in case of anomalies of the fans, prescribes the

operation of a substitute one. This procedure can cause a delay in the extraction smoke (about 4 minutes according to the experimental tests in normal operating conditions). The analysis of the smoke front upstream and downstream the fire, allows to establish that 500 m of tunnel are occupied by the smoke and that 240 seconds are needed to confine it in the extraction zone after the fans activation. The knowledge of these data is particular important for the definition of the emergency procedure and the 1D network model can be used to explore several scenario.

The 1D models have also been applied for the thermal analysis of ground heat exchangers. In fact, the heat exchange in these systems is similar to that occurs in sanitary ventilation systems within the underground infrastructures. The model has been validated against experimental data demonstrating its accuracy also for the prediction of the thermal behaviour. It has been used for simulating different operating conditions of small GCHP systems constituted by two vertical boreholes, in an optimization strategy based on the entropy generation minimization (EGM). A parametric analysis has been performed in order to identify the minimum of entropy generation in various operating conditions and in presence of anomalies such as ovalization and fouling, or different installation depth. Results have shown that, when no design anomalies affect the system, the minimum entropy generation is achieved by a mass flow rate equally distributed between the two vertical U-tubes. In contrast, when design or operational anomalies occur, an optimal adjustment of the mass flow rate allows one recovering a significant amount of the exergy losses.

In the field of the ventilation systems for underground infrastructures, two innovative modelling strategies have been proposed for the optimization of the design, operation and control of such complex systems. The first one is the proper orthogonal decomposition. This is a model order reduction technique characterized by accuracy and a reasonable computational time. The construction of the reduced

models starting from the non-dimensional form of the phenomena of interest, adds the quality of the flexibility to other cited characteristics. The reduced model does not depend on the geometry, source terms, boundary conditions and initial conditions. It can be used to explore different designs and operating conditions.

The POD technique has been proposed for the sanitary ventilation (in particular for the pollutant control) of the Padornelo tunnel during the excavation phase. The reduced model of the non-dimensional mass transport equation has been tested with experimental data confirming its accuracy. The comparison with the full models has also underlined the significant reduction of the CPU time that varies from the 75% to the 82% depending on the extension of the computation domain. The POD model has been used for the development of a Fuzzy Logic Control (FLC) algorithm for the ventilation system. An optimization analysis has allowed to identify the crisp value the FLC with the aim to reduce the electricity consumptions and to ensure an adequate quality of air. The developed algorithm has been implemented and tested in the Padornelo tunnel confirming the correct control of the air quality with an energy consumption reduction of about 24% respect with the fan operation at constant velocity.

In order to show the potentiality of POD technique for the optimization strategies and the real time simulations, the boreholes thermal energy storage (BTES) systems supplied by a cogeneration plant have been considered as possible application. The design and the storage temperature affect the charging times and the operations of BTES systems and cause high initial costs. Because investment costs and performances are competing objective functions, a multi-objective optimization (MOP) strategy has been applied to investigate the optimal design of a BTES system. The different operating conditions simulated by the reduced model can be distinguished in three different stages: charging time to achieve the design temperature in the ground; discharging time i.e. the effective operation to supply energy demand of domestic users; recharging time between two winter seasons.

The selected objective functions are the unit exergoeconomic cost and the second law efficiency. The Pareto front that is the result of the MOP strategy reports each optimal point for the design in term of pitch between the tube and installation depths. The unit exergoeconomic cost varies moderately from 0.031 €/kJ to 0.064 €/kJ. The exergetic efficiency presents a minimum value equal to 6% while the maximum one is of about 18.2%. The selection of the optimum solution depends on the preferences and criteria of the decision maker, suggesting that different points can be selected as for the optimum solution depending on the specific needs. The POD model has been used to perform fast and accurate simulation of the BTES system for a real time optimization of its operation. In fact, the operating conditions of this system is mainly subjected to the thermal energy demand of buildings, to the state of charge, to the availability of additional energy to store and to the energy market. An optimization algorithm has been proposed in order to discover the optimal time for storing and retrieving additional thermal energy during the operation. Various scenarios are explored taking into account the daily prediction of thermal and electrical energy consumptions as well as electricity market prices. Three different cases have been compared considering the same period of operation. In the first one, The BTES is regulated by the proposed algorithm to establish the daily time for the additional storage. In the second scenario, the operation is characterized by prefixed daily time for the additional storage (2 hours per day) and in the last one any daily storage are not considered. The results show that a significant improvement of the second law efficient (18.8%) and a large economic profit can be achieved using this algorithm.

As well known, the 1D models and the corresponding reduced models are based on the assumption of a homogenous behaviour of the fluid flow in each cross section. This make such models unsuitable to simulate the fluid behaviour in regions at high temperature gradients or in region at velocity gradients without the introduction of

proper corrections and empirical correlations. CFD codes are largely used as engineering tools for the analysis of both normal operating conditions and emergence conditions i.e. in the case of fire. The accuracy of CFD in the prediction of local flow field data i.e. velocity and temperature fields, is affected by the mesh size used for the domain discretization with significant computational resources for vast domain as in network infrastructures several kilometre long. In fact in most of the applications, the computational domain is limited to a small region i.e. close to the fire and the velocity and temperature profile in the rest of the domain are assumed known.

For these reasons, the second proposed innovative modelling strategy is the multiscale approach and in particular the development of a multiscale simulator. In general the multiscale modelling is based on the physical decomposition of the domain. This approach assigns a 3D model in the *near field* e.g. the sub-domain characterized by gradients (as the region close to the fire source), ensuring the accuracy of the CFD in such regions. Instead the *far field* e.g. the sub-domain where gradients in the transversal direction are negligible (as in cold flow conditions or in fire conditions that some distance downstream of the *far field),* is modelled by the 1D model with a low computation cost.

In the tunnel ventilations field, this type of approach has been developed through a direct-indirect coupling of commercial CFD codes and a 1D network that does not include the mass transport equation and it is limited to simple geometry.

The open source code FDS presents a 1D model called HVAC and it can be used as unique code for the multiscale modelling. The current version of the HVAC routine implemented in FDS is characterized by two major limitations for the multiscale modelling of complex systems.

First limitation is due the absence of 1D mass transport for the different species that is particularly interesting in the case of back layering of smoke thanks to the computation of the exhaust gas diffusion from the CFD domain and the relative

concentration. Second limitation is due to the energy conservation form that does not include the heat losses through the walls and does not allow one to analyzing the temperature evolution along a duct, which is very interesting in the case of semi-transversal ventilation.

For these reasons a multiscale simulator has been created through the fully integration of a 1D continuity, momentum, energy and mass transport equation in FDS modifying its source codes. The integration between FDS domain and the 1D network model occurs in a new special vent type called EXCH, added to the Vent name-list group of the FDS for specifying the type of 1D-3D boundary condition exchanged. The default air composition has been modified adding the Soot and CO species to allow the exchange of boundary conditions for the mass transport at the interface.

The exchange of all the boundary conditions does not occur at each iteration of FDS calculation but after a prefixed times step (that can be modified by the user) ensuring a temporal convergence of thermodynamic variables. The preliminary version of the multiscale simulator that has been presented in this work, allows to couple only two 1D domains with the CFD. This means that in the boundaries of the FDS domain, the EXCH vent and the OPEN vent can be used. A guide has been provided to suggest the localization of these two surfaces depending of the type of the ventilation system.

Several tests have been performed to compare the multiscale simulator with the corresponding full 1D model and the full FDS model. The tests have involved both in cold flow that in fire scenario. They have shown a significant accuracy of the multiscale simulator both for the prediction thermal fluid-dynamic behaviour that for the mass transport analysis. For the test in presence of fire, the use of the multiscale simulator has caused a reduction of the CPU of about 55%.

The multiscale simulator has been applied for modelling the ventilation system of the Monte Cuneo road tunnel in case of fire. It presents a semi-transversal ventilation system with accelerators and dumpers for the air extraction. The multiscale model has been validated with experimental data in three different points of measure. The comparison have shown an acceptable error that varies from 3.7% to 6.7%. The model has been used to simulate a fire scenario of 30 MW. Results have demonstrated that smoke might not be fully confined, depending on the atmospheric conditions at portals. The installation of larger extraction dumpers (1.8 x 2.3 m^2) and deflectors on the jet fans allows an increase in the exaction capacity in of about 16.5%. The new redesigned configuration ensures a correct smoke control with, a zero velocity in the fire area and converging velocities on both sides and significant improvements in terms of safety conditions.

Considering the results achieved in this thesis, in the author's opinion the two proposed strategies deserve further developments, as discussed in the following.

The POD models could be applied on the 1D fluid-dynamic and energy equations for the optimization algorithms of the design and operation of the ventilation systems for underground infrastructures. In fact, they allow to explore different configurations with accuracy in short time and are suitable for the implementation in advanced algorithms.

As results show, the POD model is appropriate for the real time simulations and it could be used as the *predictive controller* in the control algorithms of the ventilation. On the basis of the real data related to the traffic intensity and the weather conditions, the model might simulate the fluid-dynamic behaviour in the facility considering the latter as a non-linear dynamic system.

In the field of fire safety, the POD model can be integrated in the virtual reality simulators to train fire fighters. Unlike the actual virtual simulators, the POD model can reproduce different situations and change the parameters of the simulation in

real-time. As previously discussed, for the use of the 1D model in fire scenario, proper corrections have to be introduced in order to consider the non-homogeneity caused by the stratification, the thermal and fluid-dynamic gradients. Similar corrections should be introduced in 1D reduced models. As an alternative a POD model based on the 3D fields could be developed.

As regards the multiscale simulator, the increase of the number of interfaces 1D-3D (that are 2 in the presented version) is currently being developed. This will allow to reproduce all the components of the complex facilities, modelling air ducts, ventilation rooms with the network model. Moreover, this modification will give the possibility to use more 3D domains for the same system. This could be interesting in the case of longitudinal ventilation in long tunnels to model the areas near the jet fans with the 3D domains or in the case of fully transversal ventilation in which the ventilation strategy presents more points of extraction (e.g. the opposite supply strategy for the Frejus tunnel).

The multiscale simulator will tested in fire scenario comparing results with that obtained by the full CFD model in FDS. The multiscale simulator will be applied on longer underground infrastructures as the Frejus tunnel to test and compare the results with experimental data.

The application field of the multiscale simulator can be extended to the analysis of the smoke diffusion and temperature distribution in tall buildings such as skyscrapers.

Because the multiscale simulator has been obtained from an open source CFD code (FDS), it will be available for all the scientific community also to be subjected to additional tests from other users and it could be integrated in a next version of FDS.

References

Adjiski, V., Mirakovski, D., Despodov, Z. & Mijalkovski, S., 2015. Simulation and optimization of evacuation routes in case of fire in underground mines. *Journal of Sustainable Mining,* 14(3), pp. 133-143.

Ang, C., Rein, G., Peiro, J. & Harrison, R., 2016. Simulating longitudinal ventilation flows in long tunnels: Comparison of full CFD and multi-scale modelling approaches in FDS6. *Tunnelling and Underground Space Technology,* Volume 52, pp. 119-126.

ASHRAE, 2013. *ASHRAE Handbook - Fundamentals.* Atlanta: The American Society of Heating, Refrigerating and Air-Conditioning Engineers..

Atam, E. & Helsen, L., 2016. Ground-coupled heat pumps: part 1–Literature review and research challenges in modeling and optimal control. *Renew. Sustain. Energy <http://dx.doi.org/10.1016/j.rser.2015.10.007>,* Volume 54, p. 1653–1667.

Bandos, T. et al., 2009. Finite line-source model for borehole heat exchangers: effect of vertical temperature variations. *Geothermics ,* Volume 38, pp. 263-270.

Bangia, A. K., Batcho, F. P., Kevrekidis, G. I. & Karniadakis, E., 1997. Unsteady Two-Dimensional Flows in Complex Geometries: Comparative Bifurcation Studies with Global Eigenfunction Expansions. *Journal of Scientific Computing,* 18(3), pp. 775-805.

Beer, G., Reichl, T. & Lenz, G., 2002. *VIRTUALFIRES a virtual reality simulator for tunnel fires.* Graz, International Conference „Tunnel Safety and Ventilation.

Beer, G., Reichl, T. & Lenz, G., 2004. *VIRTUALFIRES a virtual reality simulator for tunnel fires.* Granz, International Conference „Tunnel Safety and Ventilation.

Bejan, A., Tsatsaronis, G. & Moran, M., 1996. *Thermal design and Optimization.*. New York: Wiley.

Beltrami, E., 1997. *Mathematics for Dynamic Modeling.* 2nd ed. San Diego, CA: Accademic Press.

Bender, E. A., 2000. *An Introduction to Mathematical Modeling.* New York: Dover.

Berkooz, G., Holmes, P. & LuMSey, J. L., 1993. The proper orthogonal decomposition in analysis of turbulent flows. *Annual review of fluid mechanics,* 25(1), pp. 539-575.

Bernier, M. A., 1986. Ground-coupled heat pump system simulation. *ASHRAE Transactions*, Volume 107, pp. 605-616.

Besselink, B. et al., 2013. A comparison of model reduction techniques from structural dynamics, numerical mathematics and systems and control. *Journal of Sound and Vibration,* Volume 332, pp. 4403-4422.

Bogdan, S., Birgmajer, B. & Kovačić, Z., 2008. Model predictive and fuzzy control of a road tunnel ventilation system. *Transportation Research Part C: Emerging Technologies,* Volume 16, pp. 574-592.

Bozhiiov, V., Shoushoulov, G., Kovachev, L. & Paunchev, D., 1997. *Ventilation and air-conditioning during operation in deep mines-a foremost engineering task.* Ankara, 15th Mining Congress of Turkey.

Bracke, G., Alkan, H. & Müller, W., 2006. Modelling Underground Ventilation Networks and Radon Flow for Radiological Protection Using VUMA. In: B. J. Merkel & A. Hasche-Berger, eds. *Uranium in the Environment.* Berlin: Springer, pp. 593-599.

Brahim, K., Mourad, B., Afif, E. C. & Ali., B., 2013. Control of smoke flow in a tunnel. *Journal of Applied Fluid Mechanics,* 6(1), pp. 49-60.

Brenner, T. A. et al., 2012. A reduced-order model for heat transfer in multiphase flow and practical aspects of the proper orthogonal decomposition.. *Computers & Chemical Engineering,* Volume 43, pp. 68-80.

Buljak, V., 2012. *Inverse Analyses with Model Reduction.* Berlin: Springer-Verlag.

CETU, Centre d'études des tunnels, 2003. *Giude des dossier de sécurité des tunnels routiers. Fascicule 4. Le études spécificues des dangers,* France: Ministère de l'Equipement, des Transports, du Logement, du Tourisme et de la Mer.

Chandrashekar, M. & Wong, F., 1982. Thermodynamic system analysis – a graph-theoretic approach. *Energy,* 7(6), pp. 539-566.

Chen, P. H., Lai, J. H. & Lin, C. T., 1998. Application of fuzzy control to a road tunnel ventilation system. *Fuzzy Sets and Systems ,* Volume 100, pp. 9-28.

Chu, B. et al., 2008. GA-based fuzzy controller design for tunnel ventilation systems. *Automation in Construction,* Volume 17, pp. 130-136.

Claesson, J. & Eskilson, P., 1988. Conductive heat extraction from a deep borehole thermal analysis and dimensioning rules. *Energy,* Volume 13, pp. 509-527.

Colella, F., 2010. *Multiscale Modelling of Tunnel Ventilation Flows and Fires.* Politecnico di Torino, Dipartimento di Energetica: PhD thesis.

Colella, F., Rain, G., Verda, V. & Borchiellini., R., 2011. Multiscale modeling of transient flows from fire and ventilation in long tunnels. *Computers & Fluids,* Volume 51, pp. 16-29.

Colella, F. et al., 2009. Calculation and design of tunnel ventilation systems using a two-scale modelling approach. *Build Environ,* Volume 44, pp. 2357-2367.

Colella, F., Rein, G., Borchiellini, R. & Torero, J., 2011. A novel multiscale methodology for simulating tunnel ventilation flows during fires. *Fire Technology,* 47(1), pp. 221-253.

Colella, F. et al., 2010. Analysis of the systems in the dartford tunnels using a multiscale modelling approach. *Tunnell Undergr Space Technol 2010,* Volume 25, pp. 423-432.

Colella, F., Verda, V., Borchiellini, R. & Rein, G., 2012. One-dimensional and multi-scale modelling of tunnel ventilation and fires. In: *Handbook of Tunnel Fire Safety-Second edition.* s.l.:Istitution of Civil Engineers, pp. 365-390.

Cosentino, S. et al., 2014. *Optimal Operation and Sensitivity Analysis of a Large District Heating Network Through POD Modeling.* Montreal, ASME 2014 International Mechanical Engineering Congress and Exposition.

Cosentino, S. et al., 2015. *Identification of the optimal operational strategy of a large district heating networks through POD modeling.*. Pau,France, ECOS-The 28th International Conference on Efficiency, Cost, Optimization, Simulation and Environmental Impact of Energy Systems.

Cosentino, S., Sciacovelli, A. & Verda, V., 2015. *Energy and exergy analysis of ground thermal energy storage: optimal charging time in different operating conditions.* Pau, France, ECOS-The 28th International Conference on Efficiency, Cost, Optimization, Simulation and Environmental Impact of Energy Systems.

Cosentino, S., Sciacovelli, A. & Verda, V., June 25–27, 2014.. *Optimal operation of small geothermal systems through entropy generation analysis.* Copenhagen, Denmark, ASME 2014:12th Biennial Conference on Engineering Systems Design and Analysis, ESDA 2014.

Cosentino, S., Sciacovelli, A., Verda, V. & Noce, G., 2016. Optimal operation of ground heat exchangers in presence of design anomalies: An approach based on second law analysis. *Applied Thermal Engineering ,* Volume 99, pp. 1018-1026.

Cosentino, S., Sciacovelli, A. & Verda, V., November 13-19, 2015,. *Thermoeconomic design of borehole thermal energy storage systems.* Houston, Texas, USA., IMECE 2015-ASME International Mechanical Engineering Congress and Exposition.

Dai, G. & Vardy, A., 6-8 July,1994. *Tunnel temperature control by ventilation.* Liverpool, UK, Proceedings of 8th international symposium on the aerodynamics and ventilation of vehicle tunnels.

Danziger, N. H. & Kennedy, W. D., 1982. *Longitudinal ventilation analysis for the Glenwood canyon tunnel.* York, England, Proceedings of the Fourth International Symposium Aerodynamics and Ventilation of Vehicle Tunnels.

Deo, N., 2004. *Graph Theory with Applications to Engineering and Computer Science.* London: Prentice-Hall.

DETEC, Département fédéral de l'environnement des transports de l'énergie de la communication, 2008. *Ventilation des galeries de sécurité des tunnels routiers,* France: ASTRA 13002.

Domańsk, R. & Fellah, G., 1998. Thermoeconomic analysis of sensible heat, thermal energy storage systems. *Applied Thermal Engineering,* Volume 8, pp. 693-704.

Dowell, E. H. et al., 2006. *Reduced Order Models in Unsteady Aerodynamic Models, Aeroelasticity and Molecular Dynamics.* Lisbon, Portugal, III European Conference on computational mechanics, solids, structures and coupled problems in engineering.

Ferrovial Agroman, 2013. *Etùnel Aire: Sistema Automatizado de Mediciòn y Diluciòn de Gases en Construcciòn de Obras Subterràneas,* Madrid: Ferrovial.

Ferrovial, 2017,. *Lanzamiento del proyecto de innovación "etúnel-aire".* [Online]
Available at: http://www.ferrovial.com/es/prensa/noticias/lanzamiento-proyecto-innovacion-etunel-aire/
[Accessed 16 Febrary 2017].

Florides, G. & Kalogirou, S., 2007. Ground heat exchangers-A review of systems, models and applications. *Renewable Energy,* Volume 32, pp. 2461-2478.

Florides, G. & Kalogirou, S., 2007. Ground heat exchangers-A review of systems, models and applicationsy. *Renew. Energy,* Volume 32, p. 2461–2478.

Formaggia, L., Gerbeau, J., Nobile, F. & Quarteroni, A., 2001. On the coupling of 1D and 3D Navier–Stokes equations for flow problems in compliant vessels. *Comput Methods Appl Mech Eng,* Volume 191, pp. 561-582.

Gao, Q. et al., 2008. Review of development from GSHP to UTES in China and other countries.. *Renew. Sust. Energ* , Volume 4, pp. 1383-1394.

Gehandler, J., 2015. Road tunnel fire safety and risk: a review. *Fire Science Reviews*, Volume 4, pp. 2-27.

Gershenfeld, N., 1999. *The nature of mathematical modeling.* Cambridge, UK: Cambridge University Press.

Grant, G. & Jagger, S., 2012. The use of tunnel ventilation for fire safety. In: A. Beard & R. Carvel, eds. *Handbook of Tunnel Fire Safety- Second edition.* s.l.:Istitution of Civil Engineers, pp. 177-217.

Greenshields, C. J., 2016. *OpenFoam User Guide v.4.0.* s.l.:s.n.

Guelpa, E., 2016. *Modelling strategy for multiple scenario adn fast simualtion in large systems: application to fire safety and energy engineering.*. s.l.:PhD Thesis, Politecninco di Torino.

Guelpa, E., Sciacovelli, A., Verda, V. & Ascoli, D., 2016. Faster prediction of wildfire behaviour by physical models through application of proper orthogonal decomposition. *International Journal of Wildland Fire*, 25(11), pp. 1181-1192.

Gu, Y. & O'Neal, D., 1998. Development of an equivalent diameter expression for vertical U-Tubes used in ground-coupled heat pumps. *ASHRAE Trans*, Volume 104, pp. 347-355.

Houzeaux, G. & Codina, R., 2004. A Dirichlet/Neumann domain decomposition method for incompressible turbulent flows on overlapping subdomains. *Computers & Fluids*, Volume 33, pp. 771-782.

Inc., ANSYS, 2013. *ANSYS, Fluent User Guide v.15.* s.l.:s.n.

Ingason, H., 2005. Fire Dynamics in tunnel. In: *The handbook of tunnel fire safety.* London, UK.: Ed. A. Beard and R. Carvel, Thomas Telford..

Ingason, H., 2009. Design fire curves for tunnels. *Fire Safety Journal*, Volume 44, pp. 259-265.

Ingason, H., Zheni, Y. L. & Lönnermark, A., 2014. *Tunnel Fire Dynamics.* New York: Springer.

Kizilkan, O. & Dincer, L., 2015. Borehole thermal energy storage system for heating applications: Thermodynamic performance assestment. *Energy Conversion and Management,* Volume 90, pp. 53-61.

Konaka, A., Coitb, D. W. & Smith, A. E., 2006. Multi-objective optimization using genetic algorithms: A tutorial. *Reliability Engineering and System Safety ,* Volume 91, pp. 992-1007.

Kunsch, J. P., 2002. Simple model for control of fire gases in a ventilated tunnel. *Fire Safety Journal,* Volume 37, pp. 67-81.

Lassila, T., Manzoni, A., Quarteroni, A. & Rozza, G., 2014. Model order reduction in fluid dynamics: challenges and perspectives. In: *Reduced Order Methods for Modeling and Computational Reduction.* Cham: Springer, pp. 235-273.

Li, M. & Lai, A., 2015. Review of analytical models for heat transfer by vertical ground heat exchangers (GHEs): A perspective of time and space scales. *App. Energy,* Volume 151, p. 178–191..

Lundh, M. & Dalenback, J., 2008. Swedish solar heated residential area with seasonal storage in rock: initial evaluation. *Renewable Energy,* Volume 33, pp. 703-711.

McGrattan, K. et al., 2013. *Fire Dynamics Simulator (Version 6), User's Guide.*. Gaithersburg, Maryland,: NIST Special Publication 1019.

McGrattan, K. et al., 2013. *Fire Dynamics Simulator Technical Reference Guide: Volume 1: Mathematical Model.* Gaithersburg, Maryland: NIST Special Publication 1018 Sixth Edition.

McPherson, M., 1993. Ventilation network analysis. In: *Subsurface Ventilation and Environmental Engineering.* s.l.:Springer, pp. 209-240.

Merci, B. & Beji, T., 2016. *Fluid Mechanics Aspects of Fire and Smoke Dynamics in Enclosures.* London, UK: Taylor & Francis Group.

Mine safety operation divisions, 2008. *Guideline for the management of diesel engine pollutants in underground environments,* Maitland: NSW Department of Primary Industries.

Musinet Engineering S.p.A., 2011. *Reports and documentations about Monte Cuneo Tunnel road,* Torino: Musinet.

Nagendra., S. & Khare., M., 2002. Line source emission modelling. *Atmospheric Environment,* 26(13), p. :2083–2098.

Nordell, B., Grein, M. & Kharseh, M., 2007. *Large-scale utilisation of renewable energy requires energy storage.* s.l.:Lulea University of Technology.

NTIS, 1990. *User's guide for the TUNVEN and DUCT programs.* s.l.:Publication PB80141575.

Oka, Y. & Atkinson, G., 1995. Control of smoke flow in tunnel fire. *Fire Safety Journal,* Volume 25, pp. 305-322..

Ostrowsky, Z., Bialecki, R. & Kassab, A., 2005. *Advances in application of proper orthogonal decomposition in inverse problems.* Cambridge, UK, s.n.

Ozgener, L., Hepbasli, A. & Dincer, I., 2005. Enegy and exergy analysis of Salihli geothermal district heating system in Manisa, Turkey.. *Int J Energy Res,* Volume 29, pp. 393-408.

Patancar, S., 1980. *Numerical Heat Transfer and Fluid Flow*. New York: Tayor & Franci.

Perdikaris, P., Grinberg, L. & Karniadakis, G. E., 2016. Multiscale modeling and simulation of brain blood flow. *PHYSICS OF FLUIDS* , Volume 28, pp. 021304-16.

PIARC Committee on Road Tunnels, 1995. *Tunnel routiers: emission, ventilation, environnement.* Paris: s.n.

PIARC: Technical Committee C4 Road Tunnels Operation, 2012. *Road Tunnels: vehicle emissions and air demand for ventilation,* France: World Road Association (PIARC).

Price, J., 2015. *Coupled 1D-3D simulation of flow in subway transit networks.* s.l.:PhD Thesis, Imperial College London.

Quartaroni, A., 2008. *Modellistica numerica di problemi differenziali.* Milano: Springer.

Quarteroni, A., 1994. Domain decomposition methods for the incompressible Navier-Stokes equations. In: *Computational Fluid Dynamics.* s.l.:John Wiley & Sons Ltd, p. 72–77.

Quarteroni, A. & Valli, A., 1999. *Domain Decomposition Methods for Partial Differential.* Oxford: Oxford Science Publications.

Ragot, J. & Lamotte, M., 1993. Fuzzy Logic Control. *Internation Journal of Systems Science,* Volume 24, pp. 1825-1848.

Raines, K., 2009. *Underground Passenger Comfort. Rethinking the current thermal and lighting standards.* Quebec City, Canada, PLEA2009 - 26th Conference on Passive and Low Energy Architecture..

Riess, I., Bettelini, M. & Brandt, R., November 2000. *Sprint – a design tool for fire ventilation.* Boston, s.n.

Rosenfeld, A. & Kak, A. C., 2014. *Digital picture processing.* s.l.:Elsevier.

Schilders, W., 2008. Introduction to model order reduction. In: *Model order reduction: Theory, research aspects and applications* . Berlin: Springer , pp. 2-32.

Sciacovelli, A., 2016. Toward efficient control of energy systems: an application of proper generalized decomposition to thermal storage. *International Journal of Thermodynamics,* Volume 19, pp. 19-27.

Sciacovelli, A., Verda, V. & Borchiellini, R., 2013. *Numerical Design of Thermal Systems.* Torino: Clut.

Sharqawy, M. et al., 2009. Energy, exergy and uncertainty analyses of the thermal response test for a ground heat exchanger. *Int J Energy Res,* Volume 33, pp. 582-592.

Sibbitt, B. et al., 2012. The performance of a high solar fraction seasonal storage district heating system five years of operation. *Energy Procedia* , Volume 33, pp. 856-865.

Sirovich, L., 1987. . Turbulence and the dynamics of coherent structures, Parts I, II and III. *Quarterly of applied mathematics,* Volume XLV, pp. 561-590.

Steinbrecher, A. & Stykel, T., 2013. Model order reduction of nonlinear circuit equations. *International Journal of Circuit Theory and Applications,* Volume 41, p. 1226–1247.

Taylor, S. et al., 1997. *SMARTFIRE: an Integrated Computational Fluid Dynamics Code and Expert System for Fire Field Modelling.* Greenwich, London, UK, Fire Safety Science: Proceedings of the Fifth International Symposium. International Association for Fire Safety Science.

Teodosiu, C., Ilie, V., Dumitru, R. & Teodosiu, R., 2016. Numerical evaluation of ventilation efficiency in underground metro rail transport systems. *Energy Procedia,* pp. 539-549.

Thomas, P., 1968. The Movement of Smoke in Horizontal Passages Against an Air Flow. In: *Fire Research Note.* Watford, UK.: Fire Research Station, p. no. 723.

Tsatsaronis, G., 1993. Thermoeconomic analysis and optimization of energy systems. *Prog. Energy Combust. Sci.* , Volume 19, pp. 227-257.

U.S., Bureau of Mines, 1995. *MFIRE Users Manual Version 2.20,* Minneapolis, MN: Twin Cities Research Center.

Vermesi, I. et al., 2017. Reducing the computational requirements for simulating tunnel fires by combining multiscale modelling and multiple processor calculation. *Tunnelling and Underground Space Technology,* Volume 64, pp. 146-153.

Versteeg, H. K. & Malalasekera, W., 2007. *An Introduction to Computational Fluid Dynamics: The Finite Volume Method.* Harlow: Pearson Education Limited.

Versteeg, H. & Malalasekera, W., 2007. *An introduction to computational fluid dynamics, the finite volume method..* Glasgow: Pearson Prentice Hall.

West, A., Vardy, A., Middleton, B. & Lowndes, J., 28-30 Nov 1994. *Improving the efficacy and control of the Tyne Tunnel ventilation system'.* Basel, Switzerland, s.n.

Wołoszyn, J. & Gołas, A., 2013. Modelling of a borehole heat exchanger using a finite element with multiple degrees of freedom. *Geothermics,* Volume 47, pp. 13-26.

Wu, W. et al., 2014. Evaluation of ground source absorption heat pumps combined with borehole free coolinge. *Energy Convers Manage,* Volume 79, pp. 334-343.

Wu, Y. & Bakar, M., 2000. Control of smoke fkow in tunnel fires using longitudinal ventilation systems-a study of the critical velocity. *Fire Safety Journal,* Volume 35, p. 363–390.

Yang, H., Cui, P. & Fang, Z., 2010. Vertical-borehole ground-coupled heat pumps: A review of models and system.. *Applied Energy,* Volume 87, pp. 16-27.

Zen., Y. H., Diao, N. R. & Fang, Z., 2002. A finite line-source model for boreholes in geothermal heat exchangers. *Heat Transfer-Asian Research,* Volume 31, pp. 558-567.

Zeng, H., Diao, N. & Fang, Z., 2003. Heat transfer analysis of boreholes in vertical ground heat exchangers. *Int. J. Heat Mass Transf,* Volume 46, pp. 4467-4481.

Zhai, X. Q. & Yang, Y., 2011. Experience on the application of a ground source heat pump system in an archives building. *Energy and Buildings,* Volume 43, pp. 3263-3270.

Zhu, H., Shen, Y., Yan, Z. & Guo, Q., 2016. A numerical study on the feasibility and efficiency of point smoke extraction strategies in large cross-section shield tunnel fires using CFD modeling. *Journal of Loss Prevention in the Process Industries,* pp. 158-170.

Zubair, M., Affan-Badar, M. S. & Al-Farayedhi, A., 1993. Second law-based thermoeconomic optimization of a sensible heat thermal energy storage system. *Energy,* Volume 18, pp. 641-649.